Efficient Generation of Hyperpolarized Molecules Utilizing the Scalar Order of Parahydrogen

Thesis by
Valerie Ann Norton

In Partial Fulfillment of the Requirements
for the Degree of
Doctor of Philosophy

CALIFORNIA INSTITUTE OF TECHNOLOGY
Pasadena, California
2010
(Defended 11 May 2010)

Acknowledgements

I would like to thank my thesis advisor, Dan Weitekamp, for his invaluable support which has allowed me to work on interesting and diverse projects in my time at Caltech. He has given me a truly unique opportunity to work on both experimental and theoretical aspects of these projects. His keen insights have provided the means to surmount the obstacles along the way.

I would also like to acknowledge Pratip Bhattacharya whose drive and passion brought PASADENA back to Pasadena. Without him, my part on the project would not have been possible. He and his colleagues at HMRI have been instrumental in all aspects of the experimental work. Eduard Chekmenev has brought a practicality to the process. Jan Hövener was a great help in making the wavelet phase experiments happen. All three, as well as Kent Harris and Raymond Weitekamp, have had their hands in building the polarizers and keeping them in working shape.

I would also like to thank Jim Kempf, Gary Leskowitz, and Lou Madsen for being so welcoming when I first joined the group. I would like to thank Bruce Lambert, Ramez Elgammal, and Mark Butler for all their support during much of my time here. And I would like to thank Jessica Pfeilsticker who has been making the final few years here most interesting and hopeful, for it is her task to continue the effort to hyperpolarize ever more molecules.

Abstract

This dissertation describes methods that polarize the spin of a specific nucleus in molecules synthesized by molecular addition of parahydrogen to a precursor molecule. Nuclear magnetic resonance (NMR) pulse sequences are designed to perform efficient transfer of spin order by way of the scalar spin couplings between the two nascent protons and a heteronuclear spin label target. The result is an increase in the NMR signal from that nucleus by several orders of magnitude, approaching unity polarization. Algorithms are presented to effect the desired unitary evolution of this three-spin system over the range of couplings found in diverse molecules and in the presence of interfering spins. These methods are explored theoretically and comparisons are made to select the most advantageous method given a specific problem.

Issues concerning the choice of target molecule, portable equipment, and automation are discussed. Some design choices made for convenience in one aspect of the execution of the methods raise difficulties in other aspects. These difficulties are elucidated and methods of mitigation are discussed.

Pulse design issues are elucidated with numerical calculations which confirm analytical results for the time dependence obtained in the multiply rotating frame approximation. Failures of this approximation at low frequencies are explored numerically leading to novel pulse sequence design rules which ameliorate undesirable phenomena peculiar to low field NMR, enabling its employment for this and other

applications requiring precise control of the spin degrees of freedom. Experimental results, primarily aimed at biomedical applications, are reviewed.

Table of Contents

Table of Figures

Nomenclature

AWG	arbitrary waveform generator
DAQ	data acquisition card
HEP	2-hydroxy-ethylpropionate
INEPT	insensitive nuclear enhancement by polarization transfer
MLEV	Malcolm Levitt's decoupling sequence
MRI	magnetic resonance imaging
NMR	nuclear magnetic resonance
NOE	nuclear Overhauser effect
PASADENA	parahydrogen and synthesis allow dramatically enhanced nuclear alignment
TFPP	2,2,3,3-tetrafluoropropyl 1-^{13}C-propionate-d_3

Constants and parameters

B_0	static magnetic field magnitude
B_1	oscillating magnetic field magnitude
f	quality factor for scalar spin order
I	spin quantum number
$\mathbf{I}_i$	the nuclear spin angular momentum operators on the i^{th} proton with Cartesian components I_{ix}, I_{iy}, I_{iz}, $i = 1, 2$

$\overline{J}_{12}$	J-coupling between protons in radians per second
$\overline{J}_{1S}$, $\overline{J}_{2S}$	heteronuclear J-coupling in radians per second
J_{ij}	J-coupling constants in Hz
k	Boltzmann's constant
P	polarization
$\mathbf{S}$	the nuclear spin angular momentum operators on the target nucleus with Cartesian components of S_x , S_y , S_z
T	temperature
T_1	time constant for longitudinal nuclear spin relaxation
γ_H	gyromagnetic ratio of hydrogen
γ_S	gyromagnetic ratio of the target nucleus
ϕ	pulse carrier phase
ϕ_w	pulse wavelet phase
θ	angular parameter classifying the 3-spin system and the pulse sequences derived from the J-coupling constants
ρ	density operator of the spin system
τ_{1l} , τ_{2l} , τ_{3l}	duration of the three sections of the large θ pulse sequence algorithm
τ_{1m} , τ_{2m} , τ_{3m}	duration of the three sections of the medium θ pulse sequence algorithm

$\tau_{1s}, \tau_{2s}, \tau_{3s}$	duration of the three sections of the small θ pulse sequence algorithm
ω	reference angular frequency defining the rotating frame

I. History and Introduction

The technique of Nuclear Magnetic Resonance (NMR) has its origins in Rabi's molecular beam experiments (*1*) measuring the intrinsic magnetic moment of atomic nuclei predicted to exist by quantum mechanics. Guided by these experiments and Gorter's attempt (*2,3*), Purcell (*4*) and Bloch (*5*) showed the same measurements could be performed on hydrogen in solid and liquid samples, respectively, using inductive detection similar to that utilized today.

The presence of other nuclear and electron magnetic moments near the measured nuclear magnetic moment would be expected to affect the measurement. One way this effect manifests is in the dependence of line positions on sample orientation in single crystal solids shown by Purcell (*6*). This single effect was enough to begin the use of NMR to probe chemical properties. The power of the technique was first demonstrated by Pake (*7*) to measure the hydrogen spacing in $CaSO_4 \cdot 2H_2O$ using both a single crystal and a powdered sample.

Other more subtle effects were expected (*8*), but were beyond the abilities of the equipment. Refinement in equipment and an ever increasing library of tested samples led quickly to new discoveries. In metals, Knight found resonances that were at higher frequencies than had been observed for salts of those metals (*9*) giving the Knight shift due to coupling to rapidly relaxing electron paramagnetism. In simultaneous discoveries, it was found that the resonances of ^{14}N (*10*) and ^{19}F (*11*) were

dependent upon the chemical compound in which they were found giving the chemical shift. Scalar couplings were found in $NaSbF_6$ (*12*) although it was not correctly explained for another year (*13*).

These and other discoveries have formed the basis by which the nucleus becomes a sensitive probe of the local molecular environment. Using them, it is now possible to find the structure of molecules in solution, even aqueous proteins (*14*). Kinetic studies (*15-17*) are routinely done, including on systems at chemical equilibrium, for which NMR is uniquely capable of probing rates of reaction and diffusion.

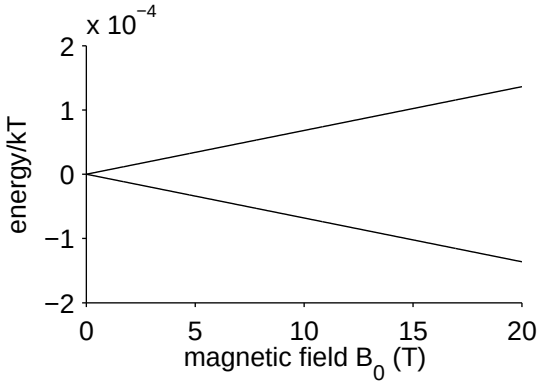

Figure 1. The separation of energy levels between states of protons with their magnetic moment aligned with the field and against the field is dependent upon the magnitude of the field. This energy separation is small compared to kT at room temperature even in high field magnets.

As powerful as NMR is as a sensitive probe of the molecular structure and dynamics, it is highly insensitive as well. NMR is fundamentally a spectroscopic technique studying differences in energy levels that are small compared to kT at ambient conditions (Fig. 1). As a result, the system is highly disordered and the excess

population of the lower energy level is only a few parts per million even in the high fields, up to about 20 T, in use today. It is possible to increase the equilibrium order at low temperatures, but relaxation times in the solid state can grow impractically long at low temperatures and the spectra desired for chemical and biological applications are often required to be in the liquid state.

A. Increasing polarization

The signal in NMR is proportional to the polarization of the nucleus that is being detected. The fractional polarization of a nucleus is given by

$$P = \frac{N_+ - N_-}{N_+ + N_-} \tag{1}$$

where N_+ is the number of spins aligned with the magnetic field and N_- is the number of spins aligned against the field. A few techniques have been developed in order to combat this problem of low signal by manipulating the populations of energy levels. Some enhance certain population differences at the expense of others that are less important or more rapidly refreshed. For example, an increase in the polarization of an insensitive nucleus may be generated at the expense of proton polarization where the gain factor includes the ratio of the gyromagnetic ratios. Saturation of hydrogen transitions in heteronuclear systems leads to small enhancements by the nuclear Overhauser effect (NOE), an example of cross relaxation between spins (*18*). Somewhat larger enhancements can be achieved by using resolved scalar couplings between

isotopes in a more sophisticated pulse technique such as insensitive nuclear enhancement by polarization transfer (INEPT) (*19*). While these techniques do increase the polarization available for detection of these heteronuclei, it is by factors on the order of the ratio of the gyromagnetic ratios. This is at most an order of magnitude for typical isotopes. Although these are important improvements over the equilibrium values, the actual population difference remains the same order of magnitude as for protons at equilibrium.

B. Hyperpolarization

Substantially greater order can be imposed on the system by using some external perturbation in a few select nonequilibrium situations. One example of this is chemically induced dynamic nuclear polarization (*20*), where ultraviolet light is used to break apart a molecule and the following geminate radical recombination is directed in part by the nuclear state. When the products have different resonant frequencies, large absorption and emission lines can be seen from each of the products due to the order imposed by sorting of nuclear spin in the recombination process. Another example is optical pumping with circularly polarized light of systems where unpaired electrons interact with the nucleus. The optical pumping orders the unpaired electron which in turn helps to order the nucleus. In gases, this has been used to polarize ^{3}He (*21*) and ^{129}Xe (*22*) mixed with Rb as high as 70%.

The technique of PASADENA (parahydrogen and synthesis allow dramatically

enhanced nuclear alignment) (*23-25*) (Fig. 2) applies the idea of chemically combining an easily generated, highly ordered, component with a disordered component as the initial step of the experiment. The system generated from chemical reaction of these two materials has a source of order that may be manipulated in an effort to generate the spin order desired by the experimenter. The disordered element is a precursor molecule that will become the desired molecule after molecular addition of hydrogen. The ordered element is hydrogen in the para state, which is easily generated by passing molecular hydrogen over a catalyst that speeds equilibration of spin isomers at sufficiently low temperature. Removed from such catalytic particles, parahydrogen may be stored at room temperature for days without significant equilibration of the spin state. The signal gain possible from the technique is dependent upon the purity of the spin state of the reactant hydrogen. The figure of merit for this purity is $f = \left(4\chi_p - 1\right)/3$ where χ_p is the mole fraction of parahydrogen.

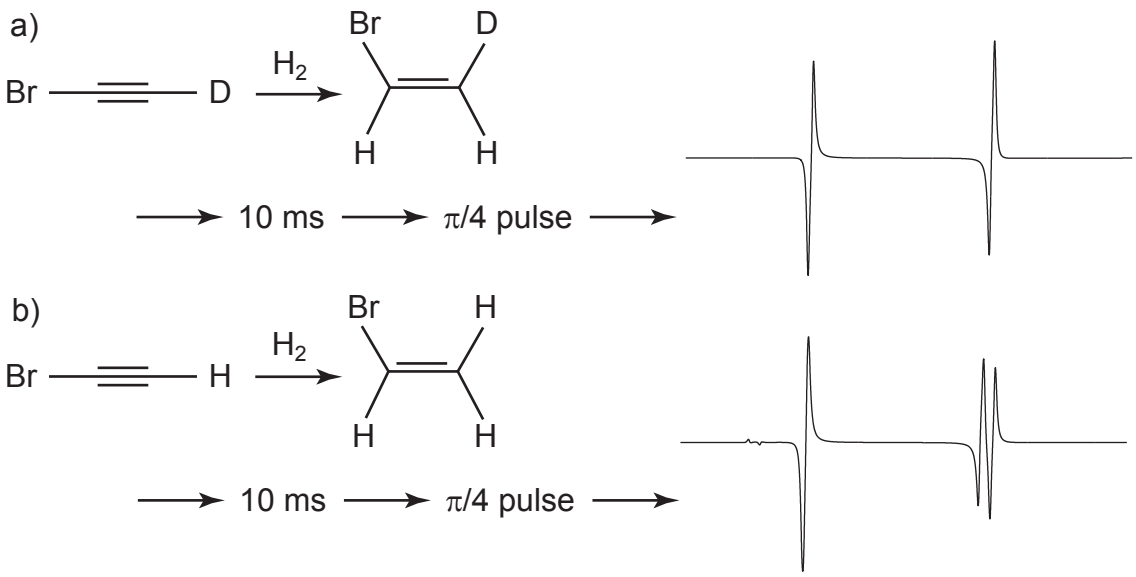

Figure 2. Simulated PASADENA spectrum 10 ms after reaction for a) the reaction of 1-bromo-2-deutero-ethylyne with parahydrogen to form 1-bromo-2-deutero-ethylene and b) the reaction of bromoethylyne with parahydrogen to form bromoethylene.

In the original proposal (*23*) and experimental demonstration (*24,26*), the newly introduced proton pair evolves under the new molecular Hamiltonian for a short time, on the order of seconds, while the hydrogen product accumulates. Radiation of the system with a $\pi/4$ pulse shows strong antiphase peaks (Fig. 2) from these coupled, inequivalent protons. As well as enhancing the signals from specific protons that were derived from a chemical reaction with parahydrogen, those initial papers presented methods by which neighboring protons could be highly polarized as well. The unitary evolution under the chemical shift differences and scalar couplings can ideally lead to $P = f$ on a particular site (*23*). In order to reach this limit experimentally, it is necessary to retard evolution out of the singlet state during the reaction, for instance by

coherently averaging the chemical shift difference of the protons to zero with a train of π pulses (*27,28*). In practice, any method of sufficiently strong proton decoupling is suitable for this (*29*).

Later experiments observed enhanced antiphase multiplets upon a spin ½ heteronucleus coupled to the nascent protons from parahydrogen in response to a single pulse (*30*). This was quantified (*31*) using the same idea as for the homonuclear case: the scalar order of parahydrogen is projected onto the eigenstates of the product molecule to give the spin density operator at the beginning of the NMR experiment. While this one-pulse experiment is inefficient, it ideally has the capacity to generate polarization of nearly $f/3$ for spin systems with advantageous coupling constants (Fig. 3), a significant increase compared to equilibrium.

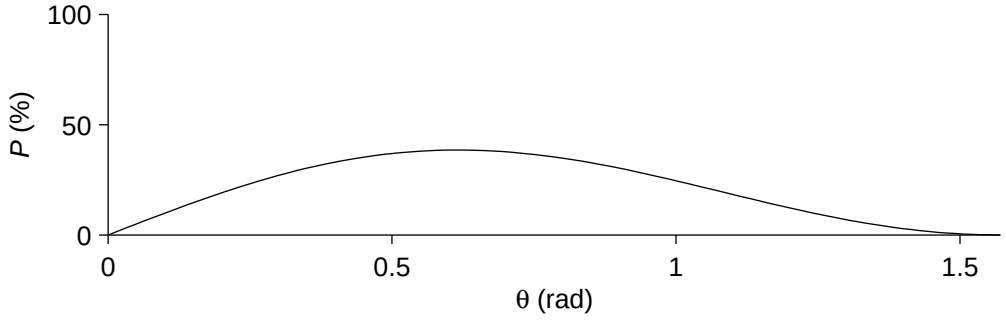

Figure 3. Maximum polarization on the heteronucleus using a single pulse technique is found using the formula $P = f\cos^2\theta\sin\theta$. The value of θ is dependent upon the scalar coupling constants of the system as defined in Eq. (17).

C. Recent advances

Proposals in the context of other experiments utilizing parahydrogen (*27,28*) as a source of scalar order demonstrate the use of a decoupling scheme to arrest the evolution of spin states in the product molecule. This serves to "suspend time" such that all molecules are in the same initial state when the decoupling stops. In addition to the work utilizing parahydrogen as a source of spin order, other experimenters have shown that equivalent scalar or "singlet" spin order can be prepared from Zeeman polarization and is long-lived in systems with inequivalent hydrogen sites under sufficiently strong proton decoupling (*32,33*).

The use of proton decoupling during the chemical reaction for preservation of the singlet state and increased lifetime has lead to the development of a more complicated but efficient three pulse sequence for the transfer of spin order to a heteronucleus (*34,35*), which is discussed in section III.A. This sequence is capable of the theoretical maximum polarization $P = f$ for advantageous spin systems. In this way, the nuclei can be made to be nearly fully aligned with the applied magnetic field increasing the signal by several orders of magnitude. In practice, absolute polarization levels of 15-20% have been achieved (*36*).

Efforts are now being made to expand the number of molecules which can be hyperpolarized subsequent to formation from parahydrogen and also to increase the spectroscopic environments in which externally generated molecules, hyperpolarized by

any method, may be used, particularly in biological applications. Hyperpolarized ^{129}Xe has long been used for magnetic resonance imaging (MRI) of lung where sparse proton density and drastic magnetic susceptibility gradients make traditional methods difficult (*37*). Also showing potential medical relevance, subsecond angiography was performed by real time imaging of a hyperpolarized tracer molecule, revealing flow in major blood vessels in rats and lung vasculature in pigs (*38*). This was quickly followed by angiography utilizing more biologically relevant solutions (*39*).

These hyperpolarized MRI methods are intrinsically transient in nature, but utilize pulse sequences usually associated with the unrelated method of steady state free precession (SSFP). These sequences consist of hundreds of gradient echo experiments repeated at intervals of several ms to create 2D and 3D images. For hyperpolarized studies, they are repurposed to gather unique data as quickly as possible where averaging is not required due to the high signal level (*38*). This repurposing was improved by utilizing methods that refocus the magnetization at the end of each data collection window instead of discarding it with spoiling gradients, enabling 3D imaging with a single hyperpolarized sample (*40,41*).

Once injected hyperpolarized molecules are moving in the vascular system, it is of interest to study interactions of the molecules with some aspect of that system, such as their transport, binding, and metabolism. To that end, an amphiphilic probe 2,2,3,3-tetrafluoropropyl 1-^{13}C-propionate-d_3 (TFPP) that binds with lipid bilayers was developed (*42*). When a binding event occurs, the chemical shift of this probe changes

sufficiently to be distinct from that of the molecule in solution, enabling chemical shift imaging (CSI) *in vivo* (*43*). With a similar method, tissue pH has been studied *in vivo* (*44*) by measuring the relative concentration of $H^{13}CO_3^-$ and $^{13}CO_2$ which have a significant chemical shift difference.

In addition to these simple interactions, molecules that are expected to react and form new molecules in the accessible time period can be introduced to a system and monitored. This application of CSI is used for metabolic imaging with pyruvate (*45*) and with succinate (*46*). When the injected molecule reacts to form daughter molecules that are also hyperpolarized, those new molecules are initially at much lower concentration than the initial molecule, so have much lower signal. It is useful to use large angle pulses in order to see the product molecules, but large angle pulses on the initial molecule drastically reduces the time large polarizations are available. Also, the signal from the initial molecule may overwhelm signal from the lower concentration products. In order to mitigate dissipation of spin order by observation of the initial species, shaped pulses have been developed that excite the products selectively while leaving the initial reactant largely unperturbed (*47*).

The Faraday-law signal level from a heteronucleus is not as large as that from an equally polarized proton by a factor of $\left(\gamma_S/\gamma_H\right)^2$. When the heteronucleus is being used in an MRI application, larger gradients by a factor of γ_H/γ_S must be used in order to acquire the same spatial resolution as with protons. On the other hand, protons

generally have much shorter lifetimes than heteronuclei, allowing the polarization to decay away before the molecule can be placed in a useful molecular environment. With these limitations in mind, it has been shown that the long-lived nucleus can be used for storing the polarization while a molecule is transported to the location where it reacts. When the experiment is ready to be performed, the polarization can be moved to the more sensitive protons (*48*). Further work has been done to improve this method in the complicated spin systems of interest here using selective recoupling of a subset of the scalar couplings to direct the polarization as desired (*49*).

D. Overview of thesis sections

Section II is used to set up some of the mathematical tools required to understand the later sections. First, parahydrogen is described in detail illustrating the scalar order it contains and its origin in rotational energy splittings. Next, the early PASADENA experiments are briefly reviewed, demonstrating the quantification of this spin order with spin density operator methods. After that, a "time suspension" prescription for preserving the order during chemical reaction is described. Finally, the theoretical methods needed for the specific problem at hand, polarizing a third target heteronucleus, are introduced.

Section III describes the methods for efficiently using parahydrogen as a source of order to generate very large polarizations that are referred to as hyperpolarization. The prior art method of efficient order transfer from parahydrogen to a target nucleus

that results in theoretical polarization $P = 1$ for a small class of molecules is described in detail and its effective range of applicability to molecules is increased by modifications to the algorithm for choosing pulse timing. Then two further methods are developed to address molecules that are not well addressed by the existing method. These entail novel uses of coherent averaging to effectively change the average spin Hamiltonian. Finally, a comparison is made of the various algorithms.

Section IV describes the hardware and software used to implement these methods. Calibration procedures are illustrated. Drawbacks to this particular hardware are shown, particularly difficulties using pulsed techniques in a low field, where the usual multiply rotating frame approximation fails. Solutions that address these problems are discussed.

Theoretical calculations are used throughout in order to support and illustrate the points made. These calculations are performed with GAMMA (*50*), a library of NMR functions written in C++ to facilitate modeling of NMR systems to varying degrees of exactness. The calculations performed here are either ideal or lab frame calculations. Ideal calculations make use of certain simplifications such as the rotating frame approximation and ideal pulses. Lab frame calculations more closely model the systems in question using audio frequency pulses with real shapes and this work introduces such exact techniques to the GAMMA environment. Relaxation effects are discussed qualitatively to motivate experimental design.

II. Background

A. Parahydrogen

Molecular hydrogen is a diatomic gas at standard temperature and pressure. Hydrogen is found in two stable isotopes of which ^{1}H is vastly more common. The ^{1}H nucleus is a spin ½ particle, so the symmetrization postulate demands that the overall wavefunction must be antisymmetric with respect to interchange of particle labels. This nuclear wavefunction is a product of translational, vibrational, rotational, and spin functions.

$$\psi\left(\mathbf{R}, r, \theta, \phi\right) = \psi_t\left(\mathbf{R}\right)\psi_v\left(r\right)\psi_r\left(\theta, \phi\right)\psi_s \tag{2}$$

The translational portion of the function depends only on the location $\mathbf{R}$ of the center of mass, so is unchanged by exchange of particles and is necessarily symmetric in nature. The vibrational portion may be approximated by the eigenfunctions of the linear harmonic oscillator for sufficiently small vibrations. These are only dependent upon the change of the magnitude of r, the distance between the nuclei, so are likewise unchanged by the exchange of particles. Since these are both symmetric, the antisymmetric nature of the overall wavefunction must come from either the rotational or spin functions.

The rotational portion of the wavefunction is characterized by the eigenfunctions of the rigid rotor. These are given by the spherical harmonics

$$\psi_r(\theta,\phi) \propto e^{im\phi} P_l^{|m|}(\cos\theta) \tag{3}$$

where l and m are the quantum numbers corresponding to the total angular momentum and its projection along an axis defined by $\theta = 0$ and $P_l^m(u) = \sqrt{(1-u^2)^m}\,\frac{d^m}{du^m} P_l(u)$ where $P_l(u)$ are the Legendre polynomials. The exchange of particle indices is equivalent to changing $\theta \to (\pi - \theta)$ and $\phi \to (\phi + \pi)$. Under this change, all ψ_r with even l are symmetric and all ψ_r with odd l are antisymmetric with respect to exchange.

The spin portion of the wavefunction is made up of linear combinations of the direct product basis states. The required linear combinations are eigenfunctions of the total angular momentum I of the system which can be 1 or 0. There are $2I+1=3$ states for $I=1$ which comprise a triplet that is symmetric with exchange and 1 state with $I=0$, a singlet that is antisymmetric with exchange:

$$\begin{aligned} |\psi_s\rangle_T &= \begin{cases} |\alpha\alpha\rangle \\ \frac{1}{\sqrt{2}}\left(|\alpha\beta\rangle + |\beta\alpha\rangle\right) \\ |\beta\beta\rangle \end{cases} \\ |\psi_s\rangle_S &= \tfrac{1}{\sqrt{2}}\left(|\alpha\beta\rangle - |\beta\alpha\rangle\right) \end{aligned} . \tag{4}$$

To achieve the overall antisymmetry of the system, physical states with odd l must be in any one of the triplet states while states with even l only exist in the singlet state.

The lowest energy state of the system is the one where $l=0$ and the system is in the spin singlet state. This correlation of rotational and spin states allows a method

of generating a sample of hydrogen in a pure spin state by bringing it to equilibrium at a sufficiently low temperature. In practice, a catalyst is required to allow mixing of the spin states sufficiently to bring a sample to equilibrium in a reasonable time. For our experiments, hydrogen gas was flowed over an iron oxide catalyst at roughly 18 K in order to get 97% or better purity. This would be sufficient to generate nearly pure parahydrogen if it was brought fully to equilibrium at this temperature (Fig. 4). Once the gas is removed from the catalyst, it may be warmed to room temperature and stored for up to a week while maintaining high spin purity.

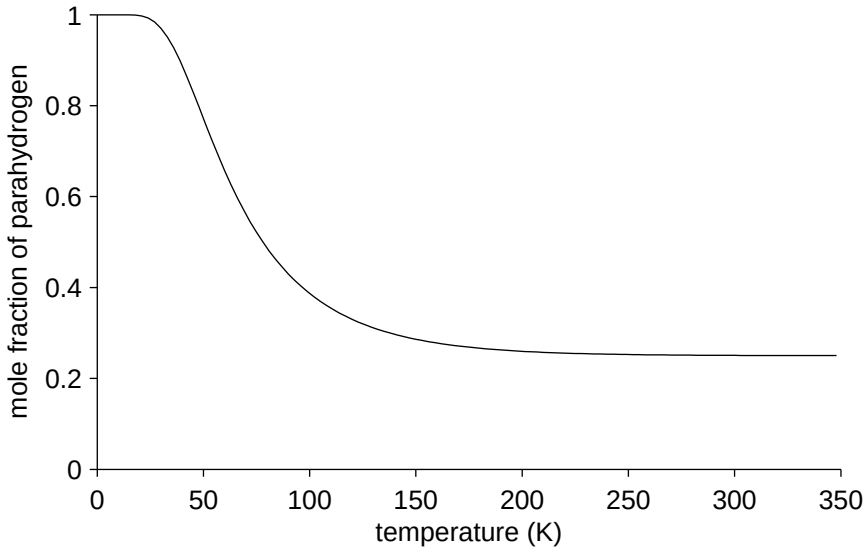

Figure 4. The mole fraction of parahydrogen in a hydrogen sample as a function of temperature.

B. PASADENA

The technique of PASADENA utilizes the spin order found in parahydrogen to generate strong NMR signals from specific magnetic spins in the molecule. By itself,

parahydrogen is invisible to NMR since the overall spin of the system is 0. In order to generate signal from this system, the symmetry must be broken in some way. This is achieved by chemical synthesis of a molecule of interest by adding the parahydrogen molecule across a double or triple bond in a manner that preserves the spin state of the two protons.

It has been found (*24,38,40*) that Wilkinson's catalyst (*51*) and similar cationic Rh complexes that add hydrogen molecularly such that both nascent protons are on the same side of a double or triple bonds also preserves the spin order of the protons. This need for a molecular addition hydrogenation reaction mechanism sets a limit on the particular molecules that may be studied by the method.

The initial condition of the product spin system is given, using the sudden approximation, as the state of the reactant system. For the spins that come from the hydrogen molecule, this initial state is given by the density operator

$$\rho_H = \frac{1}{4} - \frac{1}{3}\left(4\chi_P - 1\right)\mathbf{I}_1 \cdot \mathbf{I}_2 = \frac{1}{4} - f\,\mathbf{I}_1 \cdot \mathbf{I}_2 \tag{5}$$

where χ_P is the mole fraction of parahydrogen and $\mathbf{I}_i$ is the total spin operator for spin i. This state has been variously described interchangeably as symmetrization order, scalar order, or singlet order. It is fully characterized by f (Eq. (5)), which has the range $-1/3 \le f \le 1$, the extremes exemplified by pure orthohydrogen and pure parahydrogen, respectively.

The spins that are initially on the precursor molecule are at thermal equilibrium

with the environment so the density operator of spins 3 through N is given by

$$\rho_X = \exp\left(-\frac{\hbar\hat{H}}{kT}\right) \approx \mathbf{1} - \sum_{i=3}^{N} \frac{\hbar\omega_i I_{z,i}}{kT} \tag{6}$$

where ω_i is the frequency of the spin in the applied magnetic field, k is Boltzmann's constant, and T is temperature. The total density operator is the tensor product of these two operators.

$$\rho = \rho_H \otimes \rho_X \tag{7}$$

Once the hydrogen is incorporated into a molecule where the symmetry is broken, the singlet state is no longer an eigenstate of the system but mixes with the triplet state that has 0 projection along the z-axis. For a fluid system of only the two protons from hydrogen, the Hamiltonian is

$$\hat{H} = \omega_1 I_{z1} + \omega_2 I_{z2} + \bar{J}_{12}\mathbf{I}_1 \cdot \mathbf{I}_2 \tag{8}$$

where $\bar{J}_{12} = 2\pi J_{12}$ is the scalar coupling between the protons in radians per second, and the eigenstates are given by

$$\begin{aligned}
|1\rangle &= |\alpha\alpha\rangle \\
|2\rangle &= \cos\left(\tfrac{\kappa}{2}\right)|\alpha\beta\rangle + \sin\left(\tfrac{\kappa}{2}\right)|\beta\alpha\rangle \\
|3\rangle &= -\sin\left(\tfrac{\kappa}{2}\right)|\alpha\beta\rangle + \cos\left(\tfrac{\kappa}{2}\right)|\beta\alpha\rangle \\
|4\rangle &= |\beta\beta\rangle
\end{aligned} \tag{9}$$

where $\tan\kappa = \bar{J}_{12}/(\omega_1 - \omega_2)$. In the above eigenbasis of the Hamiltonian, the density operator ρ_H has the matrix representation

$$\rho = \begin{bmatrix} \frac{1-f}{4} & 0 & 0 & 0 \\ 0 & \frac{1+f}{4} - \frac{f}{2}\sin\kappa & \frac{\cos\kappa}{2} & 0 \\ 0 & \frac{\cos\kappa}{2} & \frac{1+f}{4} + \frac{f}{2}\sin\kappa & 0 \\ 0 & 0 & 0 & \frac{1-f}{4} \end{bmatrix}. \quad (10)$$

The off-diagonal coherences are lost if the spread of reaction times is long compared to the period of the coherence unless a method to suspend evolution is used. When this system is subjected to the pulse sequence $\tau_w - \frac{\pi}{4}$, a signal with antiphase doublet peaks separated by $\overline{J}_{12}$ is seen at each chemical shift.

This signal has been used directly as a sensitive probe of protons in low population and short lived species such as in catalytic systems (*24,25,52,53*).

C. Order Preservation

Each molecule is formed in a coherent superposition of the eigenstates of the spin Hamiltonian, and so is evolving in time starting from the creation of the molecule from precursor and parahydrogen. The spread of reaction times necessarily averages the ensemble density operator over time, however, dissipating that part of the ensemble spin order which corresponds to these time dependent terms in the density operator. In order to fully utilize this order, it would be necessary that the reaction happen in a time scale short compared to the coherence period, which is $2\pi \Big/ \sqrt{\overline{J}_{12}^2 + \left(\omega_1 - \omega_2\right)^2}$ (*23,25*). For typical values of these spin Hamiltonian parameters, this requires that the reaction be completed in a small fraction of a second. This

requirement is impractically severe for known reactions.

In the proposal of a related parahydrogen experiment, in which optical detection of f substitutes for NMR detection of P (*27,28*), it was pointed out that a train of π pulses delivered during reactions, in this case during an initial adsorption or hydrogenation and a final desorption or dehydrogenation, would serve to preserve the spin order during those periods. For the two spin case (*23*), this "time suspension" of the spins, while the chemical reaction product accumulates, increases the attainable polarization P by a factor of two, enabling $P = f$, ideally. Although the protons are on the catalyst for a much shorter time than on the molecule, this "time suspension" is also important at these times to prevent mixing on the catalyst.

Carravetta *et al*. (*29,32*) have demonstrated in a separate experiment that when the scalar order, created in this case from ordinary polarization, is preserved by decoupling, such as a π train, the lifetime of that state is under some circumstances greatly extended beyond the lattice relaxation time T_1, typically thought of as the longest time constant for NMR processes. The singlet character of the effective eigenstate protects the population from relaxation due to fluctuations of interactions that are symmetric with respect to exchange of the two hydrogen spin labels. Notably, this includes the intrapair dipolar coupling, which is time dependent in solution due to molecular tumbling and frequently an important source of spin relaxation.

Taken together, the time suspension aspect and the decreased spin-lattice

relaxation allow for reaction times of some seconds while preserving the scalar spin order. Evolution under the Hamiltonian in Eq. (8) then starts at the cessation of the proton decoupling instead of the moment of product formation. Thus, decoupling allows all of the order from the parahydrogen to be accessible to the experimenter within a new molecule.

D. Three Spin System

The system of interest (Fig. 5) for heteronuclear PASADENA consists of three spins: the protons derived from addition of parahydrogen $\mathbf{I}_1$ and $\mathbf{I}_2$, which are the source of spin order in the system, and a relatively insensitive spin ½ nucleus $\mathbf{S}$ which is the target for spin order. Transferring spin order to the $\mathbf{S}$ spin has many advantages that include its longer spin lattice relaxation time, lower background signal from unpolarized molecules in a mixture, and the greater chemical specificity of the NMR spectrum. For the initial discussion, other spins in the molecule will be assumed to be noninteracting.

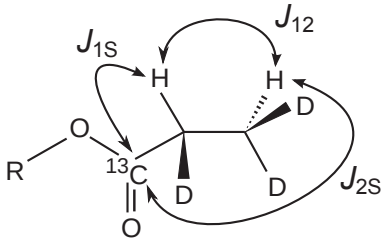

Figure 5. The 3-spin system with the homonuclear and heteronuclear coupling constants defined on a representative molecule.

Immediately following the addition of parahydrogen to a precursor molecule, the spin state of the nascent protons is unchanged, therefore the initial condition is

$$\rho_i = \rho_H \otimes \rho_X \approx \tfrac{f}{8}\left(1 - \mathbf{I}_1 \cdot \mathbf{I}_2\right) \tag{11}$$

and the rotating frame Hamiltonian for this fluid system in a static field is

$$\hat{H} = \omega_S S_z + \omega_1 I_{z1} + \omega_2 I_{z2} + \overline{J}_{12}\mathbf{I}_1 \cdot \mathbf{I}_2 + \overline{J}_{1S}\mathbf{I}_1 \cdot \mathbf{S} + \overline{J}_{2S}\mathbf{I}_2 \cdot \mathbf{S} \tag{12}$$

where $\overline{J}_{ij}$ are the scalar coupling constants between spins in rad/s. The desired evolution of the system is entirely mediated by the scalar coupling in the system so can be made nearly invariant to the applied static field so long as it is high enough to separate Larmor frequencies allowing selective excitation of the different isotopes. The field used in experiments is 1.8 mT, corresponding to a proton frequency of 75 kHz and carbon frequency of 19 kHz, which is sufficiently low that the chemical shift difference of the protons may be neglected but high enough to neglect the flip-flop coupling terms between heteronuclei. Thus the Hamiltonian in the doubly rotating frame may be simplified to

$$\hat{H} = \overline{J}_{12}\mathbf{I}_1 \cdot \mathbf{I}_2 + \overline{J}_{1S} I_{z1} S_z + \overline{J}_{2S} I_{z2} S_z . \tag{13}$$

For the discussion, it is useful to represent the protons with the pseudo-spin $\mathbf{K}$, defined as

$$\begin{aligned} K_x &= I_{1x} I_{2x} + I_{1y} I_{2y} \\ K_y &= I_{1y} I_{2x} - I_{1x} I_{2y} \\ K_z &= \tfrac{1}{2}\left(I_{1z} - I_{2z}\right) \end{aligned} \tag{14}$$

where $\overline{J}_{\Delta} = \left(\overline{J}_{1S} - \overline{J}_{2S}\right)/2$. This pseudo-spin has the commutation relations of an angular momentum spin operator. In this system, the initial condition, with f set to 1, and Hamiltonian may be written as

$$\rho_i = \tfrac{1}{8}\left(1 - 4K_x - 4I_{1z}I_{2z}\right) \tag{15}$$

$$\hat{H} = \overline{J}_{12}K_x + \overline{J}_{\Delta}2K_zS_z + \overline{J}_{+}\left(I_{1z} + I_{2z}\right)S_z + \overline{J}_{12}I_{1z}I_{2z} \tag{16}$$

where $\overline{J}_{+} = \left(\overline{J}_{1S} + \overline{J}_{2S}\right)/2$. Of the three terms in the initial state, only the second term evolves under this Hamiltonian. Of the four terms in the Hamiltonian, only the first two lead to important evolution. The third and fourth terms in the Hamiltonian commute with the other terms and with the initial density operator so are not considered further.

The spin order that is important for evolution under this Hamiltonian is in the off diagonal elements represented by K_x. It is therefore important that some method of order preservation be applied to this system. Unlike the Hamiltonian in Eq. (8), the symmetry breaking element is scalar coupling to a third nucleus rather than a difference in chemical shift. Time suspension pulses, operationally the same as proton decoupling, suffice during the reaction period in order to preserve the product molecules in the singlet state so that all product molecules start evolving under the Hamiltonian at the same time.

This time suspension additionally has the fortuitous side effect that the singlet spin state on the protons has a much longer lifetime than that associated with ordinary Zeeman magnetization (*32*). The polarization on protons typically decays on time scales

on the order of a second while the order of the singlet state may decay on time scales on the order of tens of seconds. This allows for longer reaction times without significant loss of order.

The individual molecular systems are well categorized based upon the value of

$$\theta = \tan^{-1}\left|\bar{J}_{12}/\bar{J}_{\Delta}\right| \tag{17}$$

which ranges on the interval $0 < \theta < \pi/2$. An algorithm for systems with $\theta = \pi/4$ has been developed by Goldman *et al*. (*34,35*). This algorithm will be discussed in detail. Then a method of extending the effectiveness of the algorithm will be discussed and two new algorithms will be added so that there is an appropriate algorithm for the hyperpolarization of a heteronucleus in any molecular system made up of the requisite three spins with spectrally resolved J-couplings.

III. Pulse sequence algorithms

The goal is to find pulse sequences by which the spin system can be manipulated from singlet order into Zeeman polarization in a time short compared to the irreversible dephasing. Qualitatively, one might expect that if the three scalar couplings are well resolved this might be practical. The effective strategy turns out to depend nontrivially on the ratio of coupling through the parameter θ (Eq. (17)). An established method exists for systems where $\theta \approx \pi/4$, the medium range. As θ nears the extremes of 0 and $\pi/2$, this evolution under the initial Hamiltonian is no longer advantageous leading to inefficiencies ($P \ll f$) or pulse sequences that are too long. To better address these cases, new algorithms are introduced that use pulses on the system to effectively change the average Hamiltonian by turning off parts of the Hamiltonian in Eq. (16) during one or more evolution periods are developed. These new algorithms share a basic structure with the original algorithm and understanding it is helpful to understanding them, so the existing algorithm will be described in detail as well.

A. Medium range pulse sequence algorithm

The medium range is characterized by $\theta \approx \pi/4$. Goldman *et al.* (*34,35*) developed an efficient pulse sequence algorithm designed specifically for the $\theta = \pi/4$ case. This sequence is less effective as θ diverges from that value. Extra pulses, either before or after the algorithm, increase the efficiency so that, in principle, any molecule

may be polarized to near unity with this algorithm. However, the pulse sequences become very long, so as a practical matter, those molecules that diverge greatly from the optimal value of θ are not effectively addressed.

1. Algorithm for $\theta = \pi/4$

The algorithm, based on the pulse sequence shown in Fig. 6, utilizes the relevant intrinsic Hamiltonian, which is given by

$$\hat{H} = \overline{J}_{12} K_x + \overline{J}_{\Delta} 2K_z S_z \tag{18}$$

after removing those pieces of Eq. (16) that are not important as described previously, throughout the generated sequence to efficiently develop Zeeman polarization from the initial singlet order. Under this Hamiltonian, the evolution of the pseudo-spin $\mathbf{K}$ is to precess in the operator space defined by $\left(K_x, 2K_y S_z, 2K_z S_z\right)$ around a field in the direction $\zeta = \overline{J}_{12}\hat{\mathbf{x}} + \overline{J}_{\Delta}\hat{\mathbf{z}}$ with characteristic angular frequency $\overline{J}_K = \sqrt{\overline{J}_{12}^2 + \overline{J}_{\Delta}^2}$ (Fig. 7).

The evolving portion of the initial state, $\rho_i = -K_x/2$, evolves under the intrinsic Hamiltonian as

$$\begin{aligned} K_x \rightarrow & \left[\sin^2\theta + \cos^2\theta \cos\left(\overline{J}_K t\right)\right] K_x \\ & + \cos\theta \sin\left(\overline{J}_K t\right)\left(2K_y S_z\right) + \sin\theta\cos\theta\left[1 - \cos\left(\overline{J}_K t\right)\right]\left(2K_z S_z\right) \end{aligned} . \tag{19}$$

Application of a $\pi/2_y$ pulse on $\mathbf{S}$ generates antiphase transverse order on the heteronucleus. Specifically, the new states $2K_z S_x$ and $2K_y S_x$ are created while anything left in K_x will continue as before. Under the intrinsic Hamiltonian, the

evolution of each of these two new states is described by

$$2K_yS_x \to \tfrac{1}{2}\sin\theta\cos\theta\left[1-\cos\left(\bar{J}_Kt\right)\right]\left(S_y-4I_{1z}I_{2z}S_y\right) + \left[\cos^2\theta+\sin^2\theta\cos\left(\bar{J}_Kt\right)\right]\left(2K_yS_x\right)+\sin\theta\sin\left(\bar{J}_Kt\right)\left(2K_zS_x\right) \tag{20}$$

$$2K_zS_x \to \tfrac{1}{2}\cos\theta\sin\left(\bar{J}_Kt\right)\left(S_y-4I_{1z}I_{2z}S_y\right)-\sin\theta\sin\left(\bar{J}_Kt\right)\left(2K_yS_x\right) + \cos\left(\bar{J}_Kt\right)\left(2K_zS_x\right). \tag{21}$$

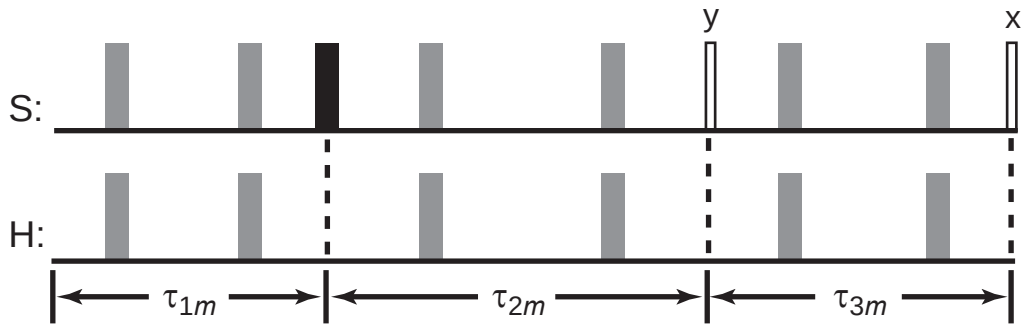

Figure 6. Schematic of the medium θ pulse sequence algorithm. The main pulses of the algorithm are shown in black and recommended echo pulses are shown in grey. Solid pulses are π and open pulses are $\pi/2$. The echo pulses occur at $1/4$ and $3/4$ on the time of each wait period.

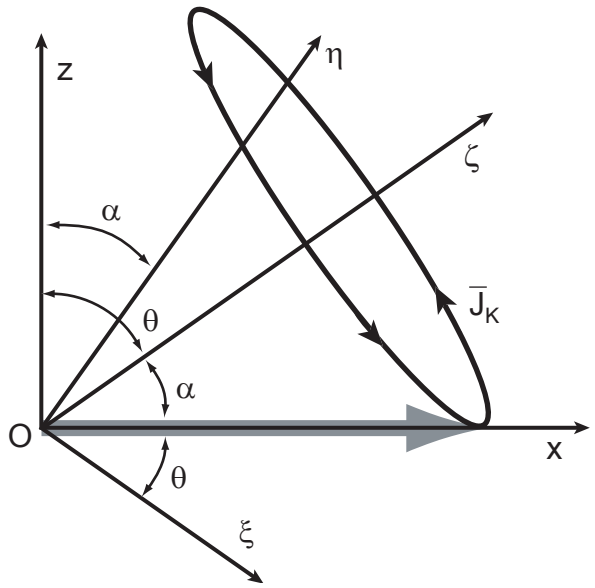

Figure 7. Coordinates for graphically describing the evolution of K_x under the intrinsic Hamiltonian.

When $\theta \geq \pi/4$, the most advantageous evolution is from the state $2K_yS_x$ which takes advantage of relation (20) to generate Zeeman order on $\mathbf{S}$. The algorithm is designed to pass the system through this exact state. Briefly, hydrogen decoupling for time suspension during the reaction is followed by τ_{1m} - π - τ_{2m} - $(\pi/2)_y$ - τ_{3m} - $(\pi/2)_x$ on $\mathbf{S}$. The first two wait periods τ_{1m} and τ_{2m} of the algorithm are optimized to place the system entirely into the $2K_yS_z$ state. The final wait period τ_{3m} allows transverse polarization to develop which is finally stored along z.

However, when $\theta > \pi/3$, the first two periods are no longer sufficient to reach the state $2K_yS_z$. Further wait periods $\tau_{pre} = \pi/\bar{J}_K$ followed by π pulses executed before the sequence, referred to as prepulses, allow efficient conversion to this state

(*34,35*). The number of prepulses n required is given by

$$n = \left\lceil \theta / \left(\pi - 2\theta \right) \right\rceil - 1 . \tag{22}$$

Under the experimentalist's discretion, "pump" pulses may be applied after the completion of the basic sequence in order to increase the final order. These are further wait periods $\tau_{pump} = \pi / \overline{J}_K$ followed by pulses of varying angles (*34,35*). The wait allows more of the state $\frac{1}{2}\left(S_y - 4 I_{1z} I_{2z} S_y \right)$ to form from the leftover multi-quantum order. Once this forms, the overall polarization $\mathbf{S}$ is no longer in the z direction, so an appropriate small angle pulse is used to put it there. The maximum polarization obtainable by this sequence algorithm as described, including any required prepulses but no pump pulses, is $\sin\left(2\theta\right)$.

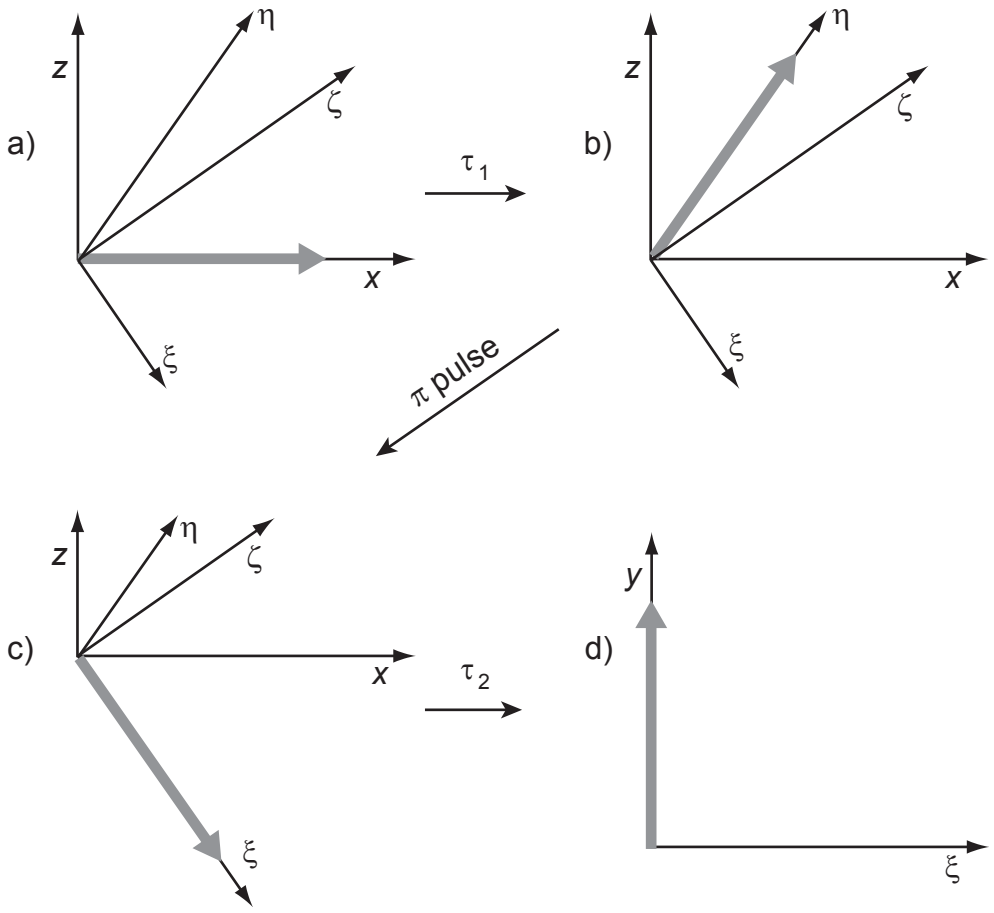

Figure 8. Evolution of the system during the first two wait times. In the space defined by the operators $\left(K_x, 2K_yS_z, 2K_zS_z\right)$, ρ (grey arrow) starts out along x (a) and precesses around ζ. When the projection of ρ onto the xz plane is along η (b), a π pulse is given which causes the projection of ρ onto the xz plane to be along ξ (c), that is ρ is in the ξy plane which is perpendicular to ζ. A second wait brings ρ along y (d). The next pulse moves the system into a different operator space.

The timing required to achieve this was described in terms of the geometric model (Fig 8). The state of ρ is first allowed to precess until its projection in the Oxz plane makes the angle θ with Ox. At this point, the pulse will place ρ in a plane

perpendicular to the fictitious field about which it precesses. It is allowed to continue to precess until it comes parallel with Oy, which corresponds with being entirely in the desired state. This recipe yields the times

$$\begin{aligned}\tau_{1m} &= \arccos\left[\cot(2\theta)\tan(\theta-\phi_\alpha)\right]\Big/\bar{J}_K \\ \tau_{2m} &= \left\{\pi - \arctan\left[\frac{\csc(2\theta)\tan(\theta-\phi_\alpha)}{\sqrt{1-\cot^2(2\theta)\tan^2(\theta-\phi_\alpha)}}\right]\right\}\Big/\bar{J}_K \\ \tau_{3m} &= \pi/\bar{J}_K\end{aligned} \tag{23}$$

where $\phi_\alpha = n(\pi - 2\theta)$.

These first two steps are efficient for placing the system entirely into the $2K_yS_z$ state. The final step is only efficient for $\theta = \pi/4$. All other cases lead to losses of order into undesired states. If these losses can be removed over some range, the algorithm will be more effective.

2. Modifications for a larger range

The cases in which $\theta = \pi/4$ are very few. Most likely, the actual value will be larger or smaller than this ideal value. Looking again at relations (20) and (21), it can be seen that in the cases when $\theta < \pi/4$, the most advantageous evolution during τ_{3m} is from a linear combination of the two states present during τ_{1m} and τ_{2m} rather than one or the other. The optimal linear combination for ρ after the second pulse in the algorithm that leads to perfect conversion is

$$\rho = \tan\theta\left(2K_yS_x\right) + \sqrt{1-\tan^2\theta}\left(2K_zS_x\right). \tag{24}$$

Variation of the timing of the sequence from that first prescribed by the algorithm above suffices to allow the creation of this state and leads to theoretically perfect conversion of the singlet spin order to Zeeman polarization for a much larger range of molecules. For the region where $\arctan\left(1/\sqrt{2}\right) < \theta < \pi/4$, the optimal wait times are given by

$$\begin{aligned}
\tau_{1m} &= \text{arc}^{-1}\left[\tfrac{1}{4}\csc\theta\sec^2\theta\left(2\sqrt{\cos(2\theta)} - \sin\theta + \sin(3\theta)\right)\right]\Big/\bar{J}_K \\
\tau_{2m} &= \text{arc}^{-1}\left[\frac{\csc\theta\sec^2\theta}{-8\sqrt{\cos(2\theta)}}\left(\begin{array}{l}2\cos(2\theta) + 2\cos^{\frac{5}{2}}(2\theta)\csc\theta + \\ \csc\theta\sqrt{-\left(\begin{array}{l}1+\cos(2\theta)+\cos(4\theta)+ \\ \cos(6\theta)+8\cos^{\frac{5}{2}}(2\theta)\sin\theta\end{array}\right)}\end{array}\right)\right]\Big/\bar{J}_K \\
\tau_{3m} &= \text{arc}^{-1}\left[-\tan^2\theta\right]\Big/\bar{J}_K
\end{aligned} \tag{25}$$

and on the region where $\theta \le \arctan\left(1/\sqrt{2}\right)$, the optimal times are given by

$$\begin{aligned}
\tau_{1m} &= \text{arc}^{-1}\left[\tfrac{1}{4}\csc\theta\sec^2\theta\left(-2\sqrt{\cos(2\theta)} - \sin\theta + \sin(3\theta)\right)\right]\Big/\bar{J}_K \\
\tau_{2m} &= \text{arc}^{-1}\left[\frac{\csc\theta}{8\sqrt{\cos(2\theta)}}\left(\begin{array}{l}2 - 2\cos^{\frac{5}{2}}(2\theta)\csc\theta\sec^2\theta - 2\tan^2\theta + \\ \csc^3\theta\tan^2\theta\sqrt{-\left(\begin{array}{l}1+\cos(2\theta)+\cos(4\theta)+ \\ \cos(6\theta)-8\cos^{\frac{5}{2}}(2\theta)\sin\theta\end{array}\right)}\end{array}\right)\right]\Big/\bar{J}_K \\
\tau_{3m} &= \text{arc}^{-1}\left[-\tan^2\theta\right]\Big/\bar{J}_K .
\end{aligned} \tag{26}$$

When the quantity under the square root for finding τ_{2m} becomes negative, when $\theta \approx 0.3532$ rad, it is no longer possible to place the system into the desired state. When using prepulses, but no pump pulses, the polarization achievable is shown for all θ in Fig. 9.

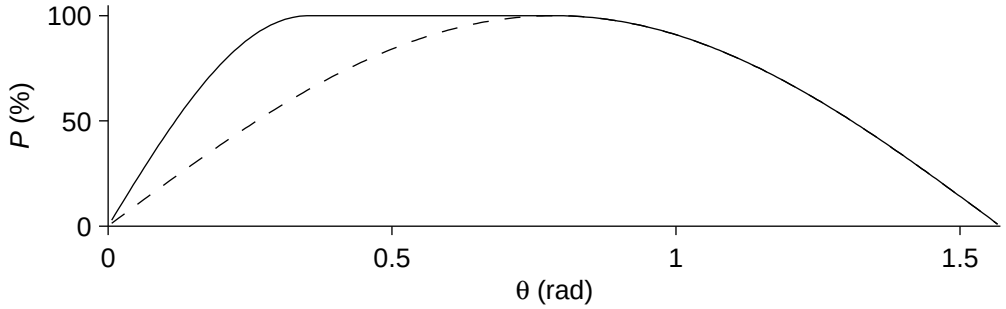

Figure 9. The resultant polarization achieved by the medium θ sequence algorithm (solid line) and original algorithm by Goldman *et al*. (dashed line) over the range of possible θ. This uses ideal calculations.

3. Operation in real systems

It is often not possible to completely isolate the spin system of a molecule of interest from all other spins. Such common atoms as hydrogen have no isotopes without spin and others would be prohibitively expensive to replace with a spin 0 isotope. Rather than completely isolate the desired three spin system, steps must be taken to mitigate the effects of spectator spins in the system. All hydrogen that may couple to the system of interest on the precursor molecule needs to be replaced by deuterium. When spectator protons are replaced with deuterons, the coupling between the spins is weakened by a factor of approximately six and, more importantly, pulses can be applied to these spins separately from protons. This allows decoupling of these undesirable spins from the system by echo pulses on protons or heteronuclear decoupling. Spins with the same isotopic identity as the target isotope that couple with the desired system must also be replaced.

The interference from spectator spins is likely to still be too great in most systems where it is needed even with the reduction in coupling strength by using deuterons for protons. To further reduce the effects of these spectator spins, echo pulses need to be added to the sequence in such a way that the overall average Hamiltonian remains unchanged from that of the three spin system. This is done simply by applying the π pulses to both protons and target nuclei. Even without spectator spins, one set is useful to refocus the chemical shift terms. With the spectator spins, a symmetric set is much more effective for refocusing of the effects of heteronuclear scalar couplings to the spectator spins, as described by Goldman et al. (*34,35*). Thus, in order to mitigate the effects of these spins reasonably well, each wait period τ in the sequence must have π pulses on both the protons and the target nucleus at times given by $\tau/4$ and $3\tau/4$ during the period. Having two pulses also allows phase cycling, which can help reduce problems due to misset pulses.

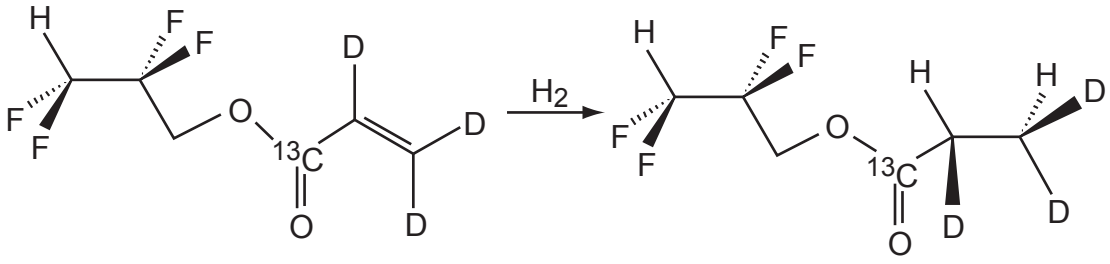

Figure 10. The molecule 2,2,3,3-tetrafluoropropyl 1-^{13}C-propionate-d_3 is derived from 2,2,3,3-tetrafluoropropyl 1-^{13}C-acrylate-d_3. It is vital to deuterate the acrylate portion of the molecule and may be important to deuterate the closer protons on the tetrafluoropropyl portion which have some small coupling with the labeled carbon.

Since the sequences are performed in a low field, some care must be taken when using molecules with spectator isotopes that have Larmor frequencies sufficiently similar to that of the protons or the target spin. As an example, the molecule TFPP in Fig. 10 was found to have some small coupling between the target ^{13}C and the protons across the ether oxygen when refocused INEPT was performed on the hyperpolarized molecule (*48*). In this molecule, the proton spectrum showed significant polarization on both added protons as well as the two nearest protons from the precursor. For a molecule with the parameters of the three spin system of TFPP, the polarization obtained on ^{13}C is reduced when there is coupling to two extra protons as seen in Fig. 11. This reduction can be mitigated by optimization of the sequence timing, numerically taking into account the entire spin system, but it cannot be completely recovered in this way (Fig 11). The molecule was chosen to have a fluorinated hydrocarbon moiety which is known to bind to lipids, so a first approach to reducing the problem might be to replace these two protons with fluorine. This helps, but since ^{1}H and ^{19}F frequencies are so close in the low field, it also requires much longer pulses than would ordinarily be used, as seen in Fig. 12, where the longest pulses, 187 μs when the proton frequency is 75 kHz, are required when coupling is strong.

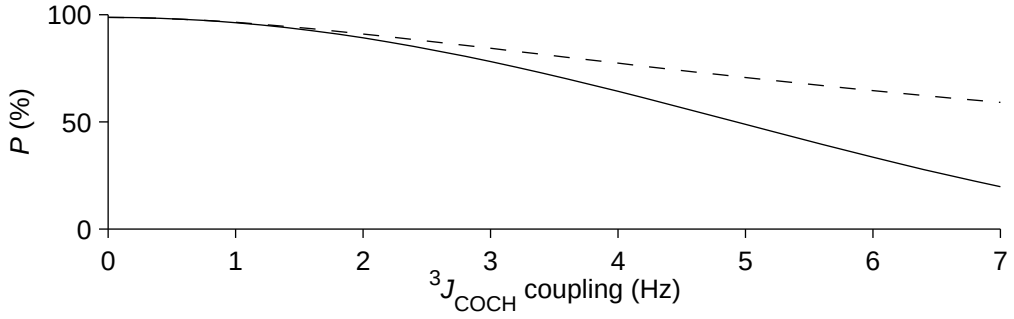

Figure 11. Polarization resulting on the heteronucleus is reduced when spectator spins act on the system. In this example, a molecule with $J_{12} = 7.57$ Hz, $J_{1S} = 7.24$ Hz, and $J_{2S} = -5.62$ Hz has an additional coupling between two identical protons and the ^{13}C target. When the system is polarized with the optimal sequence for the main three spin system, the resulting polarization on ^{13}C is reduced with stronger scalar coupling to the spectators (solid line). This reduction in efficiency may be mitigated by reoptimizing the sequence for the complete five spin system (dashed line) to regain some, but not all, of the polarization. This uses ideal calculations.

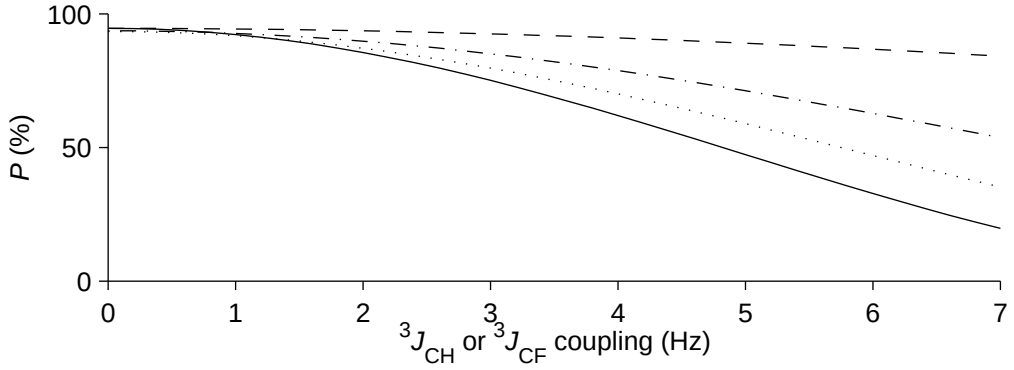

Figure 12. Spectator isotopes affect the resulting polarization on the heteronucleus. In this example, a molecule with $J_{12} = 7.57$ Hz, $J_{1S} = 7.24$ Hz, and $J_{2S} = -5.62$ Hz has an additional coupling to two identical protons (solid line) or two identical ^{19}F spins (broken lines) and the ^{13}C target. In low field, ^{19}F is sufficiently close to ^{1}H in frequency to be affected by the same pulse. This is mitigated by increasing the length of pulses in order to increase their selectivity. In this case, a π pulse with 7 cycles (dotted) is

not as good as a π pulse with 10 cycles (dash-dot), which is not as good as a π pulse with 14 cycles (dashed). They are all improvements over protons with pulses of any of these lengths (14 cycles is shown but all follow the same curve). This uses lab frame calculations.

4. Behavior under experimental error

In order to estimate how well this pulse sequence algorithm will perform in a given situation, it is useful to know how well it continues to perform in the face of common experimental errors. Errors may arise from inaccurate adjustments of the static field strength or its variation due to the movement of objects near the equipment. Other errors include the strength of pulses at the $\mathbf{I}$ or $\mathbf{S}$ Larmor frequencies and errors in determining the scalar couplings in the system.

i. Scalar coupling errors

The pulse sequences derived from the medium θ algorithm are specific to the coupling constants of the given molecule. Experimental error in determining these scalar coupling constants is in principle avoidable, but is common as the first order theory typically used is often insufficient in systems with multiple coupling constants of similar magnitude. Additionally, these couplings are sometimes dependent upon other factors such as solution pH and temperature. In some situations, the proton coupling depends upon the configuration of the precursor molecule.

An example of a molecule that displays many of these complications is 1-^{13}C succinic acid. Both homonuclear and heteronuclear scalar coupling constants of succinic

acid vary very strongly with pH near neutral due to the changing probabilities of conformations as the protonation state of the molecule changes. Two proton-proton coupling constants are found at each pH (*36,54*) in the undeuterated system. In this case, the coupling constants can be made fairly certain by performing the experiment in basic or acidic solution where there is no strong dependence. That we find two different coupling constants between the methylene groups shows that final coupling of the parahydrogen derived protons on C2 and C3 will depend on the choice of maleic acid or fumaric acid as the deuterated alkene precursor molecule since these isomers lead to different succinate isomers after hydrogenation (Fig. 13).

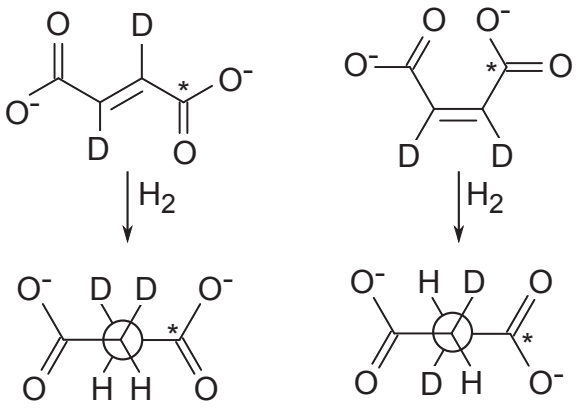

Figure 13. The geometry of the precursor selects which of the two proton-proton coupling constants available in succinate is active after hydrogenation. In conditions where the acid groups stay primarily in the *trans* position, the fumarate precursor (left) is expected to have the smaller coupling constant associated with the *gauche* geometry while the maleate precursor (right) is expected to have the larger coupling constant associated with the *trans* geometry. The location of the ^{13}C is marked with a star.

Once the appropriate scalar coupling constants have been found to some degree

of certainty, the pulse sequence can be generated. The expectation of how well a certain sequence will perform varies over the range of θ over which the algorithm is expected to be useful. An example of a molecule with θ near the high end of the medium range is 1-^{13}C-succinic acid at $\mathrm{pH} = 4.31$ with the smaller coupling constant. This molecule has $J_{12} = 6.07$ Hz, $J_{1S} = -6.80$ Hz, and $J_{2S} = 5.47$ Hz (*36*) yielding timing constants of $\tau_{1m} = 26.08$ ms, $\tau_{2m} = 45.32$ ms, and $\tau_{3m} = 54.14$ ms. Should the actual coupling constants vary from those used to generate the sequence, the resulting polarization will not be as high as shown in Fig. 14.

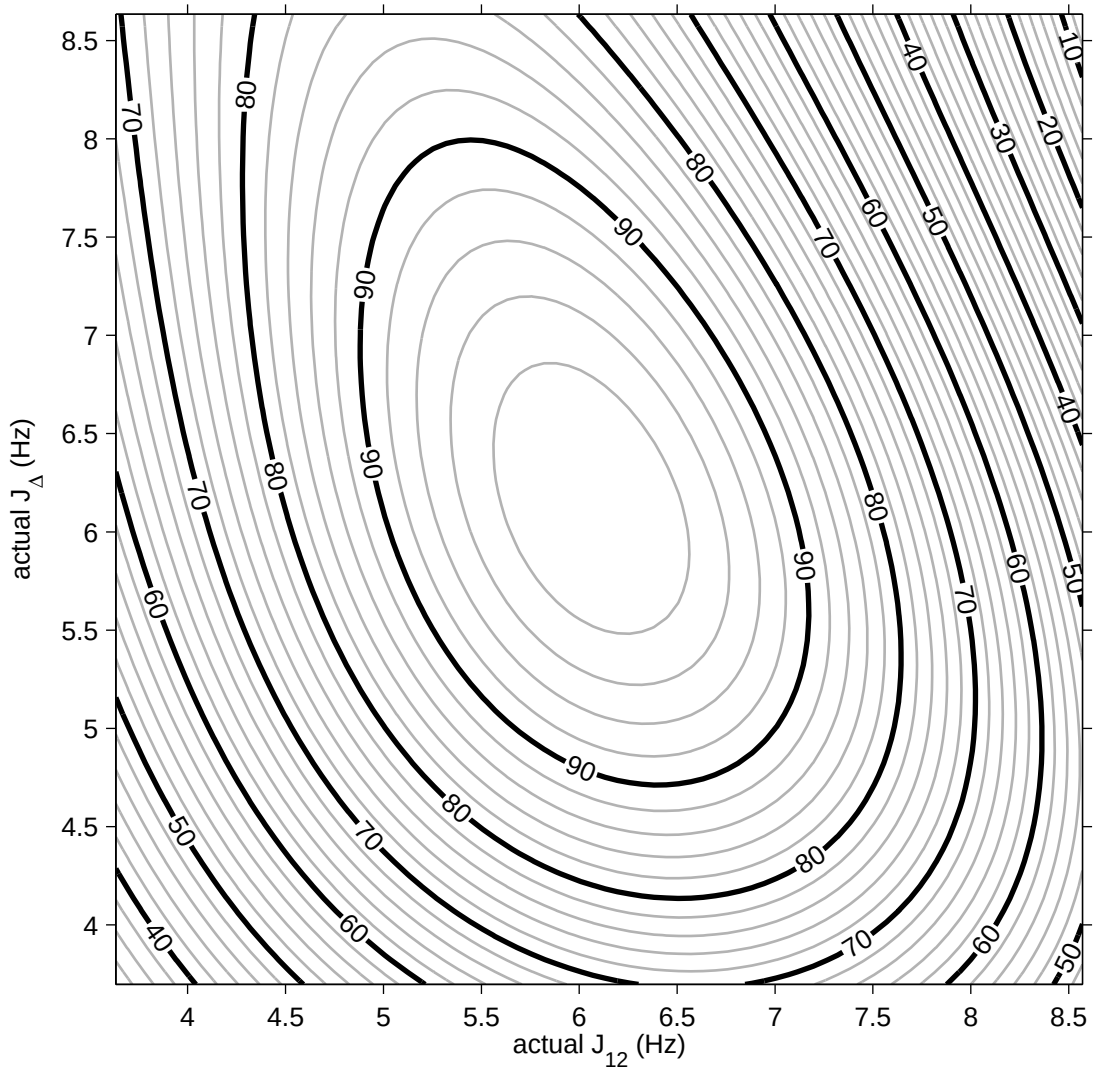

Figure 14. Contour plot of the percent of polarization on the target ^{13}C nucleus generated by the pulse sequence derived for 1-^{13}C-succinic acid at $\mathrm{pH} = 4.31$ over a wide range of similar scalar coupling constants. The major contours are marked for every 10% and the minor contours are every 2%. The pulse sequence generates 100% polarization when the coupling constants are correct. This uses ideal calculations.

An example of a molecule with θ near the small end of the medium range is 1-phenylethylphenylphosphinic acid (Fig. 15) where the target is the phosphorus atom.

This molecule has $J_{12} = 7.4$ Hz, $J_{1S} = (-)18.6$ Hz, and $J_{2S} = 16.8$ Hz (*55*). The specific signs of the constants are not indicated in the reference, but the two bond and three bond heteronuclear couplings were found to generally have opposing signs for the molecules studied. Assuming this is so, the timing required for the sequence to polarize this molecule is $\tau_{1m} = 21.68$ ms, $\tau_{2m} = 10.35$ ms, and $\tau_{3m} = 14.49$ ms. Should the coupling constants be incorrect, the resulting polarization will be reduced as shown in Fig. 16.

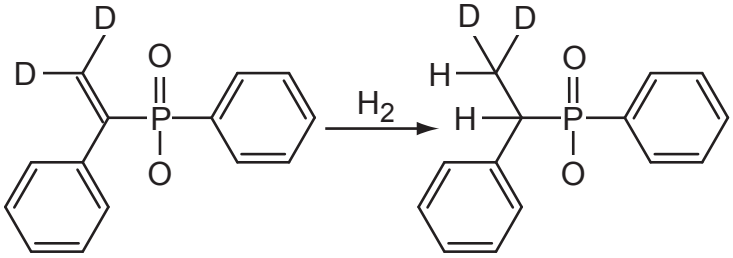

Figure 15. Precursor and product scheme for generation of partly deuterated 1-phenylethylphenylphosphinic acid. It is likely that the benzene rings will also need deuteration in order to decrease coupling to the ^{31}P.

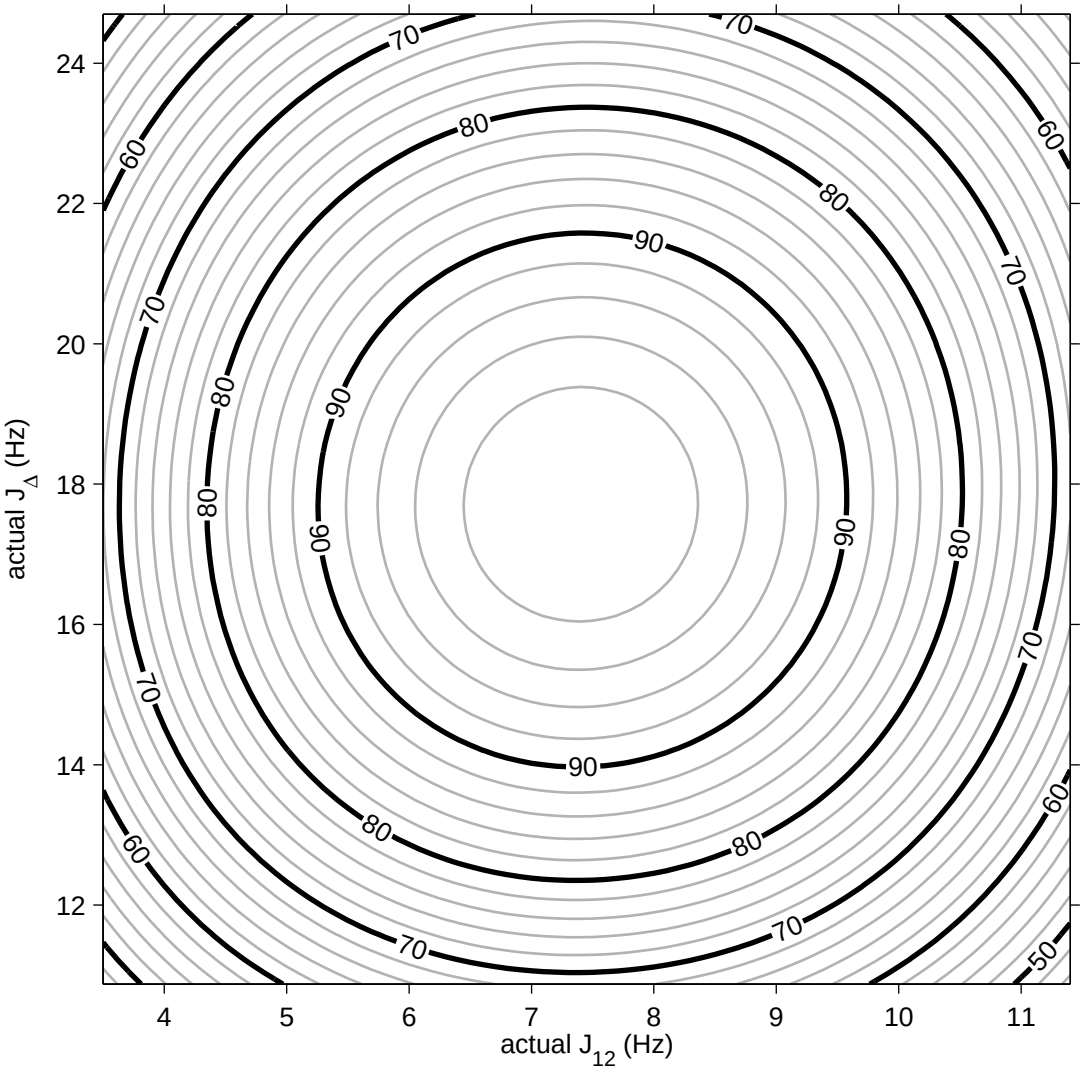

Figure 16. Contour plot of the percent of polarization on the target ^{31}P nucleus generated by the pulse sequence derived for 1-phenylethylphenylphosphinic acid over a wide range of similar scalar coupling constants. The major contours are marked for every 10% and the minor contours are every 2%. The pulse sequence generates 100% polarization when the coupling constants are correct. This uses ideal calculations.

ii. Magnetic field strength and pulse power

The interactions that generate polarization via these pulse sequence algorithms

are not dependent upon the magnetic field strength, however the pulses delivered to the system are tuned to a specific magnetic field. When the strength of the static or oscillating fields is incorrectly set, the pulse sequence is adversely affected reducing the final polarization. The extent of the harm from these effects is highly dependent upon features of the pulse sequence that do not figure in the outcome unless the pulses are not generated correctly. Phase cycling the echo pulses by applying the second around the negative axis of the first for each set of echoes significantly improves the resilience against these sorts of incorrect settings (Fig. 17). The main pulses in the sequence cannot be cycled, but pulse shaping, which is useful for other reasons and simple with the hardware used, is generally useful to decrease the dependence of the nutation angle on these factors as well. This is discussed in section VI.D.

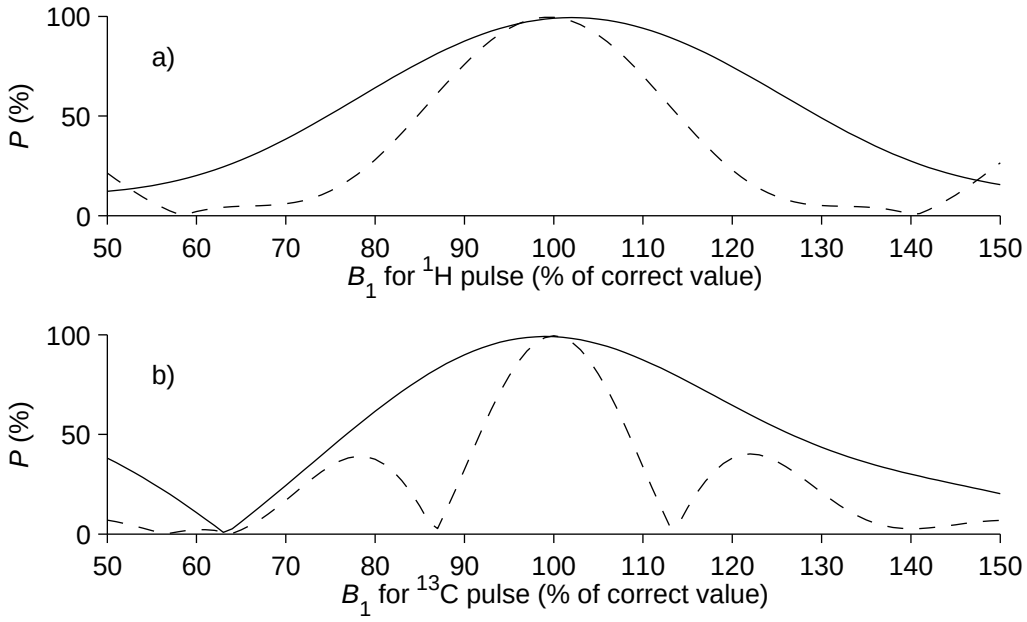

Figure 17. Using simple phase cycling (solid line) with the echo pulses improves the behavior of

the pulse sequences over not doing so (dashed line) with respect to incorrect setting of the pulse power for both a) proton pulses and b) pulses on the target nucleus. This example is a lab frame GAMMA calculation that uses the succinate molecule described in Fig. 14 and the pulse sequence described in the text for that molecule.

B. Small range pulse sequence algorithm

The small range is characterized by $\theta \lesssim 0.3532$, generally due to a large difference in the heteronuclear scalar coupling. Below the lower limit of the medium range algorithm, the effectiveness falls off sharply (Fig. 9). Pump pulses allow the experimentalist to increase the polarization by increasing the time required by the sequence, but cannot perfectly polarize the target. A different algorithm is needed for this range. Molecules with strong two-bond and three-bond heteronuclear coupling to protons, for example those with a ^{31}P target spin, and molecules where the added protons are attached directly to the target have will often fall into this range.

1. Algorithm for the limit $\theta \to 0$

The spin order transfer requires a nonzero value of both $\overline{J}_{12}$ and $\overline{J}_{\Delta}$, but becomes challenging when either one dominates. Looking at relations (20) and (21), it is clear that the most effective evolution for the system during τ_{3s} in the limit $\theta \to 0$ comes from relation (21). In order to take advantage of this, an algorithm that places the system into the intermediate state $2K_zS_x$ at time $\tau_{1s} + \tau_{2s}$ must be found. One way to more easily control the evolution of the states is to be able to turn off one part of the

other of the intrinsic Hamiltonian in Eq. (18). One method to do this is using decoupling applied to the target isotope, which is used for this algorithm. In effect, this temporarily switches the effective Hamiltonian to that of the limit $\theta \to \pi/2$ for the period τ_{2s}. This degree of freedom modifies the strategy. The form of the novel small θ pulse sequence algorithm is shown in Fig. 18.

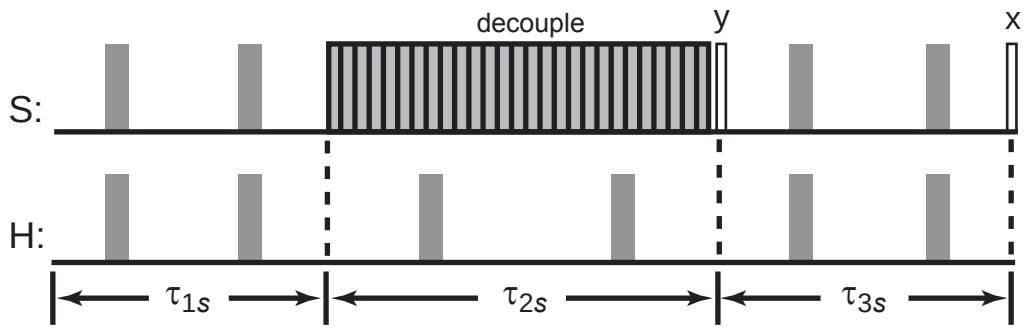

Figure 18. Schematic of the small θ range pulse sequence. The main pulses of the algorithm are dark and recommended echo pulses are light. Solid pulses are π, open pulses are $\pi/2$, and decoupling uses a typical cyclic method that returns the polarization to the starting point, such as MLEV-16.

Briefly, the initial proton decoupling during the reaction is followed by a wait of τ_{1s}, then decoupling is applied to the target for a second wait τ_{2s} until the system is in the desired intermediate state. A $(\pi/2)_y$ mixing pulse on the target after decoupling starts the evolution that develops polarization during the third wait τ_{3s}. A final $(\pi/2)_x$ pulse stores the magnetization along z. The recommended echo scheme (grey pulses) to mitigate the effects of spectator spins is largely unchanged.

In detail, first the system is allowed to evolve from the initial condition under the

intrinsic Hamiltonian until the maximum amount of $2K_yS_z$ and $2K_zS_z$ has developed. This leaves the system in a linear combination of the two states that is generally different from the desired state with no order left in the K_x state. Second, the system is subjected to coherent decoupling on the insensitive target nucleus until the system is in the desired intermediate state. Decoupling effectively changes the Hamiltonian of the system during this period such that the heteronuclear coupling does not operate leading to a new type of evolution. During this time, the average Hamiltonian in the rotating frame is given by

$$\hat{H}_{dec} = \bar{J}_{12}K_x . \tag{27}$$

Under this Hamiltonian, K_x does not evolve but the two states it evolves into interconvert such that

$$2K_yS_z \rightarrow \cos\left(\bar{J}_{12}t\right)\left(2K_yS_z\right) + \sin\left(\bar{J}_{12}t\right)\left(2K_zS_z\right) \tag{28}$$

$$2K_zS_z \rightarrow \sin\left(\bar{J}_{12}t\right)\left(2K_yS_z\right) + \cos\left(\bar{J}_{12}t\right)\left(2K_zS_z\right). \tag{29}$$

This decoupling is left on until the system evolves entirely into the $2K_zS_z$ state. After this evolution, a $\left(\pi/2\right)_y$ pulse on $\mathbf{S}$ is applied to produce the desired intermediate state $2K_zS_x$. Finally, the system is again allowed to evolve under the intrinsic Hamiltonian so that S_y-like polarization develops according to relation (21). A $\pi/2_x$ pulse on $\mathbf{S}$ is applied to store the polarization as Zeeman order when the transverse order is greatest. To follow this recipe exactly, the times are given by

$$\begin{aligned}\tau_{1s} &= \arccos\left[-\tan^2\theta\right]\Big/\bar{J}_K \\ \tau_{2s} &= \arctan\left[\cot\theta\sqrt{1-\tan^2\theta}\right]\Big/\bar{J}_{12} \\ \tau_{3s} &= \pi/2\bar{J}_K\end{aligned} \tag{30}$$

which yields a maximum polarization of $\cos\theta$ for $\theta \le \pi/4$ and $2\sin\theta\cos^2\theta$ for $\theta > \pi/4$ when using the real part of the times.

2. Modifications for a larger range

In order to make this algorithm effective for real systems, it is again useful to observe that the optimal intermediate state for $0 < \theta \le \pi/4$ is the linear combination given in Eq. (24). This sequence is easily modified to generate the correct intermediate state by simply shortening the second wait. The third wait also needs correction to generate the optimal sequence.

The optimal sequence for the range of θ then is to allow evolution from the initial state, after the time suspension, to the state with the minimum amount of K_x. Next, turn on cyclic decoupling on the target nucleus until the state is the optimal state indicated by Eq. (24). Then a $(\pi/2)_y$ mixing pulse triggers evolution generating transverse spin order on the target which is finally stored in z by a final $(\pi/2)_x$ pulse. This sequence is generated using times given by

$$\begin{aligned}\tau_{1s} = \tau_{3s} &= \arccos\left[-\tan^2(\theta)\right]\Big/\bar{J}_K \\ \tau_{2s} &= \arccos\left[2\tan(\theta)\sqrt{1-\tan^2(\theta)}\right]\Big/\bar{J}_{12}\end{aligned} \tag{31}$$

and yields the polarization of 1 for the range $0 < \theta \leq \pi/4$ (Fig. 19).

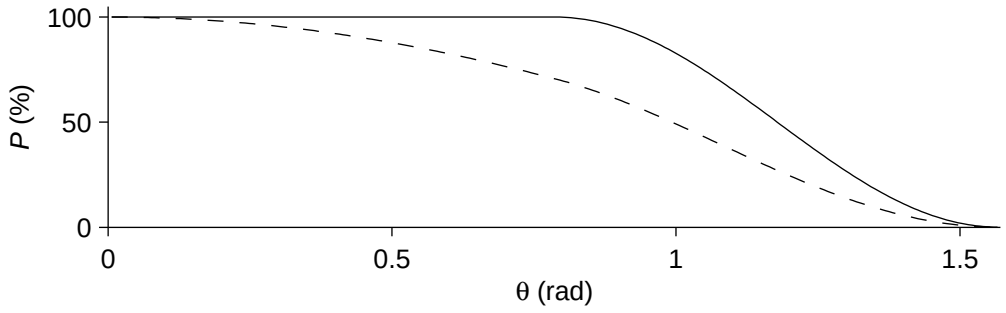

Figure 19. The theoretical polarization possible by application of the small θ sequence algorithm in with the most optimal times (solid) and as it was originally designed (dashed). This uses ideal calculations.

3. Operation in real systems

Similarly to the medium θ case, the spin system must not contain any other isotopes with the same identity as the target or protons for the pulse sequence to operate correctly. This is generally a matter of deuterating the precursor molecule to be used in reaction.

As well, echo pulses are required during the wait periods of the small θ pulse sequence algorithm to refocus what little chemical shift or resonance offset there is and to mitigate the effects of spectator isotopes. For the first and last wait periods, the same approach using two symmetric echoes on both protons and target is most effective. For the second wait period, the problem is simplified by the decoupling applied to the target isotope. In this case, symmetric echoes are only required on the protons.

4. Behavior under experimental error

Just as with the medium θ range sequence algorithm, the required parameters will only be known within some experimental error and magnetic fields are not perfect. It is useful to know how the sequence acts when these common problems occur.

i. Scalar coupling errors

To demonstrate the degree of difficulty poorly known scalar couplings cause for the generation of hyperpolarization using the small θ range pulse sequence algorithm, two molecules are selected as examples of the extremes of the range in which the algorithm would be applied. At the large end of the range, an example molecule is ethylphosphonyl dichloride where the target is ^{31}P. This molecule has $J_{12} = 6 - 8$ Hz, $J_{1S} = 30.0$ Hz, and $J_{2S} = 14.2$ Hz with the relative sign of the heteronuclear coupling constants noted as being opposite (*55*). Taking $J_{12} = 7$ Hz, the sequence generated has $\tau_{1s} = \tau_{3s} = 11.47$ ms and $\tau_{2s} = 21.06$ ms. If the system has parameters similar to these, then this sequence is applied the resulting polarization on ^{31}P can be found in Fig. 20.

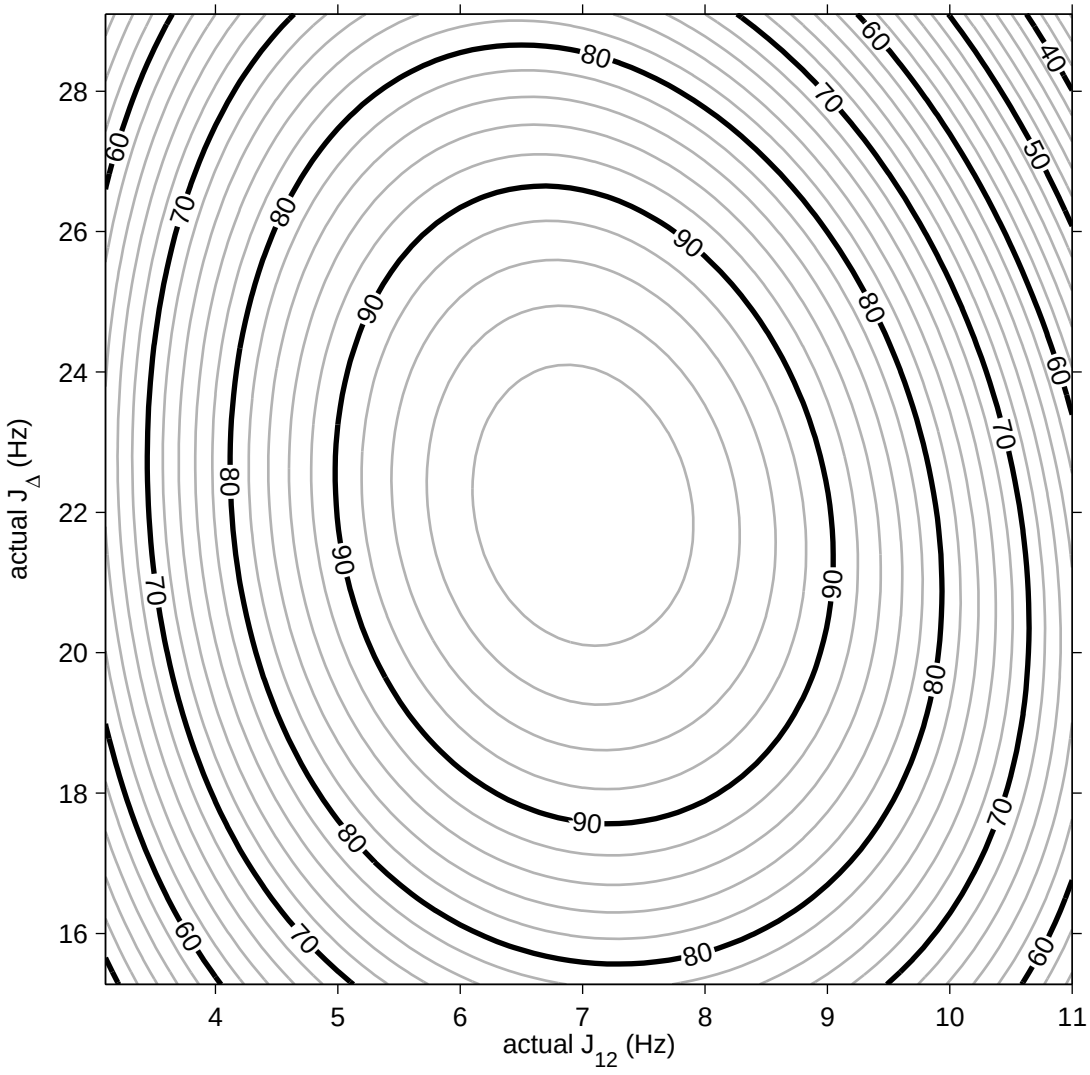

Figure 20. The polarization expected on ^{31}P of ethylphosphonyl dichloride when the pulse sequence derived from the literature scalar coupling constants is delivered to the molecule considering that the actual scalar coupling constants may differ from the literature values. The major contours are marked for every 10% and the minor contours are every 2%. The pulse sequence generates 100% polarization when the coupling constants are correct. This uses ideal calculations.

An example molecule representing the low end of the small θ range is diethyl mercury where ^{199}Hg is the target nucleus. This molecule has $J_{12} = 7.5$ Hz, $J_{1S} = 91$ Hz,

and $J_{2S} = 120$ Hz with no indication of the relative sign of the heteronuclear coupling constants (*56*). Assuming they are opposite, the pulse sequence requires $\tau_{1s} = \tau_{3s} = 2.37$ ms and $\tau_{2s} = 30.31$ ms. Given this sequence, the polarization expected for molecules with similar parameters is show in Fig. 21.

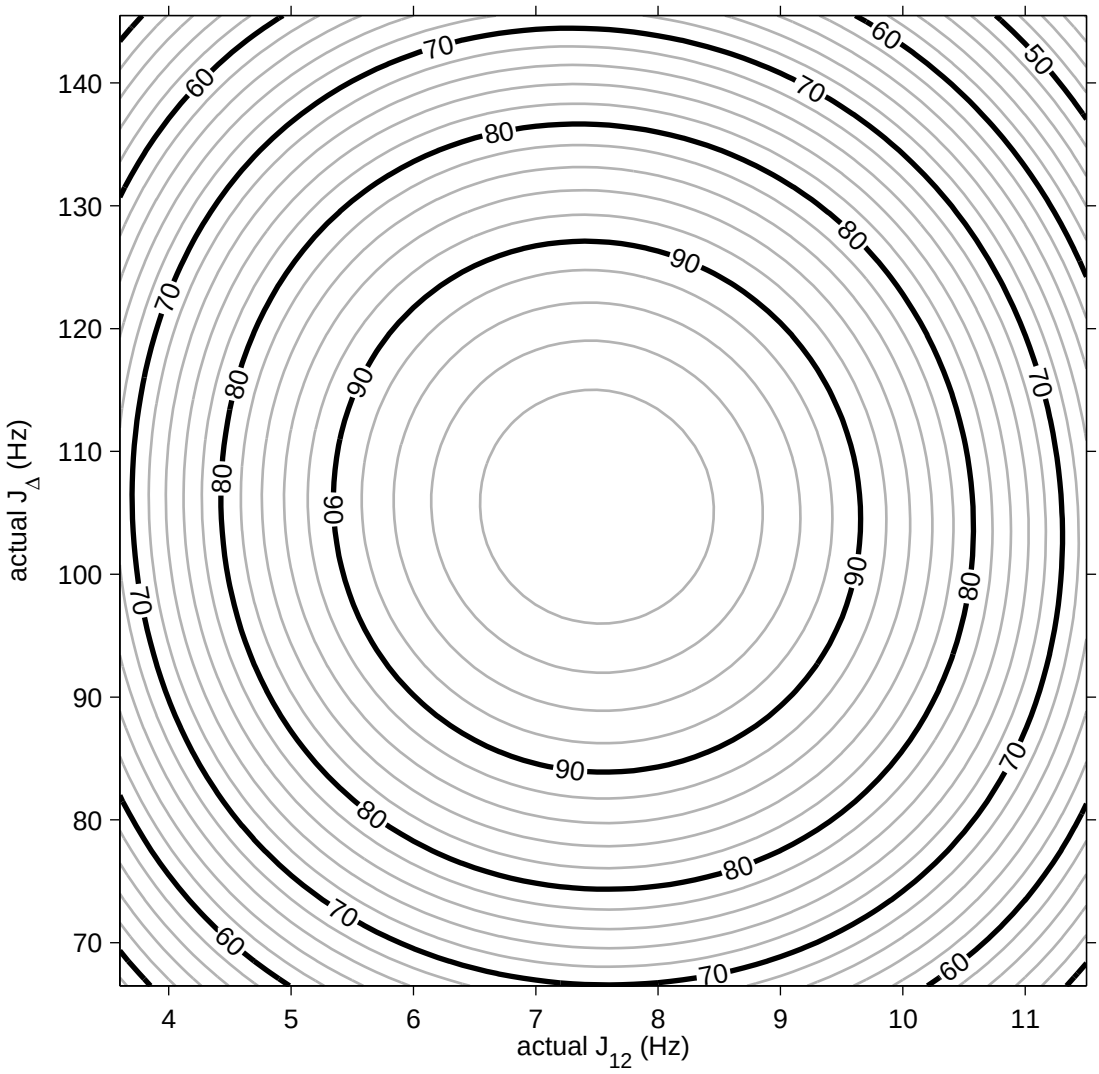

Figure 21. Polarization expected on ^{199}Hg given the sequence derived for the literature scalar coupling values for diethyl mercury when the actual scalar coupling differs. The major contours are

marked for every 10% and the minor contours are every 2%. The pulse sequence generates 100% polarization when the coupling constants are correct. This uses ideal calculations.

C. Large range pulse sequence algorithm

The large range is characterized very roughly by $\theta \gtrsim 1$, generally due to weak scalar coupling to the target nucleus. Both small and medium range sequence algorithms are ineffective over this range. Pump pulses after either sequence allow increases to the polarization, but are increasingly fruitless when they are most required and expand the sequence time beyond acceptable limits. Still another novel algorithm is needed for this range. Molecules with low γ, weakly coupling heteronuclei such as ^{15}N which promise particularly long lifetimes for the generated polarization tend to fall into this range.

1. Algorithm for the limit $\theta \to \pi/2$

In the case where $\bar{J}_{12}$ comes to dominate $\bar{J}_{\Delta}$, neither of the relations (20) or (21) generates useful evolution for this system. In order to generate the desired polarization at the end of the sequence, the intrinsic Hamiltonian needs to be changed during this period. Specifically, some method of homonuclear decoupling by which the $\bar{J}_{12}K_x$ piece in the Hamiltonian is effectively removed while the heteronuclear coupling remains, would generate useful evolution for this range. Unlike the case of decoupling heteronuclei, no general strategy is known for decoupling homonuclear scalar couplings.

The innovation here is to show that a J-synchronized train of π pulses on the $\mathbf{S}$ spins is able to generate the desired Hamiltonian. This synchronous train is a series of π pulses given twice over each period of $\tau_{res} = 2\pi/\bar{J}_{12}$ at $\tau_{res}/4$ and $3\tau_{res}/4$. Average Hamiltonian theory is used to show analytically how this affects the evolution of the system. Starting with the Hamiltonian in Eq. (18), then transforming away the pulses and the homonuclear coupling yields a time dependent Hamiltonian in the toggling frame given by

$$\begin{aligned} \hat{H}_T(t) &= \bar{J}_\Delta 2K_z S_z \cos\left(\bar{J}_{12}t\right) + \bar{J}_\Delta 2K_y S_z \sin\left(\bar{J}_{12}t\right), \quad t < \frac{\tau_{res}}{4}, \frac{3\tau_{res}}{4} < t \\ \hat{H}_T(t) &= -\bar{J}_\Delta 2K_z S_z \cos\left(\bar{J}_{12}t\right) - \bar{J}_\Delta 2K_y S_z \sin\left(\bar{J}_{12}t\right), \quad \frac{\tau_{res}}{4} < t < \frac{3\tau_{res}}{4} \end{aligned} . \tag{32}$$

Integrating this Hamiltonian over the interval τ_{res} then gives

$$\widetilde{H} = \tfrac{2}{\pi}\bar{J}_\Delta\left(2K_z S_z\right). \tag{33}$$

Thus, the homonuclear coupling has indeed been removed leaving only a heteronuclear coupling scaled down by $2/\pi$ in its place. The relevant evolution of the spin system under this Hamiltonian is given by

$$K_x \to \cos\left(\tfrac{2}{\pi}\bar{J}_\Delta t\right)K_x + \sin\left(\tfrac{2}{\pi}\bar{J}_\Delta t\right)\left(2K_y S_z\right) \tag{34}$$

$$2K_z S_x \to \tfrac{1}{2}\sin\left(\tfrac{2}{\pi}\bar{J}_\Delta t\right)\left(S_y - 4I_{1z}I_{2z}S_y\right) + \cos\left(\tfrac{2}{\pi}\bar{J}_\Delta t\right)\left(2K_z S_x\right). \tag{35}$$

The evolution in relation (35) is advantageous for generating the desired polarized state that can be stored in z with a final pulse.

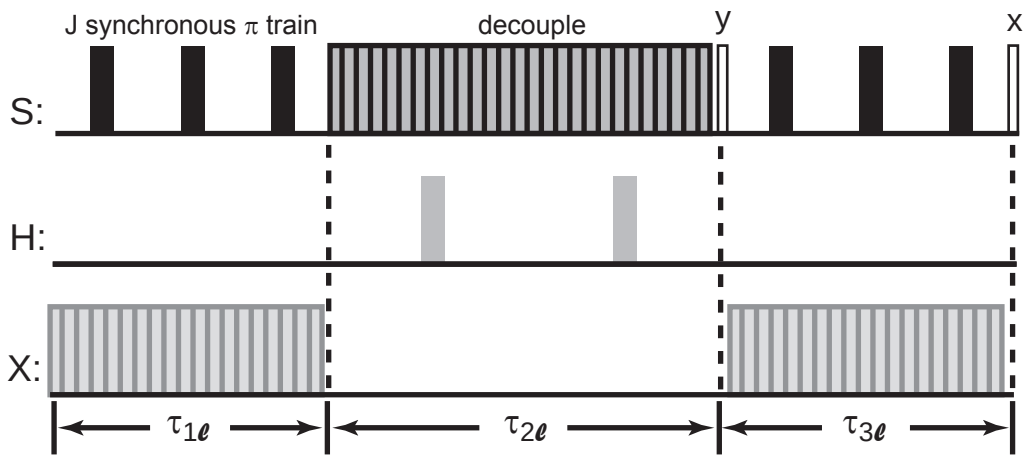

Figure 22. Schematic of the large θ range pulse sequence. The number of pulses in the J-synchronized π train should be set to the number required by the algorithm; three is used as an example. The main pulses of the algorithm are dark and recommended echoes on proton and decoupling on spectator isotopes X are light. Solid pulses are π, open pulses are $\pi/2$, and decoupling uses a cyclic method that returns the polarization to the starting point, such as MLEV-16.

In order to best utilize this evolution, the system must be placed in a state without any K_x in it. The evolution of the system under the intrinsic Hamiltonian is not useful for bringing the system into such a state, so the J-synchronized π train is also useful for the first part of the sequence, utilizing the evolution in relation (34).

An algorithm for the large range, starting when time suspension during the precursor reaction is completed, would then utilize a J-synchronized π train for a time τ_{1l} to fully convert the K_x spin order to $2K_yS_z$. Cyclic decoupling is applied to the target isotope for a time τ_{2l} until the system is in the state $2K_zS_z$. A $\pi/2_y$ mixing pulse is applied to the target isotope and second J-synchronized π train is applied to the

system for a time τ_{3l} until the transverse polarization has built up. A final $\pi/2_x$ pulse stores this as longitudinal polarization for future use. This algorithm is illustrated in Fig. 22, including a scheme for compensating for the effects of spectator isotopes. The timing required for this algorithm is given by

$$\begin{aligned} \tau_{1l} &= \tau_{3l} = \pi^2/4\bar{J}_\Delta \\ \tau_{2l} &= \pi/2\bar{J}_{12} \end{aligned} . \tag{36}$$

While formally the average Hamiltonian theory used requires a cycle of pulses that brings the system back to its original state, in practice the homonuclear decoupling operates over an odd number of pulses as well. Since the first and third waits are during J-synchronized π trains, their timing cannot freely be set to any value but must be set to an integer multiple of $\tau_{res}/2$. Therefore, the value of $\tau_{1l} = \tau_{3l}$ must be coerced to the integer or half integer multiple of τ_{res} that is nearest to the prescribed time given by Eq. (36).

2. Modifications for more consistent polarization

While the time desired for the waits $\tau_{1l} = \tau_{3l}$ is very close to an integer multiple of $\tau_{res}/2$ when θ nears the upper limit of its range, the difference between the optimal time and an allowed time can become quite dramatic as θ nears $\pi/4$ where the other algorithms start to fall off in effectiveness. This mismatch reduces the resulting polarization of the algorithm. This problem is particularly apparent near $\theta = 1.09$ where the effectiveness of the large range sequence actually drops below that of the medium

range sequence.

Numerical optimization of the sequence holding the number of π pulses steady but allowing the times to vary increases the polarization of the sequence without requiring large changes in the time needed (Fig. 23). By allowing this variation, the polarization increases to unity over an extensive range (Fig. 24).

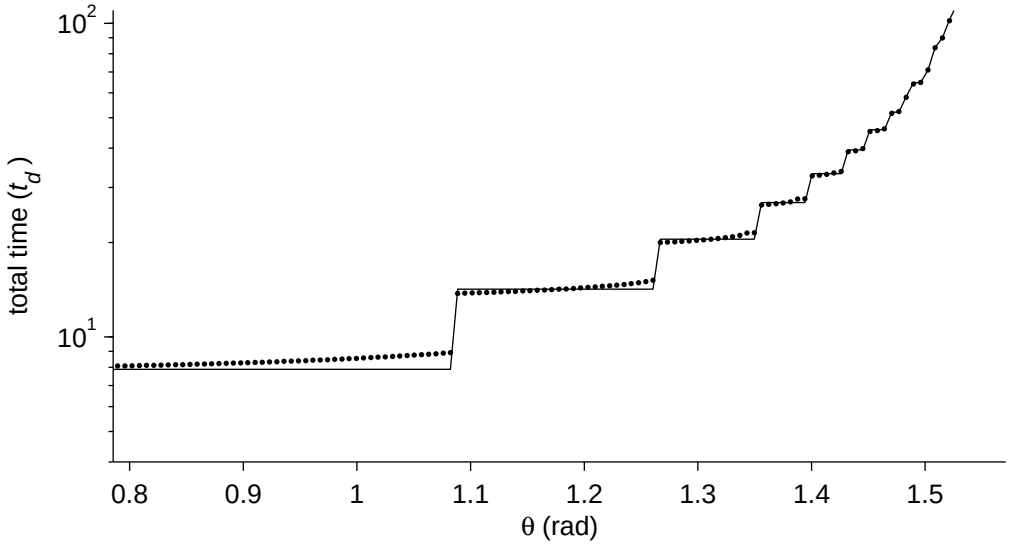

Figure 23. The wait times required by the large θ sequence algorithm generally need to be optimized in order to achieve unity polarization. The total time for the sequence as calculated (line) is compared to the total of the numerically optimized times (dots) and found to be similar. This uses ideal calculations.

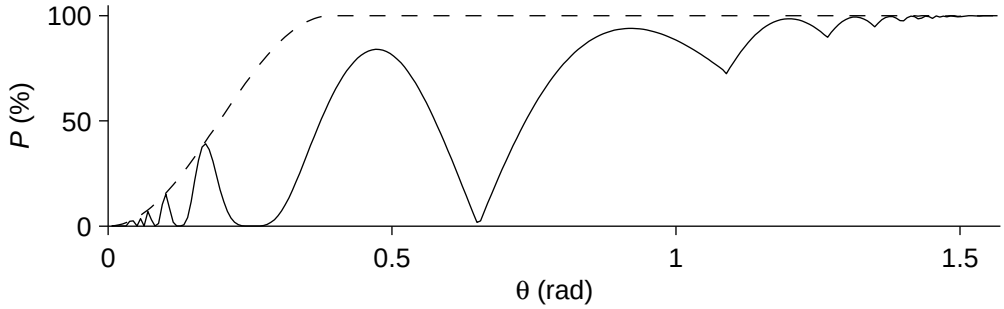

Figure 24. The theoretical polarization achievable using the large θ sequence algorithm as described with calculated times (solid) and after numerical optimization (dashed). The minimum number of π pulses in each synchronous period is 1. This uses ideal calculations.

3. Operation in real systems

Similar to the medium and small range θ cases, the spin system must not contain interfering spins of the same isotope as the target nor any interfering protons for the pulse sequence to operate correctly. This generally requires deuteration of the precursor molecule to be used in the reaction.

As well, a means of refocusing the chemical shift of the target and mitigating the effects of spectator isotopes is required. Over the second wait period, this requires symmetric echoes on the protons. Over the J-synchronized π train, this is more difficult to apply. The target chemical shift is already refocused by the pulses, but pulses on the protons to lessen the effects of deuterium will interfere with the J-synchronized π train. Over these periods, it is possible to apply decoupling to those isotopes other than the target and protons that are known to be part of the spin system. A second method is to treat each segment in the J-synchronized π train as a separate period and apply the

symmetric echoes to target and protons during each one.

4. Behavior under experimental error

To understand how well the sequence is likely to perform in a real experiment, it is useful to look at how it fails when common experimental errors occur. These are the same as for the small and medium θ range sequence algorithms.

i. Scalar coupling errors

To see how uncertain scalar coupling affects the outcome of a particular pulse sequence, it is useful to examine it at different points in the range. An example of a molecule at the low end of the large θ range is 1-^{13}C-succinate at $\mathrm{pH} = 13.3$ with the larger of the two proton-proton coupling constants. This molecule has scalar coupling constants of $J_{12} = 8.51$ Hz, $J_{1S} = -6.32$ Hz, and $J_{2S} = 4.13$ Hz (*36*). The timing for this pulse sequence, after optimization, is $\tau_{1l} = \tau_{3l} = 70.02$ ms with 1 π pulse in the J-synchronized π train and $\tau_{2l} = 21.29$ ms. This sequence performs as seen in Fig. 25.

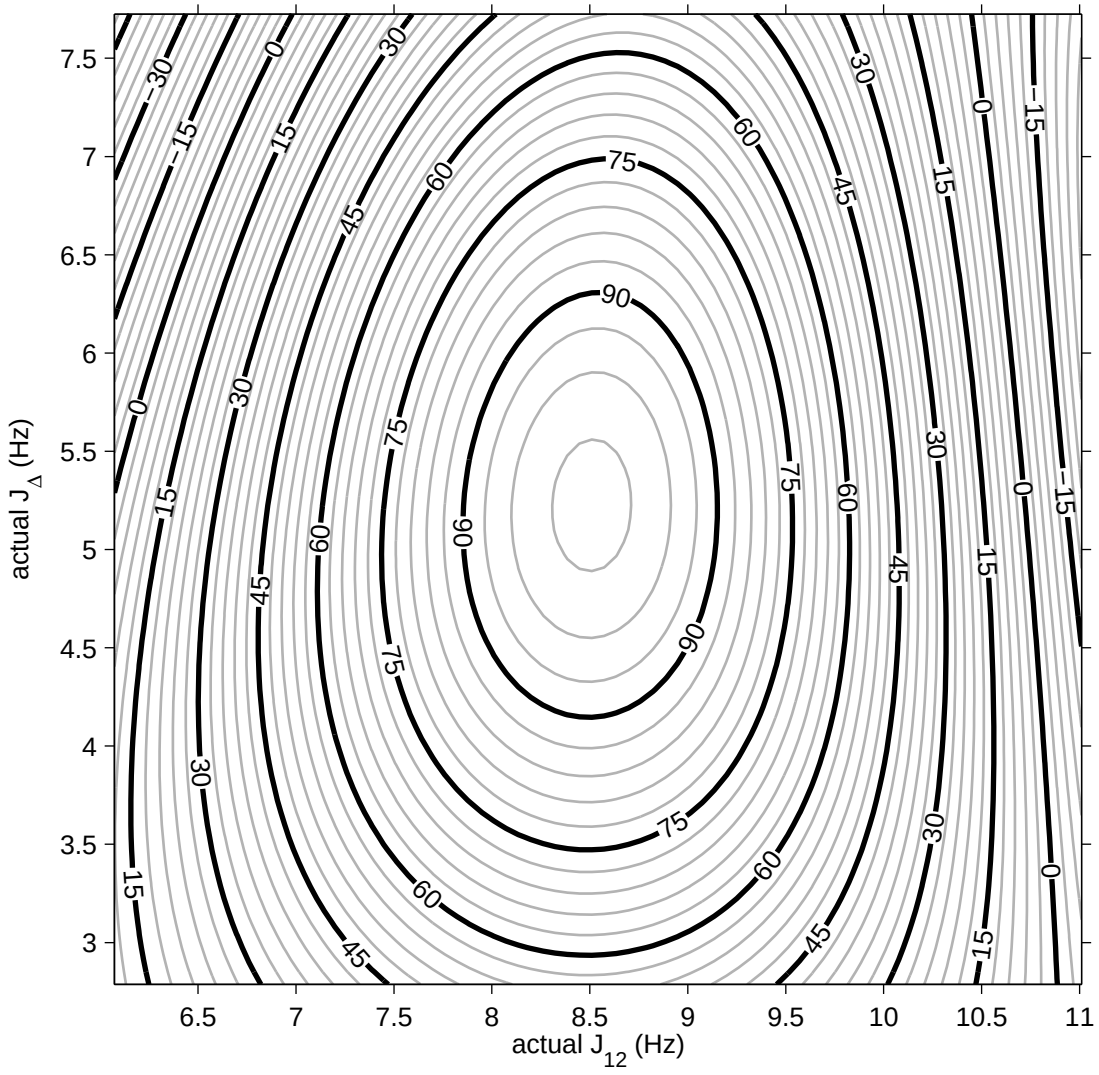

Figure 25. Pulse sequence performance for the sequence derived for 1-^{13}C-succinate in very basic solution when the scalar coupling constants diverge from those given in the literature. The major contours are marked for every 15% and the minor contours are every 3%. The pulse sequence generates 100% polarization when the coupling constants are correct. This uses ideal calculations.

An example of a molecule with somewhat larger θ is ^{15}N-choline. This molecule has $J_{12} = 3.15$ Hz or $J_{12} = 7.00$ Hz and $J_{1S} = 3.68$ Hz with only one heteronuclear

coupling corresponding to the three bond coupling observed (*57*). The pulse sequence for this molecule with the larger J_{12} value requires that $\tau_{1l} = \tau_{3l} = 214.16$ ms with 3 π pulses and $\tau_{2l} = 38.68$ ms. This sequence performs as seen in Fig. 26.

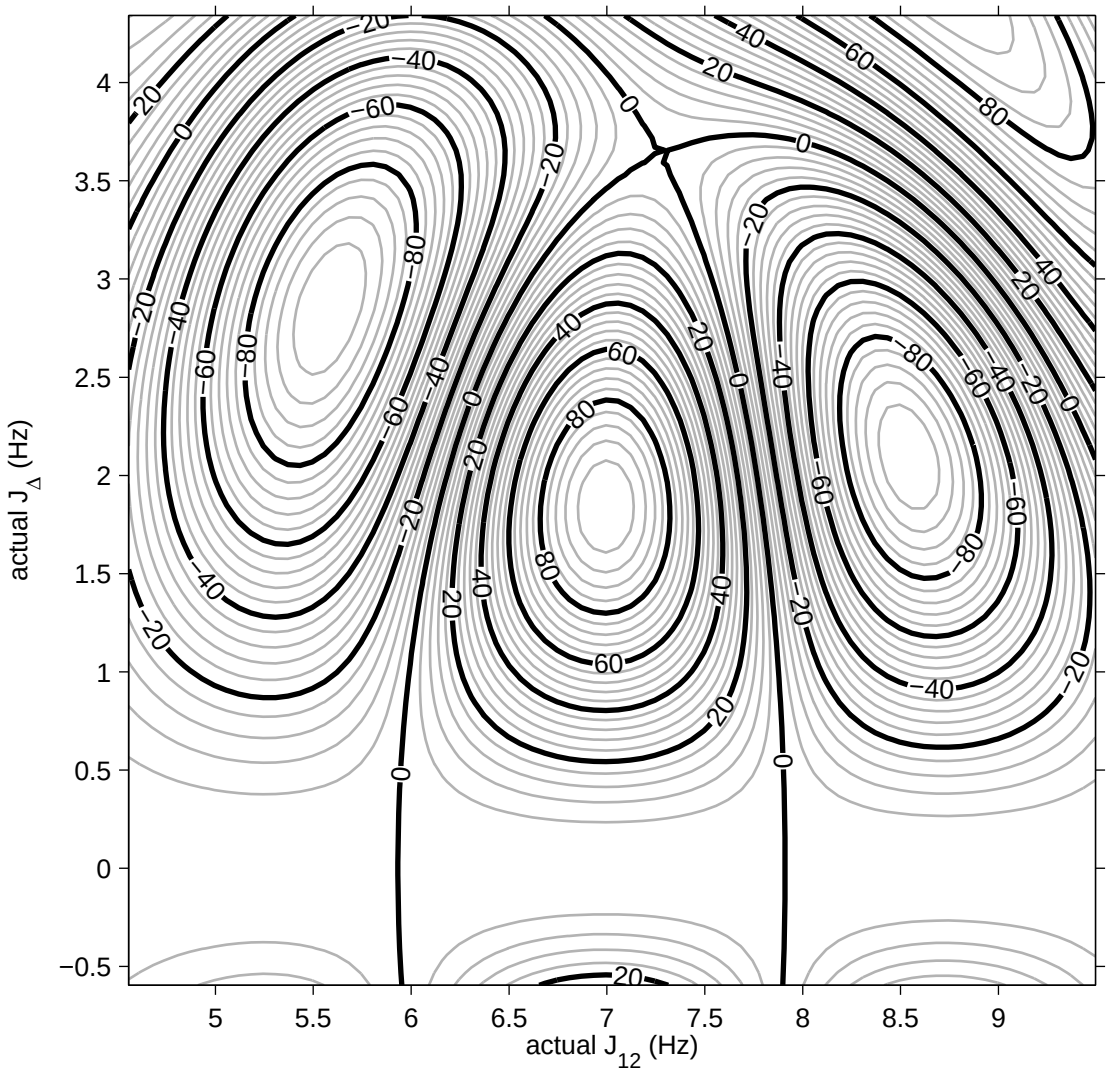

Figure 26. Expected performance of the pulse sequence derived for ^{15}N-choline should the scalar coupling values differ from those found in the literature. The major contours are marked for every 20% and the minor contours are every 4%. The pulse sequence generates 100% polarization when the coupling constants are correct. This uses ideal calculations.

Comparing Figs. 25 and 26 shows the increasing importance of having accurate scalar coupling values, particularly for J_{12}, as the value of θ increases.

D. Comparison of sequence algorithms

There is great overlap in the regions in which this set of pulse sequence algorithms is capable of generating unity polarization. In order to select between them, it is useful to examine the time requirements of each algorithm. Over the entire range, there are multiple regions that are best handled in different ways. These regions will be examined starting with the highest where $\theta \le \pi/4$ and proceeding to lower values of θ, then examine the regions where $\theta > \pi/4$. To give a better idea of the general time requirement of the pulse sequences, they are compared using the dimensionless time $t_d = \overline{J}_{12}\tau$. This is a useful comparison since the formulae generate times that depend on the values of various scalar couplings. For a given a value of θ, the value of one scalar coupling determines the rest, so the dimensionless product of one coupling and the total time is a quality factor by which sequences may be compared, for which t_d is preferred. The magnitude of $\overline{J}_{12}/2\pi$ changes over a relatively small range, generally being between $3-12$ Hz. Values of $\overline{J}_{\Delta}/2\pi$ as small as 0.5 Hz are likely practical before dephasing effects dominate, but it and $\overline{J}_{K}/2\pi$ can easily range up to 120 Hz. Using this dimensionless time will show the time behavior of the sequences over the range of θ with the least amount of distortion due to the general correlation of the other scalar

couplings with θ.

1. For the range $\theta \le \pi/4$

This is a region over which any one of the three algorithms given may operate on the system to generate unity polarization. Considerations like the time required to deliver the sequence, ease of implementation, and behavior due to common errors are also important in considering which sequence to use.

The large θ range sequence was not designed for this region and does not generate sequences with good time requirements over this region. The sequences contain one π pulse for the J-synchronized π train regions when $\theta < \pi/4$, so the time to complete the calculated sequence is $\tau\bar{J}_{12} = 2.5\pi$. The optimization generally increases this time slightly. This is significantly greater than the other two sequences. If the sequence is allowed to have 0 π pulses when θ becomes small enough, the sequence reduces to the small θ range case and is no longer interesting as a unique procedure.

The small and medium θ ranges have complicated dependencies (Fig. 27), but show three distinctive regions. The first to note is when $\arctan\left(1/\sqrt{2}\right) < \theta \le \pi/4$. Over this region, the medium range sequence is the clear winner generating the faster sequence. At $\theta = \arctan\left(1/\sqrt{2}\right)$, the two sequences are equivalent as $\tau_{2s} = \tau_{2m} = 0$. Just above this, τ_{2s} reaches the maximum value before the systems start sampling

states equivalent to those sampled at earlier times, causing the sudden jump to smaller times. Second, when $0.3532 < \theta \le \arctan\left(1/\sqrt{2}\right)$, both algorithms generate sequences that perform in a comparable manner with only slight time advantage found in using the small range sequence. Third, when $\theta < 0.3532$ rad, the medium sequence no longer achieves unity polarization, so although it does eventually gain better time performance, it is not the preferred algorithm. At the θ where the time for the sequences is equivalent, the polarization has only dropped to about 94% but is rapidly decreasing. In this range, the gains in time are not worth the losses in polarization, generally, but quantifying the tradeoff would require consideration of dephasing effects.

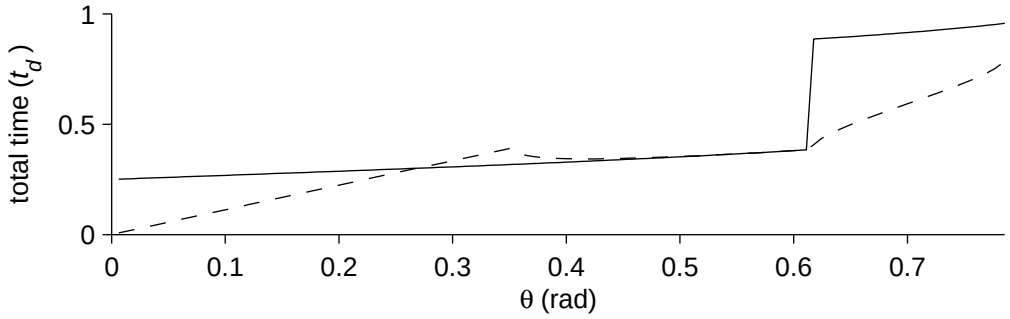

Figure 27. The time performance of the small (solid) and medium (dotted) range pulse sequences over the range in which one or both of them generates unity polarization. This uses ideal calculations.

2. For the range $\pi/4 < \theta$

The large range is characterized by weaker heteronuclear coupling and longer pulse sequences. As such, the choice between pulse sequences is often a tradeoff

between one that performs faster but does not give very good polarization and one that does give good polarization on the target, but does not perform as quickly as desired.

The large θ pulse sequence algorithm will always deliver a fully polarized target nucleus when relaxation is not taken into account. The medium θ pulse sequence algorithm is expected to give increasingly poor polarization that can be arbitrarily increased by the use of pump pulses after the main sequence is completed. After n such pump pulses, the polarization on the target is expected to be

$$P_n = \sqrt{1-\cos^{2(n+1)}(2\theta)} \tag{37}$$

when relaxation is not taken into account (*34*). This process requires an increasing number of pulses each with a unique angle that has been determined in the absence of relaxation but is changed when the relaxation constants are unequal.

By rearranging Eq. (37), it is possible to estimate the length of time that would be required to gain a minimum desired polarization using the medium θ pulse sequence algorithm. This value can be compared to the large θ pulse sequence and a choice made about which sequence to use based on whether the time savings, if there is any, justifies the loss of polarization. A few comparisons of this type are shown in Fig. 28 for examples where the medium θ sequence achieves 99%, 90%, 75%, and just 50% polarization, all of which eventually require more time than the large θ sequence requires for unity polarization.

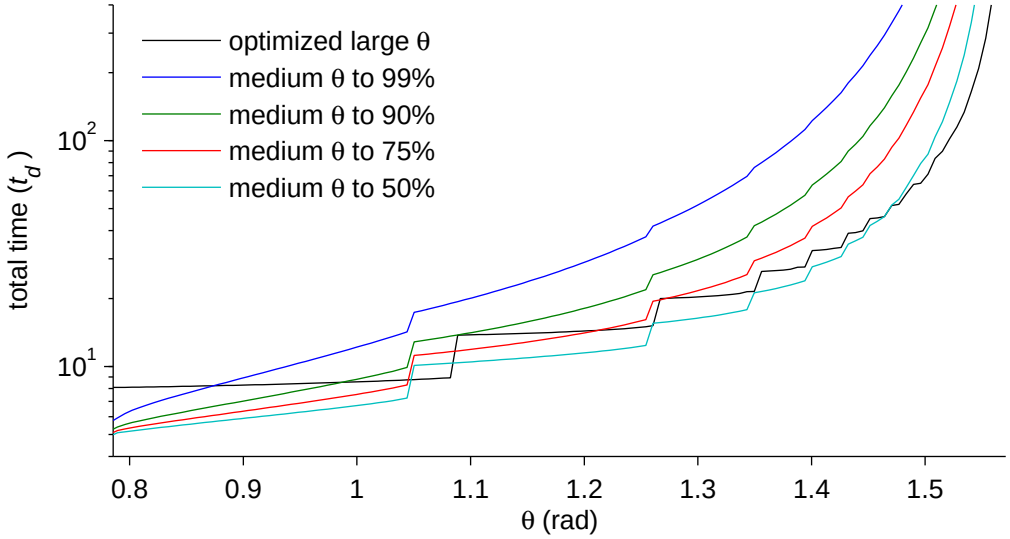

Figure 28. The time performance of the optimized large pulse sequence algorithm, compared to that of various versions of the medium pulse sequence algorithm which are able to deliver 99%, 90%, 75%, or 50% polarization to the target nucleus. The number of pump pulses has not been forced to an integer value, so the times represent a minimum estimate. This uses ideal calculations.

IV. Instrumentation and execution

The instrumentation initially used at CIT and Huntington Medical Research Institutes (*40*) to carry out the hydrogenation reaction and low field order transfer experiment to ^{13}C on was obtained from Amersham (now part of G.E.) in Malmo, Sweden on temporary loan. An improved homebuilt instrument was subsequently developed and is described here. A principal goal was to miniaturize the reactor to produce smaller samples of only 2 mL rather than approximately 12 mL, sufficient for studies on rodents, thus minimizing the costs of reagents. Faster, cheaper, more competent digital components were used, which also required fundamental changes to the computer program which controls the equipment. I designed the computer related architecture of the device and performed the significant programming of the software, including changes to handle the new controlling hardware and the computer program that automated the several functions. This section will describe the components in the system which holds reagents, delivers them to the reactor volume, which is also the locus for the low field NMR which generates the hyperpolarized molecules. It will then describe the procedure for generating hyperpolarized molecules. More details can be found in previously published (*58,59*) papers concerning an earlier version of the instrument, also based on my hardware choices and software.

A. Instrument hardware

The hardware for the system includes the reactor system and controlling hardware that interfaces with the computer. The reactor system is the hardware that holds reactants, performs product forming reactions, and executes the spin order transfer sequence. Hyperpolarized molecules are then ejected to atmospheric pressure for use in high field NMR or MRI for experiments. The heart of this system is the reactor itself. This reactor is a container consisting of a polymer cylinder that is threaded at the top and bottom. A threaded disk screws into the top and contains separate inputs at the top for parahydrogen gas and an aqueous solution of the precursor molecule and a hydrogenation catalyst. A second threaded disk screws into the bottom and has a conical indentation leading to an outlet that allows the product to be removed at the end of hyperpolarization. The piecewise structure allows for easy cleaning of the inside of the reactor. It was produced in house.

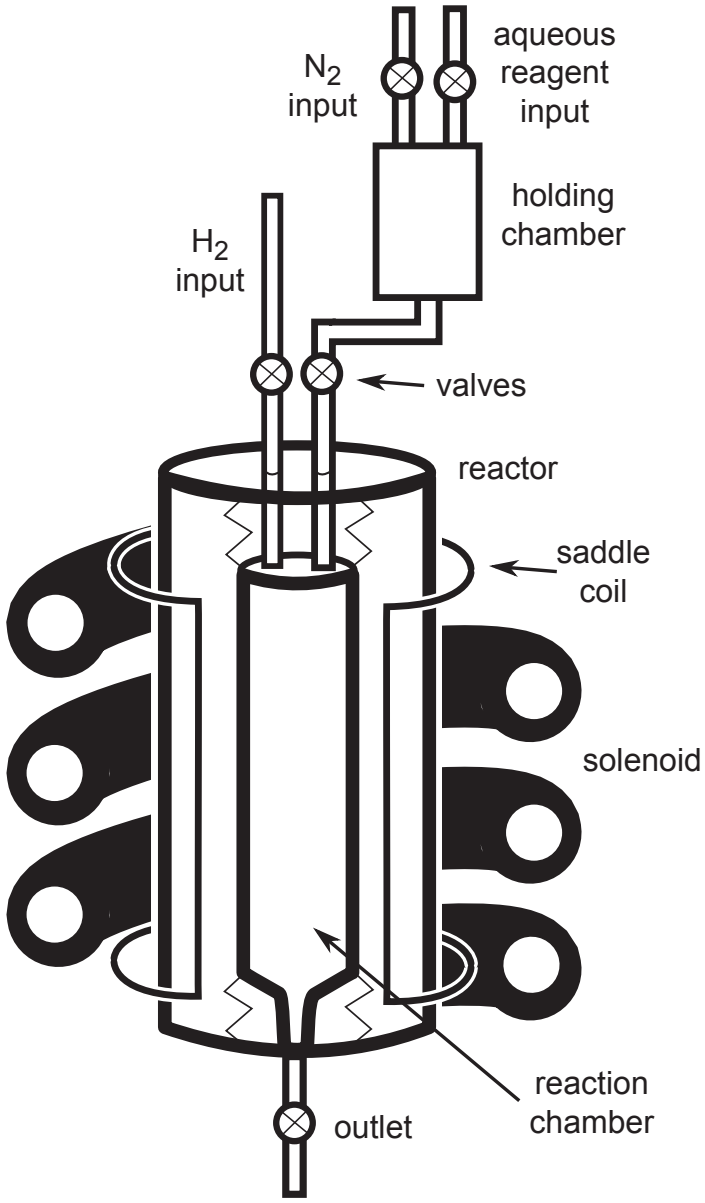

Figure 29. Schematic of the reactor system. The aqueous mixture of precursor and catalyst is placed in the holding chamber and solenoid providing B_0 is powered to prepare for hyperpolarization. The reaction chamber is filled with parahydrogen, proton decoupling initiated with the saddle coil, and precursor solution pushed into the reaction chamber under nitrogen pressure. After the spin order transfer sequence pulsing finishes, the product is removed through the outlet valve at reduced pressure.

The reactor is surrounded by a solenoid electromagnet that provides a stable magnetic field B_0 in the z direction along the axis of the reactor. An untuned saddle coil set between the solenoid and the reactor is used to deliver the audio frequency B_1 fields perpendicular to the static field. All pulses for all nuclei are generated using this coil. These were also built in house. Although the pulse coil is untuned, it does have a variable response to different frequencies due to its inductive reactance. This is manifest in that the voltage levels required in the definition of one pulse cannot be directly calculated based on another nucleus that has already been calibrated. It also causes changes in the shapes of pulses, particularly short pulses (Fig 30). In order to accurately calculate how well these pulses work for the system, it is necessary to collect data on the current passing through the coils as a result of the programmed pulses.

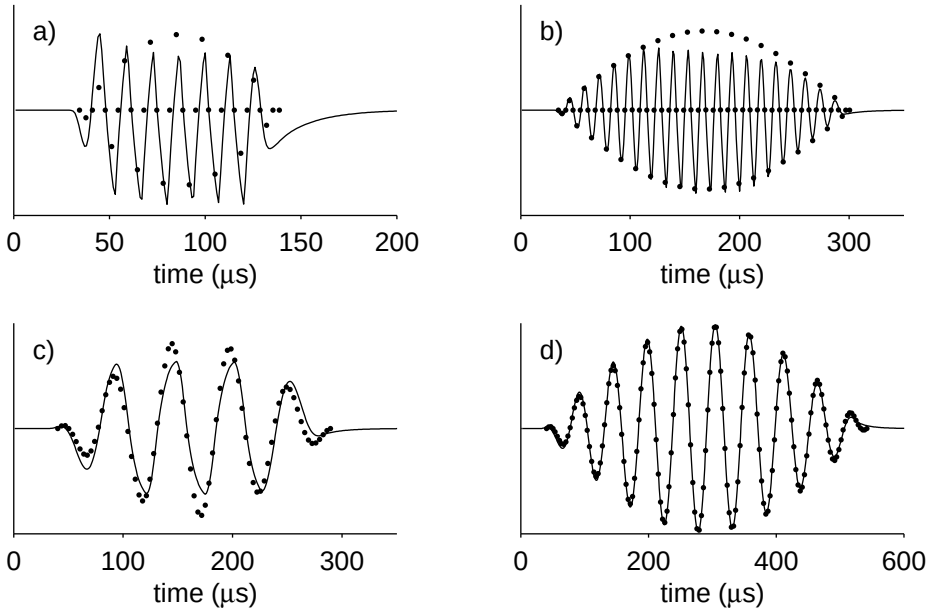

Figure 30. Actual pulse shapes (lines) measured by measuring the voltage drop across a 0.1Ω spy

resister when the defined half-sine shaped pulse (dots) is generated. The pulses are a) a short ^{1}H pulse, b) a long ^{1}H pulse, c) a short ^{13}C pulse, and d) a long ^{13}C pulse. The scaling and synchronization of the measured pulse with the defining pulse is approximate.

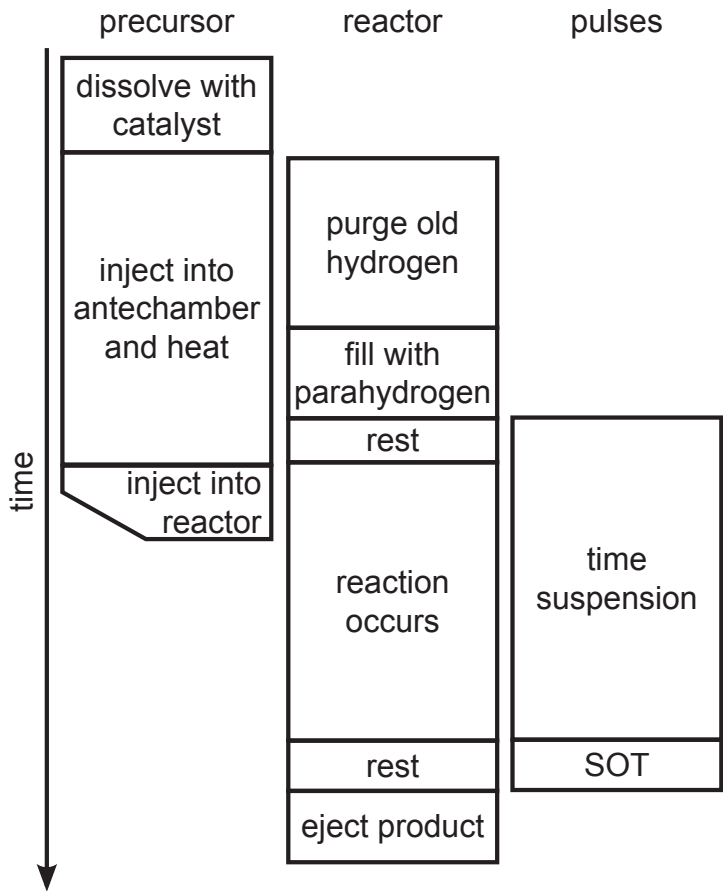

Figure 31. Timeline of a typical hyperpolarization procedure. The catalyst and precursor mixture and dissolved and warmed before being injected into the reactor already pressurized with parahydrogen. Time suspension by proton decoupling is started before the injection to insure the least amount of state mixing before the spin order transfer (SOT) pulse sequence is initiated. After the pulse sequence, the products are ejected to be used in an experiment in another instrument.

Reactants come to the reactor via Teflon tubing. Parahydrogen is supplied from a pressurized tank. The flow from the tank is controlled by solenoid valves. The

precursor and catalyst mixture is loaded into a holding chamber at the start of an experiment. This mixture is pushed from the holding chamber to the reactor through Teflon tubing using pressure supplied by a tank of nitrogen. This flow is also controlled by solenoid valves. The pressure of nitrogen (12 bar) and parahydrogen (10 bar) is set by regulators on the gas tanks. During an experiment, the reactants are sprayed into the reactor already filled with parahydrogen. An example of the order of the steps of the experiment is illustrated in Fig. 31.

The plumbing, holding chamber, and reactor are all housed in an insulated box so that the experiment may be heated to improve reaction time. During normal experiments, this system is kept at 60°C.

The reactor system is computer controlled via a National Instruments (NI) multifunction DAQ card model NI PXI-6251 in a model NI PXI-1042 chassis interfaced with a desktop computer using a model NI PXI-PCI8331 controller. Outputs from the card are made accessible using a model NI SCB-68 screw terminal connector block. The card has digital outputs that control the opening and closing of the solenoid valves via a connected NI ER-16 electromechanical relay for timed control of the movement of reactants and products through the system. The card also has analog outputs, one of which is the input to the amplifier that powers the B_1 saddle coil for generation of the pulses used to deliver the pulse sequence for hyperpolarization of the product molecules in the reactor.

B. Computer program

The computer program is written in NI LabVIEW 8.5 (*60*) and a basic flow chart of its operation is provided in Fig. 32. It dictates when valves open and close and when and how B_1 pulses are delivered. The program has two main components visible on the primary user interface. One component allows a sequence of events to be run in a prescribed order with set timing. These sequences, generally referred to as "pulse programs", can be saved and recalled for use in automatically generating hyperpolarized product with the equipment. The second component allows real time manual control of the valves during times when a pulse program is not being run.

The pulse program steps are defined by an array of clusters. The clusters contain elements that define the state of the system during each step of the array. The elements in this cluster are as follows:

1) Type. This element defines what sort of step is being performed. The type may be "timed" (the program preserves the state for a set time), "start pulse" (the program initiates the programmed pulse sequence), "finish pulse" (the program waits for the end of the programmed pulse sequence), or "wait" (the program waits for the user to click "okay" on a dialog box before continuing to the next step).
2) Time. This element defines the time that a timed step will last.
3) Valves. This is a cluster of Boolean buttons representing the valves in the

system. They are set to “off” to keep the valves closed and to “on” to open the valves.

In order to generate a pulse program, the user sets the elements in the cluster to depict the state the system should be in at a given moment. That is, the user turns the valves that are desired to be open to “on”, sets the type of step and, if needed, the time the step will last. If a “start pulse” step is used, those parameters also need to be set separately and a “finish pulse” step will need to follow at some point afterward in order to leave the DAQ card ready for another pulse. Only one type of “pulse” step can be used during a particular run of a pulse program. More steps are produced by stepping the array forward and setting the elements appropriately. The program is run by pressing a start button after which it steps through the defined steps sequentially until the last one is reached.

A secondary pulse setup program panel allows setting and testing the B_1 pulse sequence that will be delivered during a pulse program or single pulse that can be used directly for calibration purposes. Pulses are defined by an array of voltage values output from the analog out to the amplifier at a user defined frequency. The user may also select an offset from zero and a scaling factor for the pulses. A set of MATLAB® (*61*) functions has been created to easily generate the data file used to define the series of voltage values that represent a pulse. All pulse settings are kept as global variables to simplify the data flow.

The separate MATLAB® functions contain programs to generate specific pulses of

various shapes, link these pulses together in specific desirable ways, and a few helper functions. A few variables considered to be “spectrometer settings” (that a user of a pulse programmer would not frequently alter) are set as global variables. These are: “omega”, which denotes the frequency of protons in Hz; “cardfreq”, which is the word rate at which the arbitrary waveform generator (AWG) (part of the multifunctional DAQ card) outputs the voltage data points when generating a pulse; and “now”, which keeps track of the cumulative time, in seconds, that has passed during all the previous pulses and delays that have been created.

To use them, a user first declares these three variables to be global and sets them to the desired values. Usually “now” is initialized to 0 or to half the time represented by one point. Then the pulses and delays that are needed are generated in order and concatenated into a single vector. When the pulse is ready, the real part is saved with the “save_pulse” helper function which writes it in the form needed by the LabVIEW program. This program has additional functionality to save the pulse in the form needed by GAMMA programs to facilitate theoretical modeling of the pulse results.

The pulse generating functions all take three required variables and return a vector of voltage values representing the desired pulse. The first is a variable containing information about the isotope to be pulsed, the second is the nutation angle desired, and the third is the pulse phase ϕ. Some pulses, such as Gaussian pulses, have extra parameters that can be optionally supplied after these required variables. These are set

to default values if not provided. The variable containing isotope information can be generated by hand or by use of a helper function that takes a string with the isotope name as input and returns the required variable with standard values derived from the value of “omega”. This variable contains the type of isotope, the carrier frequency of the isotope at the given static field, the amplitude (which needs to be set from calibration), and the $\pi/2$ times for various pulse types. The $\pi/2$ times can be customized by supplying a second variable representing the number of periods of the carrier frequency that such a pulse should last.

In addition to the pulses, a delay function is provided. The delay function takes the number of seconds to wait as the only parameter and returns zeros that will cause a pause for the requested amount of time at the specified data rate. At the end of both pulse and delay functions, the amount of time represented by the number of points in the vector returned is added to the value of “now” so that the next pulse along will generate the correctly phased carrier. Since multiple isotopes are being pulsed, the carrier frequency is not always the same and the pulse sequence cannot be formed by concatenating envelopes for the pulses together and mixing them with the carrier as a final step.

Some preprogrammed pulse sequences exist in order to simplify their generation. One program is supplied for decoupling with MLEV-16 (*62*) which requires an isotope variable (as previously described), a time in seconds, and the type of pulses that are desired. At the end of the initial decoupling for time suspension prior to

generating sequences for heteronuclear PASADENA order transfer, the value of “now” may be reset to the initial value if desired, since phase coherence between these periods is immaterial. Distinct programs were written for the small, medium, and large θ pulse sequence algorithms including phase cycled echoes. These take the timing parameters needed by the sequence, and isotope variables for the protons and target spins as parameters.

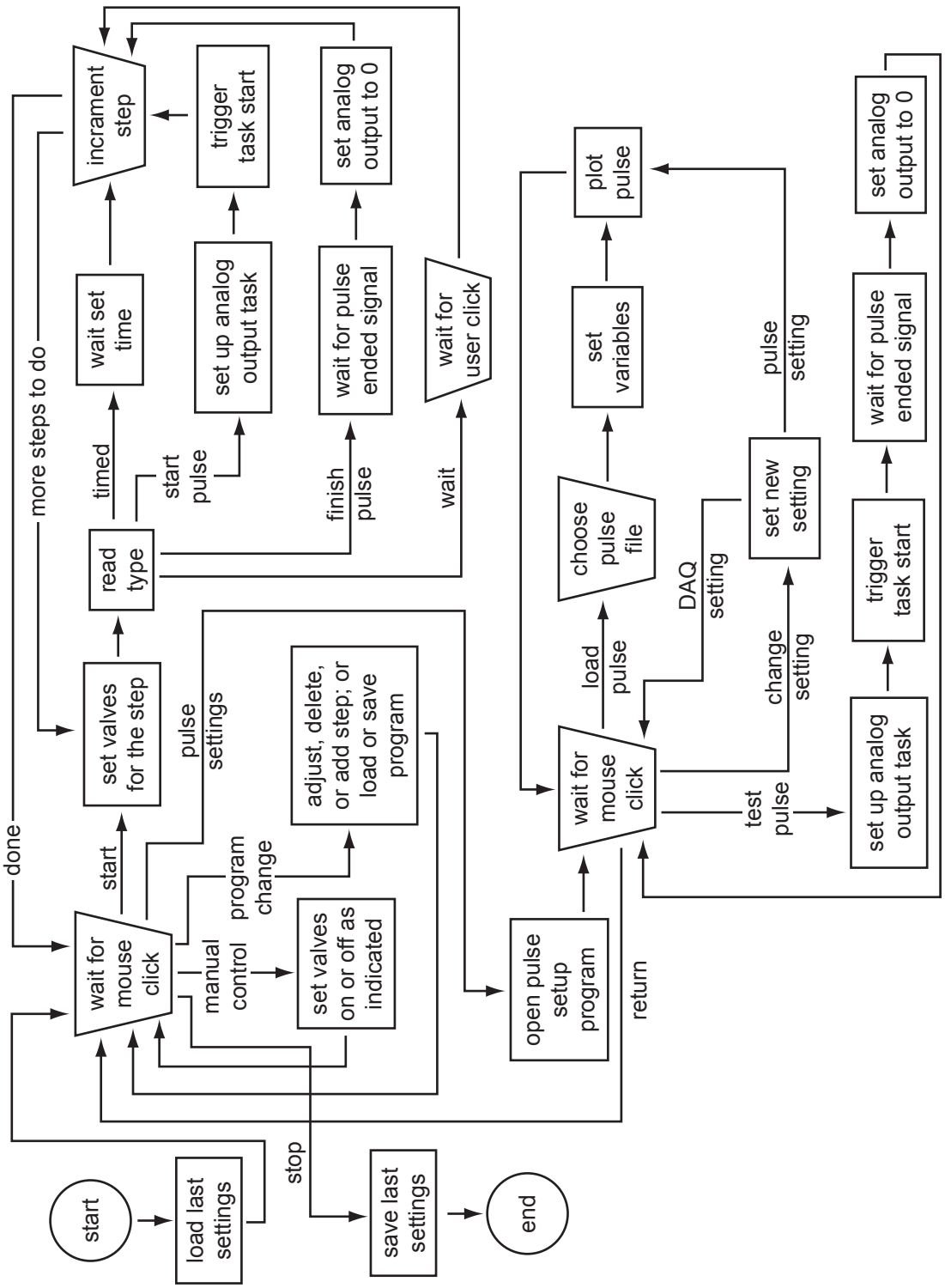

Figure 32. Flow chart of the pulse program described in the text including manual and

programmatic control of all aspects of the polarizer. Some lesser functions and checking procedures are not shown.

C. Field calibration

The secondary panel of the user interface, used for setting up and testing pulse sequences, is also used for calibration of the B_0 and B_1 fields. The low-field instrument is not set up to collect a signal from a precessing nucleus, complicating the procedure of testing the pulses delivered at a particular amplitude. Thus, this procedure relies on manually transporting a sample from a high field to the polarizer field, delivering a pulse, and transporting the sample back to high field for observation of the surviving magnetization.

Initially, the pulse power is set to a value that is expected to give a large nutation angle somewhat less than what is required to fully invert the magnetization. If too large an amplitude is used, the curve will flatten or show a local maximum at the center where the global minimum should be (Fig. 33). It is expected that the pulse power will shift the resonance frequency somewhat due to Bloch-Siegert effects (*63*) so that there are interactions between the values of B_0 and B_1 of a type that are not significant in high field NMR. If a pulse that is too small is used for the calibration, an incorrect resonance will be found due to insufficiently accounting for these interactions.

For each test, the standard sample is allowed to come to equilibrium in a high field NMR spectrometer to provide initial polarization. The sample is then carried to the

polarizer and placed within the reactor volume. The test pulse is triggered, then the sample is moved back to the high field instrument. During this second passage, all transverse polarization generated by the test pulse is lost, but longitudinal polarization remains. The sample is given a $\pi/2$ pulse in the high field spectrometer and the amplitude of the signal indicates the size of the longitudinal polarization after the test pulse. Relaxation during each passage causes some slight distortion, but does not affect the calibration so long as the timing is carefully kept the same for each passage.

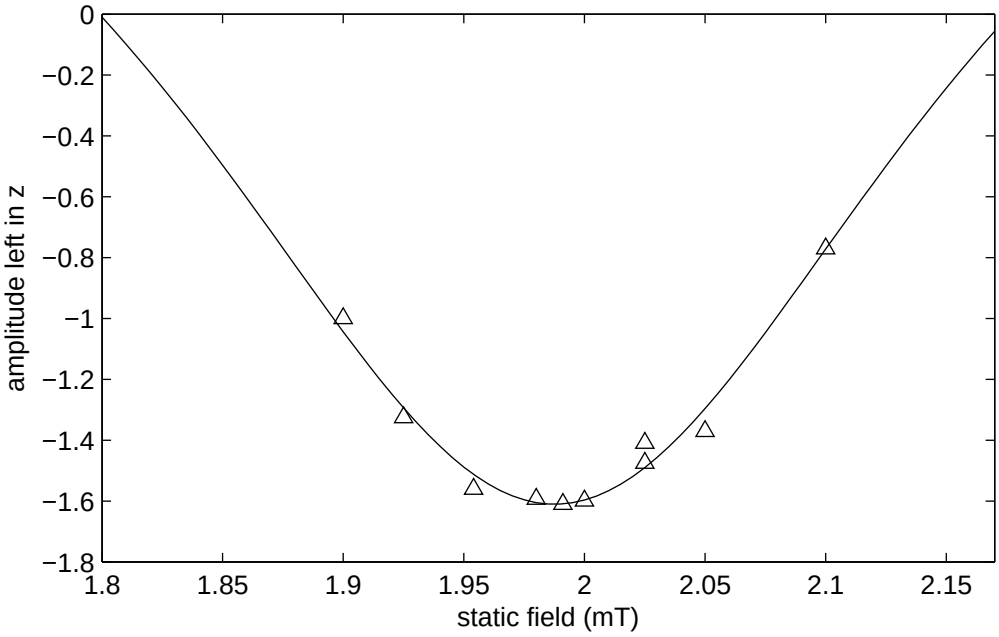

Figure 33. Experimental data points showing an example of a calibration curve for determining the static field using a ^{13}C pulse applied to deuterated and 1-^{13}C labeled acetate. The line is intended only as an aid for the eye.

D. Pulse calibration

There are two pulses in particular that need to be calibrated. The first is a π pulse for the target nucleus and the second is the π pulse for the hydrogen. In addition, it may be desirable to separately calibrate $\pi/2$ pulses for the target nucleus. In order to calibrate these pulses, a single pulse of each with a standard amplitude, generally one, is generated. Each is loaded in turn into the pulse program for calibration. This pulse is applied to a suitable standard sample at a series of amplitudes that are configured from the program panel. This polarization nominally varies as $\cos\theta$ (neglecting relaxation) with the amplitude of the delivered pulse (Fig. 34). This differs from the usual $\sin\theta$ pulse calibration curve when transverse magnetization is directly detected. The results are used to calculate the appropriate scaling required for the pulse. A similar procedure to the one used in field calibration is used to test each pulse. In this case, the static field is set to the previously calibrated value and the pulse power is varied for each test pulse.

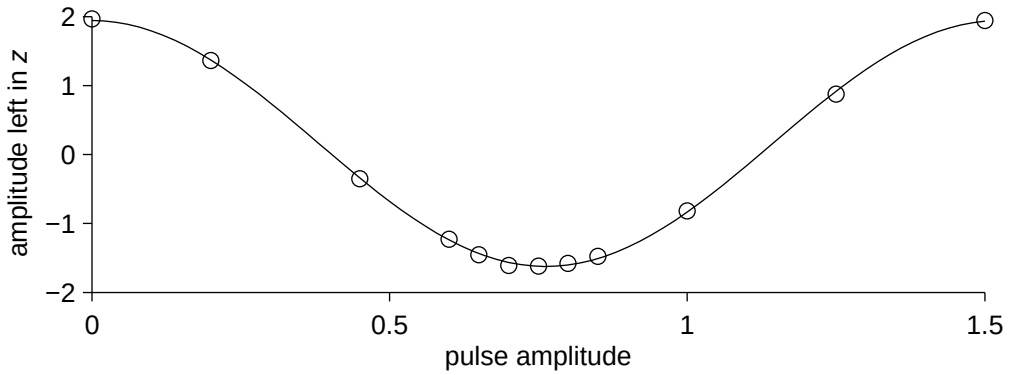

Figure 34. Experimental data points showing an example calibration curve for a ^{13}C pulse applied

to deuterated and ^{13}C labeled acetate. The sample is first polarized at 4.7 T for at least 240 s, then moved to the low field polarizer for each of the series of pulses, then moved back to sample the amplitude of the remaining polarization. The line is the least squares fit of the experimental data points to the functional form $c_3 \cos\left(\pi x/c_1\right)+c_2$ where c_i are the fitting parameters. The desired pulse amplitude from this fit is c_1.

E. Polarization

Once the pulse amplitudes have been calibrated, the pulse sequence for the molecule to be polarized is generated. This pulse contains an initial segment of time suspension proton decoupling, which defines the effective time allowed for formation of those products that will contribute to the hyperpolarized signal. This time, generally 4 s, is followed by the polarization transfer sequence. It is loaded into the pulse parameters in the LabVIEW software. A pulse program is loaded into the software to control the experiment. The mixture of precursor and catalyst is loaded into the holding chamber and the pressurized gasses are connected to their inlets. The system is closed up and allowed to come to equilibrium at the controlled temperature.

When everything is physically set up and the experimentalist is ready to generate the hyperpolarized product, the start button is pressed to initiate the pulse program. This program is usually set up to purge the reactor volume of any old parahydrogen and then fill it with fresh parahydrogen from a holding tank. Parahydrogen is given 2-4 s to pressurize the reactor volume, then the time suspension

is initiated directly before the precursor and catalyst mixture is pushed into the reactor volume by nitrogen at higher pressure than the hydrogen already in the reactor. At the end of the pulse, the product is expelled. The hyperpolarized product is then taken to the high field instrument for use. The simplest high field experiment simply supplies a pulse to check how much polarization is achieved. In some cases, the transport of the sample to the high field instrument was done pneumatically. For animal studies, the hyperpolarized product was ejected into a syringe which was carried to the prepared injection apparatus.

After the molecule is hyperpolarized, the system is flushed by running nitrogen gas through the plumbing. This is intended to remove any residual fluid from the previous to a new run.

F. Polarization verification

Many techniques exist to verify the level of polarization that has been obtained, each with strengths and weaknesses. The one commonly in use for MRI compares the signal from the relatively dilute hyperpolarized product (10 to 100 mM) to the signal from a highly concentrated sample of ^{13}C labeled acetic acid or pure natural abundance ethanol that is also in the NMR coil. These signals are easily separated by location in the reconstructed image. Using the known concentrations of the sample and standard, the signal from the hyperpolarized sample is easily compared to the thermal equilibrium polarization at the particular field of the instrument. This gives a field dependent

enhancement value which can be converted to an absolute enhancement by knowing the thermal equilibrium polarization of the standard. Implicit in the interpretation of the hyperpolarization P from such a calibration is the assumption that the original reaction went to completion by the time the spin order transfer sequence began. If it did not, then the fraction χ of the molecules that were formed sufficiently quickly actually carry the higher polarization P/χ. Comparisons of polarization based on the concentration of the sample and the standard are also biased to smaller values due to the inclusion of small gas bubbles in the sample that change the observed concentration.

Another common method of determining the polarization compares the signal from the hyperpolarized sample to itself after the polarization has decayed to thermal equilibrium in the high field magnet. This again gives a field dependent enhancement value that can be converted to an absolute polarization knowing the equilibrium polarization at that field. Since the catalyst is not removed after the set time for the time suspension, the completeness of the reaction, as measured by ordinary NMR many minutes later, may be partly attributable to reactions that occurred after the time frame of the time suspension. Currently, there is no method to stop the reaction on the second time scale, which would allow the course of the reaction to be studied by more direct means, independent of the transient hyperpolarized signal. This technique is complicated by the many orders of magnitude difference between the signal from the hyperpolarized molecule and that from the molecule at equilibrium. Higher gain

settings and, generally, extensive averaging are required to collect signal from the sample at thermal equilibrium.

An alternative method, that determines the absolute polarization directly, measures the signal not from the hyperpolarized nucleus, but from the protons that are coupled to the hyperpolarized nucleus. Since the coupling to the spin ½ heteronucleus causes the proton peaks to split into two with each peak associated with a different state of the neighboring heteronucleus, this doublet signal gives the absolute polarization, if resolved. The simplest example is a molecule with a polarized ^{13}C coupled to a single proton. Figure 35 demonstrates the peak differences seen in this case for both positive and negative polarizations of the carbon nucleus. Determining the polarization of this system is a matter of determining the area under each peak and fitting it to Eq. (1) where N_+ and N_- are these areas. This technique is complicated by the extra scalar couplings in the case of the three spin system needed for heteronuclear PASADENA. In these cases, more elaborate data fitting is required, but the systems do generate distinctive patterns when there is sufficient resolution as demonstrated in Fig. 36.

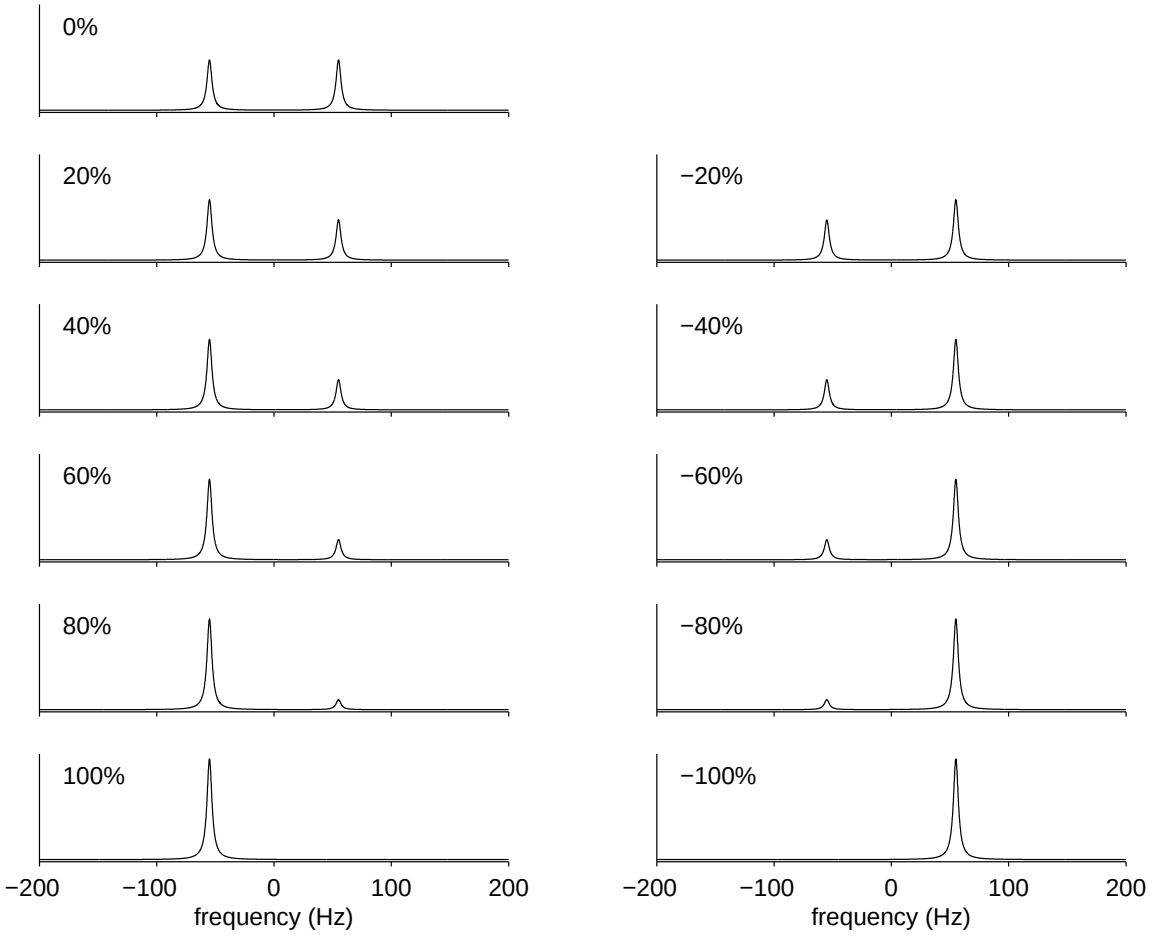

Figure 35. When a nucleus couples to a proton, the polarization of that nucleus is apparent in the peak heights of the proton spectrum, obtained from the fid subsequent to a $\pi/2$ pulse. These plots compare the relative peak heights in the proton spectrum of a single proton coupled to a ^{13}C nucleus with the indicated polarization. The coupling constant is $J_{CH} = 110$ Hz and all plots are on the same y-scale.

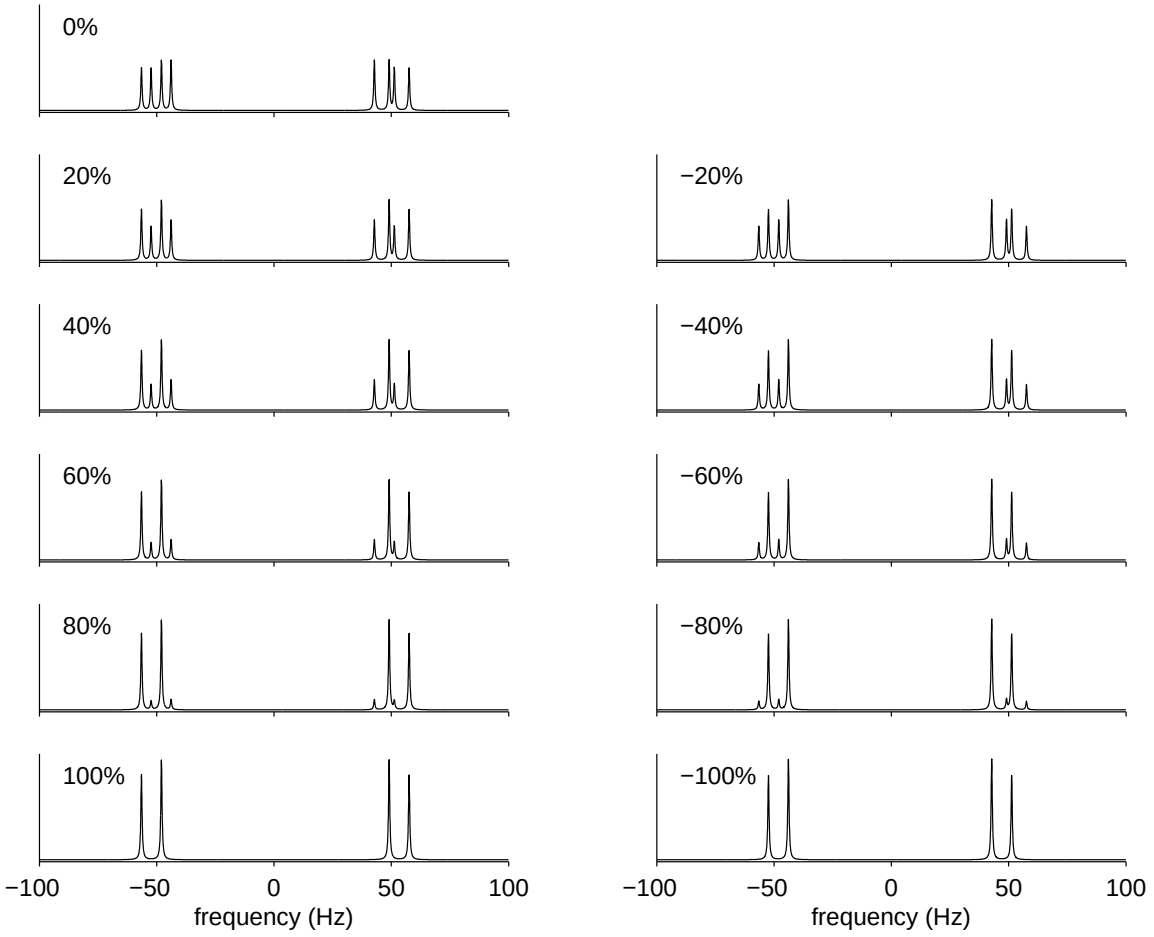

Figure 36. When a nucleus couples to two coupled protons, the polarization of that nucleus is apparent in the peak pattern of the protons. These plots compare the relative peak patterns in the proton spectrum of two protons coupled to a ^{13}C nucleus with the indicated polarization. The coupling constants are is $J_{12} = 8.51$ Hz, $J_{1S} = -6.32$ Hz, and $J_{2S} = 4.13$ Hz, the protons are split by $\delta = 0.2$ at 500 MHz, and all plots are on the same y-scale. The spectra are simulated for the case of an FID subsequent to a $\pi/2$ pulse.

In any case in which sample transport is needed prior to detection, the polarization of the sample at the end of the pulse sequence is not what is measured.

The travel time between instruments (about 10 s) allows relaxation from the hyperpolarized state. In order to estimate the hyperpolarization achieved, the measured polarization is corrected for the theoretical relaxation loss.

G. Molecule selection and characterization

The molecule to be hyperpolarized must be one that is obtainable by molecular addition of hydrogen across an accessible double or triple bond of a precursor molecule. A target nucleus near the addition point must have resolvable scalar coupling with these added hydrogen. It is possible to generate saturated molecules with specific stereochemistry with the aqueous hydrogenation catalyst that has been used for these reactions (*64,65*). Some example molecules that have been hyperpolarized are 2-hydroxy-ethylpropionate (HEP) (*40,66*), maleate (*67*), succinate (*36,67*), and the amphiphile TFPP (*48*).

1. Measurement of T_1

In general, the molecule cannot be generated in the "location" in which it will be used. Therefore, in order to reap the greatest benefit from the hyperpolarization process, the target nucleus on the molecule should have a long longitudinal relaxation time constant T_1 allowing the polarization to be stored for the greatest length of time while the molecule travels to the required location.

The typical method of T_1 measurement (*68*) involves inverting the equilibrium

magnetization and allowing it to recover for some time before measuring the amplitude of the longitudinal magnetization with a $\pi/2$ pulse. This is repeated for a number of inversions and fit to an exponential dependent upon time. After each measurement, the system must be allowed to relax for some multiple of the expected time constant; $5T_1$ is usually considered to be enough. Since these are meant to be molecules with a long relaxation time, this measurement can become quite lengthy. One method commonly employed to measure this somewhat more quickly is to saturate the magnetization and then measure the rate at which it recovers from zero instead of from a negative value. This removes the requirement of any wait between experiments and eliminates the prospect of needing to repeat a measurement because the value of T_1 has been underestimated too greatly.

In some cases, NOE or some other nonequilibrium method can be used to establish the initial polarization on the target nucleus (*69*). When this is possible, this strategy can be used to help measure the relaxation time quickly as well. In order to do this, the relaxation from the inversion of the enhanced state to equilibrium is subtracted from the relaxation from the enhanced state to equilibrium resulting in decay to zero.

It is important that T_1 be measured on the product molecule with the intended isotopic composition since deuteration will affect this value. There are two ways in which deuterium affects the relaxation of the nearby proton, one that increases the relaxation and one that decreases the relaxation in comparison to proton. Since the

deuterium gyromagnetic ratio is about one sixth that of proton, the two frequencies are significantly different and relaxation effects do not couple effectively between them. However, since deuterium is a spin 1 nucleus, it relaxes far more quickly than protons, generating a polarization sink that quickly relaxes anything that does couple with it to equilibrium.

2. Measurement of coupling constants

Once a molecule is selected, the coupling constants need to be determined to appropriate accuracy, especially when applying the large θ range pulse sequence algorithm. This is aided by undecoupled spectra of the heteronucleus. Another method is to simply perform the original PASADENA experiment on the molecule in question. This both tests that the catalytic addition of parahydrogen is working as expected and measures the required scalar coupling constants without ambiguity even when geometric considerations such as those shown in Fig. 13 are active.

3. Molecular variations

In some cases, the desired molecule may not have particularly advantageous parameters for the polarization method. One such molecule is ^{15}N labeled choline which has very weak coupling between the protons and the nitrogen target leading to a somewhat long polarization sequence. In this case it may help to vary the molecule by adding an intermediary nucleus for polarization which is then transferred to the target nitrogen label by some more traditional means such as INEPT. Specifically, a carbon

directly connected to the nitrogen and one of the added protons could be a ^{13}C intermediary. This transforms the molecule from the large θ range, which often requires long sequences, to the small θ range which generally requires quite short sequences.

V. Low field effects

The equipment constructed for generation of hyperpolarized reagents has been built with a relatively small magnetic field so that the equipment is mobile enough to be brought to where it is needed and does not cause problems with other equipment that is sensitive to magnetic fields. Using the low field also allows for the use of cheaper and more general equipment for pulse generation since the frequencies involved are in the kHz range. This low field is possible since the sequences rely upon internal scalar coupling to generate the necessary evolution that results in hyperpolarization.

Thus, while the use of low field has advantages, it also generates some problems. These problems and their solutions are to be discussed in this section.

A. Lab frame introduction

Generally, NMR calculations are conducted in the rotating frame. This is covered in the elementary texts on the subject such as that by Levitt (*70*) or Goldman (*71*). In NMR, the signal of interest contains small deviations from some large frequency. In order to be more sensitive to these small deviations, the system is transformed into a reference frame that is spinning at some reference frequency Ω. Then everything that is precessing at the reference frequency appears to be stationary and the small deviations are low frequency effects that can be easily tracked, as can be seen in Fig. 37. This leads to both conceptual and numerical simplifications.

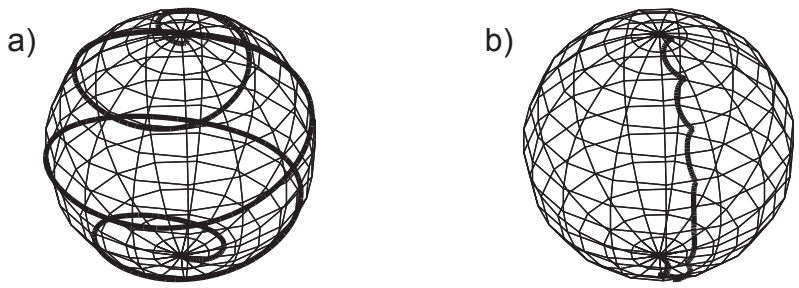

Figure 37. Comparison of the lab frame and rotating frame. The two plots follow the rotation of a unit vector of magnetization acted on by a four cycle linear square inversion pulse in (a) the lab frame and (b) the rotating frame. In the rotating frame, the deviations of the path of the magnetization from a smooth arc are clearly visible while in the lab frame these deviations are hidden by the larger effect of precession.

Pulses are described with the carrier at the reference frequency. The time dependence is piecewise-constant variations in amplitude and phase of this carrier. In typical NMR applications as well as this particular application, pulses are delivered by coils that create a B_1 field that is constant in direction, i.e. they generate linearly polarized pulses. A linearly polarized pulse at frequency Ω and phase offset ϕ is equivalent to a circularly polarized pulse at the desired frequency and a counterrotating circularly polarized pulse of equal amplitude.

$$\cos\left(\Omega t+\phi\right)=\tfrac{1}{2}\left[e^{i\left(\Omega t+\phi\right)}+e^{-i\left(\Omega t+\phi\right)}\right] \tag{38}$$

This can be transformed into the rotating frame by multiplication by $e^{-i\Omega t}$.

$$e^{-i\Omega t}\cos\left(\Omega t+\phi\right)=\tfrac{1}{2}\left[1+e^{-i\left(2\Omega+\phi\right)}\right] \tag{39}$$

This gives a stationary piece and a time dependent piece varying at a high frequency. In

order to simplify this, the rotating frame approximation is taken by tossing out the rapidly varying piece. This simplifies the calculations when the counterrotating piece can be neglected.

When there are multiple nuclei in a spin system, a multiply rotating coordinate system is used with one reference frequency for each nucleus. In this case, those pieces of the Hamiltonian that depend on the relative frequency between the nuclei are neglected. This includes the effects of pulses on the nuclei other than the one they are meant for and the transverse pieces of heteronuclear scalar coupling.

In high field NMR these simplifications are reasonable. At sufficiently low field NMR, they ignore effects as large as the ones they examine such that calculations using them are uninformative. The B_0 field of a few mT used here lies in a middle regime where rotating frame calculations can be informative but they are inadequate for the complete model of the system. In order to help understand and solve the difficulties of low field NMR, calculations in fully non-rotating frames are needed. This approach is straightforward in that the full time dependence is treated by breaking up the pulse sequences into intervals that are short compared to the period of the carrier frequencies and concatenating the evolution due to this piecewise-constant approximation of the Hamiltonian.

In order to more fully understand the implications of using low field, calculations in the lab frame are performed. These calculations make use of GAMMA (*50*), a C++ library of NMR related functions. This library has been created specifically to take

advantage of the simplifications brought about by using a multiply rotating frame but has many readymade functions that are readily adaptable to the inertial frame of the lab. As such, it offers a handy framework for modeling NMR experiments in the usual multiply rotating frame and in the lab frame for comparison.

B. Using GAMMA for lab frame calculations

Programs written in GAMMA are able to read in the parameters of a spin system, generate the initial condition density matrix, and evolve this density matrix under the effects of Hamiltonians that are static or include pulses, either ideal, square, or shaped. In order to perform calculations that model the system of interest, functions must be made that cast the problem as a sufficiently accurate piecewise constant Hamiltonian. Specifically, the initial condition and the Hamiltonians that are in effect at various times during the application of a pulse sequence need to be generated.

The initial condition of interest uses the tensor product construction in Eq. (7). The first two spins in a system are assumed to be the protons added from parahydrogen, while all other spins are at thermal equilibrium which uses room temperature as the default. This method restricts the form in which the file holding the spin system must be written in that the choice of the identity of the first two spins is not free, but does not restrict the calculation.

The GAMMA library already contains functions to generate the appropriate intrinsic Hamiltonian in the lab frame, but a new function for the Hamiltonian when

pulses are in operation must be generated. For the purpose of programming the instrument, these pulses are defined by a list of voltage levels that are each held for a set time. This form is smoothed and changed by the filtering effects of real electronics, but unless otherwise stated serves as the approximation of the pulse as a series of piecewise constant segments. The time step is typically 3.3 μs in the arbitrary waveform generator and typically this or 1 μs in the lab frame calculations. Shaped pulses in the multiply rotating frame version of GAMMA are defined as a similar series of piecewise constant segments in the rotating frame appropriate to the Larmor frequencies of each nucleus. The value of each segment is γB_1 in Hz while the value of the segments defined for the polarizer are the voltage values input to the amplifier. These values need to be multiplied by some arbitrary conversion factor to be appropriate as inputs to a GAMMA program. This factor can be found by calibrating a π pulse described in the same piecewise manner.

The existing shaped pulse function is used as a prototype for a lab frame function that calculates the effects of linear pulses delivered to multinuclear systems. This function only accounts for the effects of the pulse on one isotope since the rotating frame approximation assumes that all other isotopes are sufficiently separated in frequency to be unaffected by the pulse. The new function must account for the effects on all nuclei in the system. In order to do this for a pulse meant for isotope a, the interaction of the pulse must be applied to all nuclei of the same isotope with the given Rabi frequency as well as to the other isotopes at their appropriate Rabi frequency. For

instance, all nuclei of isotope b will need the value of $\gamma_a B_1$ scaled by γ_b/γ_a and then applied to account for the effect of the different gyromagnetic ratios.

In order to input the long vectors that define the pulses, existing functions that read in MATLAB® files were used. By doing this, the same functions that generate the pulse sequence for the polarizer can also be used for input to GAMMA programs simply by saving the file in a different way. Due to differences in the amplification of the different frequencies for hydrogen and carbon in the polarizer, the relative magnitude of pulses for each of the isotopes used must also be changed.

C. Pulse length at low field

A few considerations must be made about pulses at low field that are not needed at high field. Two considerations have to do with the length of the pulse. In high field, pulse lengths, often about 10μs, are many cycles of the carrier frequency. In a field of only 1.8mT, the proton Larmor frequency is 75 kHz and a 10 μs pulse would be less than one cycle of the carrier frequency long. Such a pulse would have large effects on all isotopes in the system and those effects would be highly dependent on the phase of the pulse. In order to render the effects of the pulse largely selective to one isotope, the pulse must be lengthened. The length needed is dependent upon the shape of the pulse, but typically must be at least a few cycles of the carrier frequency. For reasons that will be demonstrated, it is also advantageous that the length be chosen among the discrete values of time that make the pulse an integer or half integer multiple of the

carrier wave period.

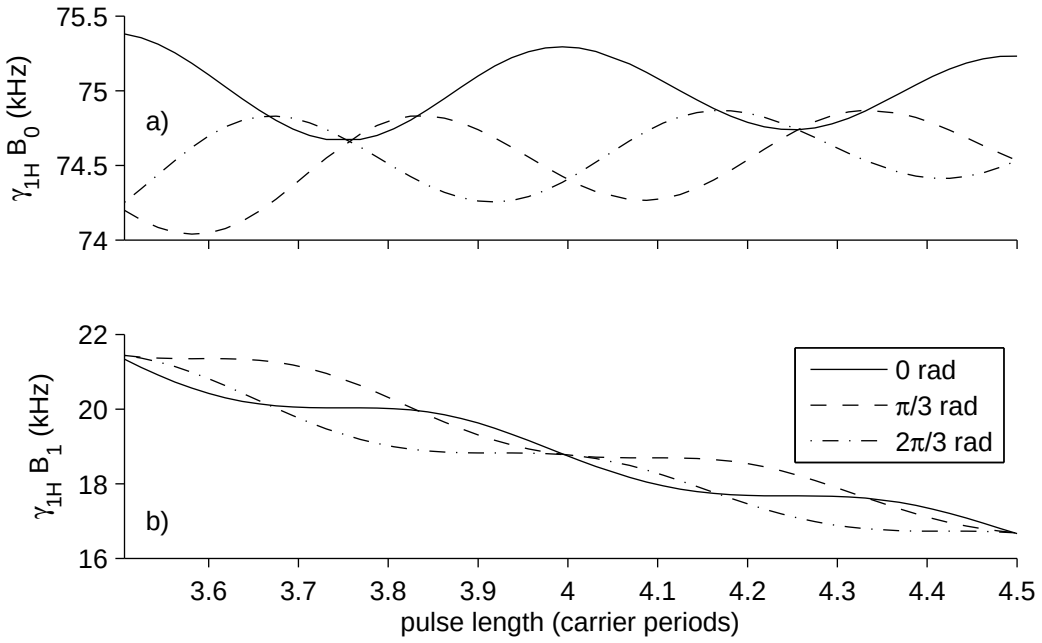

Figure 38. The optimal static field and pulse strength to give near perfect inversion with square pulses that are near four cycles of the carrier frequency long at a few example wavelet phases as shown in the legend.

Making the length such a multiple of the carrier period helps insure that the effect of the pulse is not dependent on the phase of the carrier (Fig. 38b) for purely geometric reasons. From the viewpoint of the rotating frame with the counterrotating wave discarded, the strength of B_1 for a square pulse is constant throughout the pulse so the Rabi frequency, the frequency at which the magnetization nutates about the pulse axis, is constant as well. If the pulse is started a little earlier or later, but lasts the same time, the pulse will turn the magnetization by the same amount. However, from the lab frame viewpoint, the strength of B_1 rises and falls and the instantaneous

frequency rises and falls with it (Fig. 39). If the length is not carefully chosen, then changes in when the pulse happens also change the overall rotation of the magnetization due to the pulse. Careful pulse construction where the magnitude of B_1 is dependent upon the wavelet phase could be used to help lift this pulse length restriction in applications where the wavelet phase is known before the pulse is given.

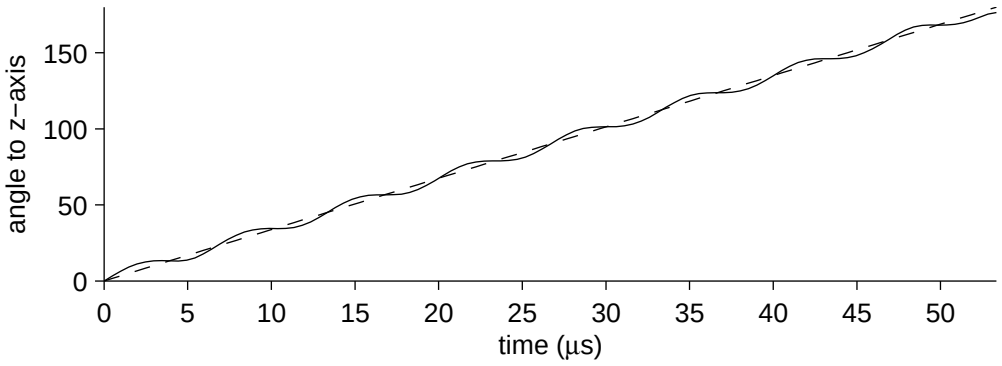

Figure 39. In the rotating frame, the linearly polarized square pulse is approximated as a circularly polarized pulse with half the amplitude. In the lab frame, the circularly polarized pulse (dotted) shows consistent Rabi frequency but the linear pulse (solid) does not and requires careful selection of the pulse length. These pulses are both π pulses that are four carrier wave periods long.

The choice of the overall length of the pulse among the lengths that are allowed is far more complicated. Shorter pulses are desirable for better time resolution, particularly in very short pulse sequences. Longer pulses are desirable for fewer non-ideal effects such as causing significant nutation on other isotopes, Bloch-Siegert effects, and wavelet phase dependence. These effects are both length and shape dependent, so require further discussion to fully understand.

It is worth noting that the non-geometric effects that control the optimal static

field of the pulse (Fig. 38a) imply that a pulse that is a quarter period longer or shorter than an integer multiple of the carrier period would be the best choice. Pulses of this length have not been explored due to the numerous other drawbacks that square pulses have in ways that are not expected to be affected by small adjustments in the pulse length.

D. Unintended nutation of other isotopes

The separation in frequency of isotopes is linearly dependent upon the strength of the static field B_0. At 1.8 mT, some isotopes that may be encountered are only separated by a few kHz. This situation requires that the pulses have sufficiently small bandwidth so as not to cause nutation on isotopes that is not intended. The bandwidth is generally dependent upon the inverse of the time of the pulse. At first glance, the fact that pulses that are quite long compared to high field practice seem to be good in this respect, but in the relative sense of the number of carrier wave periods they persist for, the pulses are much shorter than in conventional systems. It turns out that this relative sense gives the better picture of the situation. These pulses cover a much larger bandwidth in terms of their ability to rotate nearby isotopes (Fig. 40), complicating the pulse sequence design.

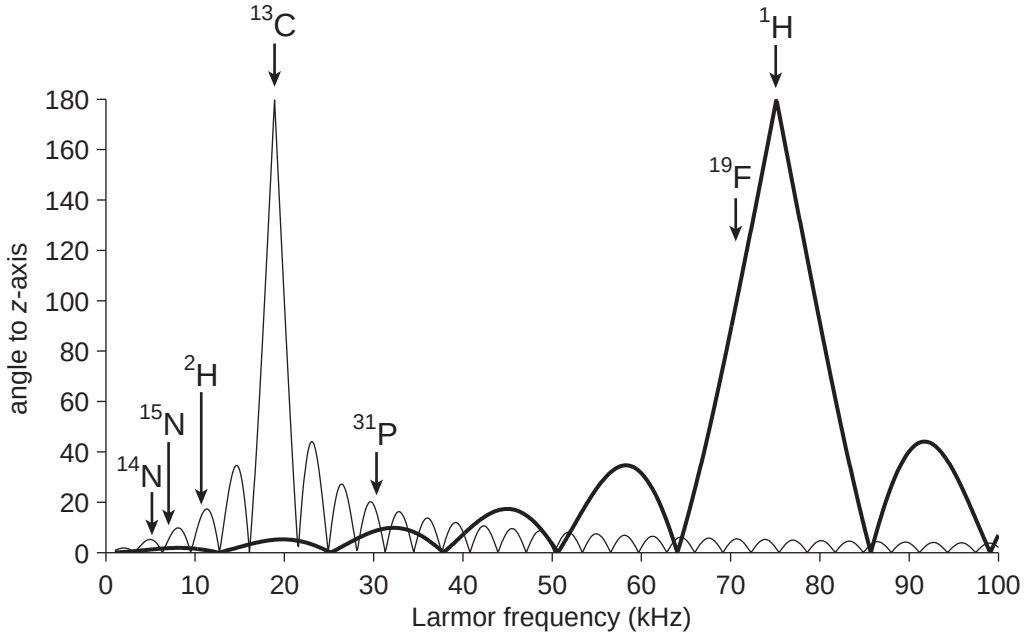

Figure 40. Pulses intended for one isotope have significant affect on other isotopes in the sample. Here are π pulses for two common isotopes, ^{1}H (thick) and ^{13}C (thin). These are square pulses that are six carrier wave periods of the target nucleus long. The locations of the reference frequencies for these isotopes and other common or useful isotopes are indicated by arrows.

The unintended nutation effects are worse for pulses intended for isotopes with a smaller gyromagnetic ratio. This is due to the relative sensitivity of the nuclei and the consequences of this sensitivity. Isotopes with a lower gyromagnetic ratio require larger amounts of power in order to achieve the same Rabi frequency as a direct consequence of the smaller magnetic moment. Also as a direct consequence, those isotopes with a larger moment are more sensitive to the power being applied. This effect can be seen in Fig. 40 in the increased size of the lobes on the higher frequency side of each pulse.

E. Bloch-Siegert effects

In the absence of any field in the transverse plane, the resonance frequency of a particular isotope is dependent only on the static field. However, when a magnetic field is turned on in the transverse place, this causes the size and direction of the field to change which in turn causes the resonance frequency to shift. When this transverse field is also static, the problem is uninteresting in that a change of axes will show it to be equivalent to the situation without the transverse field on, but with a slightly different resonance frequency. When the field becomes time dependent, the problem becomes much more interesting.

Even before the first NMR experiments were performed on stationary samples instead of molecular beams, Siegert and Bloch (*63*) contemplated the effect of the time dependent transverse field B_1 in the larger static field B_0. They studied the situation for the general problem of two independent, orthogonal fields in the transverse plane and explored the consequences for a circularly and linearly polarized field. They found that the linearly polarized case shifts the resonance of the sample by a factor of $\left(B_1/2B_0\right)^2$, to first order, and estimated that it was a negligible effect in the experiments of the time.

In the current experiments, π pulses as short as four carrier wave periods have been used, giving $B_1/B_0 = 1/8$. This gives a first order estimate of the offset as nearly 300 Hz while the actual offset due to other considerations can be as much as 1 kHz. The

first order estimate of the Bloch-Siegert shift is increasingly inaccurate as this ratio becomes large so it is insufficient to use the estimate for this situation. In practice the response is calculated numerically without recourse to an expansion in B_1/B_0.

In the case of on resonance circular polarization, there is no Bloch-Siegert shift. As such, it would be reasonable to construct an instrument capable of delivering a circularly polarized pulse in order to remove some of the difficulties inherent in using low field. However, circular polarization only helps with the on resonance isotope; the effects of each pulse on other isotopes continue to be a problem and this problem selectivity even increases in some cases.

F. Wavelet phase dependence

One unexpected result found in the course of performing lab frame calculations was a dependence of the pulse results on the wavelet phase. In the context of the rotating frame, this possibility does not arise. Such an effect implies that there is some universal time $t = 0$, seemingly violating a basic law of physics. However, without the approximations of the rotating frame, pulses with different wavelet phase are distinguishable and no physical laws are violated.

The wavelet phase is the phase that the carrier wave happens to have at the start of a pulse. NMR pulses can be thought of as a carrier wave multiplied by an envelope. The carrier is a function $\exp\left[i\left(\omega t + \phi\right)\right]$ which oscillates at the angular frequency ω near the Larmor frequency of the spin the pulse is intended to affect. The

phase ϕ is relative to the reference wave defining the rotating frame and is the usual notation of phase in high field NMR. The envelope is the shape of the pulse, for instance, for a square pulse, the envelope is a constant. In order to generate a pulse at time t_{pulse}, the carrier with the desired phase is multiplied by the desired envelope. The wavelet phase ϕ_w is the quantity $\omega t_{pulse} \bmod 2\pi$ in radians.

In the rotating frame, a π pulse delivered to a system at equilibrium at $t_{pulse} = 0$ or one delivered after a short wait should give exactly the same result because they are indistinguishable except for the time that has passed since the arbitrarily chosen initial time. In the lab frame, the pulse given by coils on a single axis is the real part of the function $\cos(\omega t + \phi)$ which does change according to the arbitrarily chosen initial time. As it turns out, these changes are important (Fig. 41).

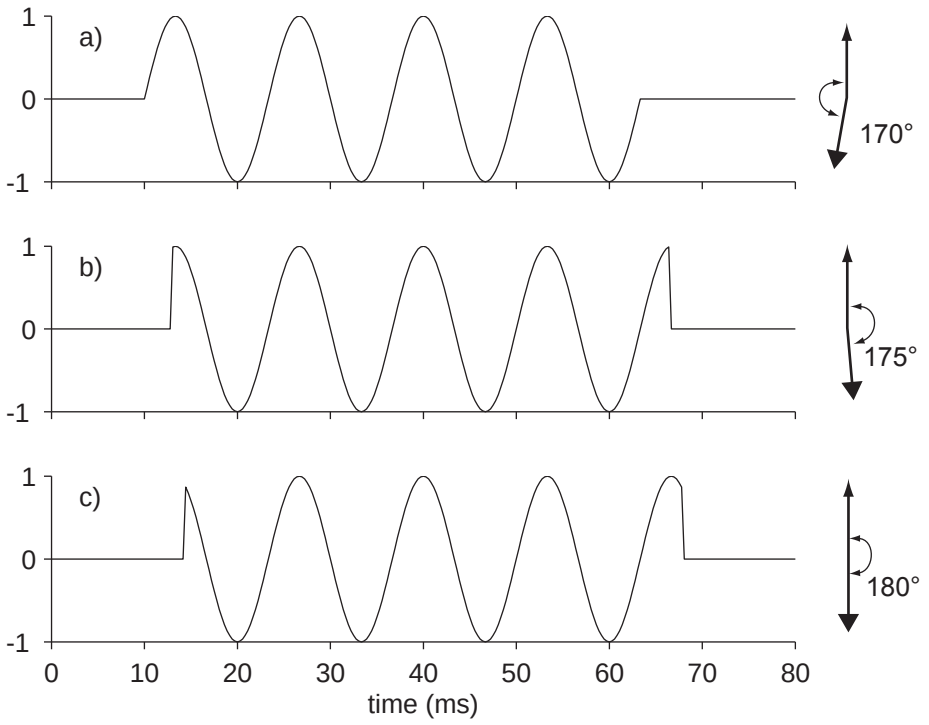

Figure 41. Examples of pulses with a square envelope with pulse phase $\phi = 0$ and wavelet phase (a) $\phi_w = 3\pi/2$, (b) $\phi_w = 0$, and (c) $\phi_w = \pi/3$. When applied with the same amplitude to a system resonating at 75 kHz, the resulting nutation axis and angle depends on the wavelet phase, to a degree which is significant for the frequencies and pulse widths of interest here, but is typically negligible in high field NMR.

The wavelet phase effects can be shown experimentally when the pulse wavelet phase can be measured or controlled. With the equipment currently in use for heteronuclear PASADENA experiments, it is the case that the wavelet phase can be controlled and an experiment has been performed to demonstrate the effect. For the demonstration, two pulses were made using six π pulses followed by a $\pi/2$ pulse. The first used the phases $x\bar{x}x\bar{x}x\bar{x}y$, where the letters denote the axis about which the pulse

operates and the over bar denotes the negative axis. This sequence is predicted to show extreme variation over the tested phases, while the second, with phases $x\bar{x}xx\bar{x}xy$, should show very little variation. The design concept of this experiment is illustrated in Fig. 42 and the results of this experiment are shown in Fig. 43 with a fit calculated using GAMMA on the same pulse shapes with the values of B_0, B_1, and an amplitude as fitting parameters. This amplitude parameter was required because the divergence found in the experiment was more than is expected from these pulses. This difference may be due to distortions in the pulse shape by the polarizer electronics such that the pulse delivered is not exactly as designed.

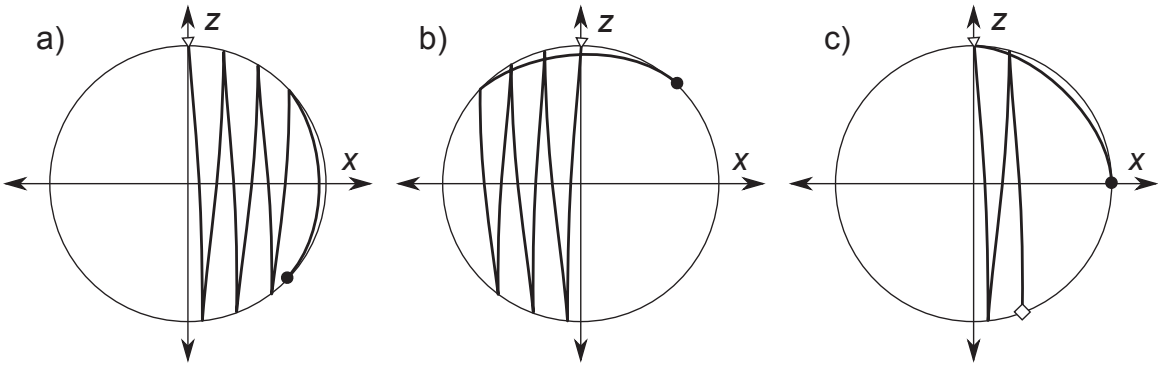

Figure 42. Schematic of the expected nutation of various series of six π pulses followed by a $\pi/2$ pulse. For a pulse with the phases $x\bar{x}x\bar{x}x\bar{x}y$ (a and b), the magnetization that starts along the z-axis at the empty triangle and nutates with ever increasing error dependent upon the wavelet phase until it finishes at the large dot. At one extreme (a), this error results in a large, negative magnitude along z after the $\pi/2$ pulse, while at the other extreme (b), this error results in a large, positive magnitude along z after the $\pi/2$ pulse. For a pulse with the phases $x\bar{x}xx\bar{x}xy$ (c), the magnetization that starts along the z-axis at the empty triangle and nutates with increasing error until the end of the third inversion (at the

diamond) after which the path is retraced back to the start so that all wavelet phases give approximately no magnetization along z after the $\pi/2$ pulse.

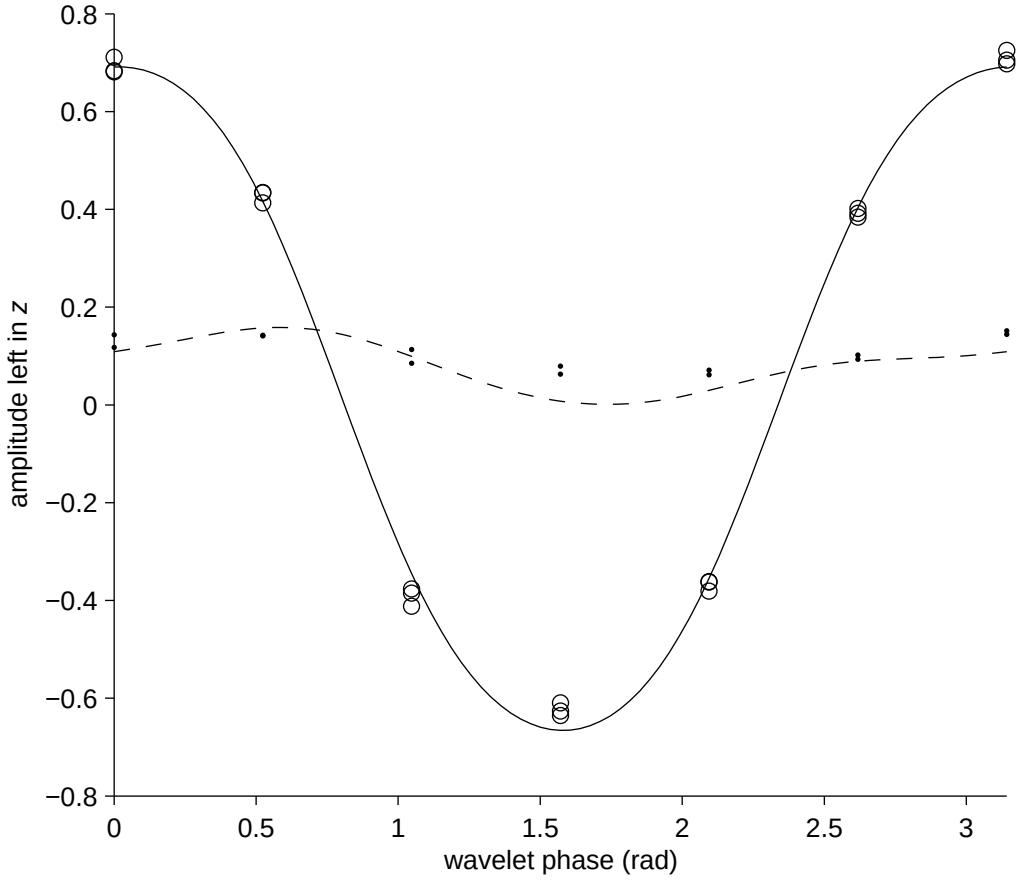

Figure 43. Experimental demonstration of wavelet phase effects. Six π pulses are applied successively followed by a $(\pi/2)_y$ pulse. These π pulses were applied with the phases $x\bar{x}x\bar{x}x\bar{x}$ (circles with solid line fit), thus increasing the divergence from the rotating frame expectation with each pulse, or with the phases $x\bar{x}xx\bar{x}x$ (points with dashed line fit), thus increasing the divergence over the first three pulses and then decreasing it over the second three pulses. The data are normalized by dividing by the signal obtained with no pulses.

Given a pulse with a certain carrier frequency, there is an optimal Larmor

frequency γB_0 and Rabi frequency γB_1 at which that pulse gives perfect inversion for any particular wavelet phase (Fig. 44). However, in a real experiment it is impractical to change the value of the static field as part of the pulse sequence. When both fields are set to particular values, only a few values of the wavelet phase will give perfect inversion while the others give poor inversion, sometimes substantially so (Fig. 45). This is not markedly improved when the value of γB_1 is optimized for each wavelet phase.

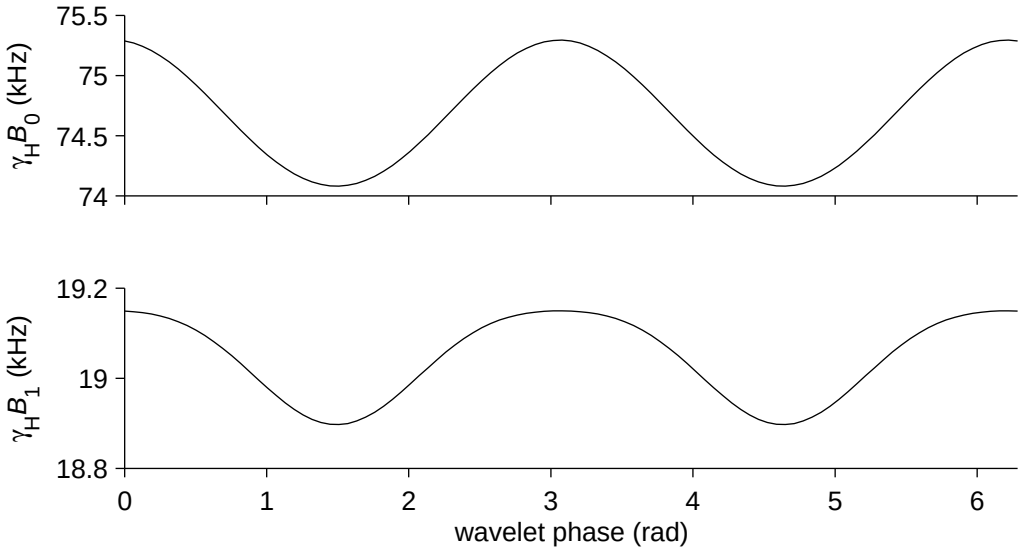

Figure 44. The optimal values for γB_0 and γB_1 for a π proton pulse with a square envelope, $\phi = 0$, and a carrier frequency of 75 kHz that lasts four cycles of the carrier for the range of possible wavelet phase values. When the pulse is used with these field strengths, it gives a perfect inversion at each wavelet phase.

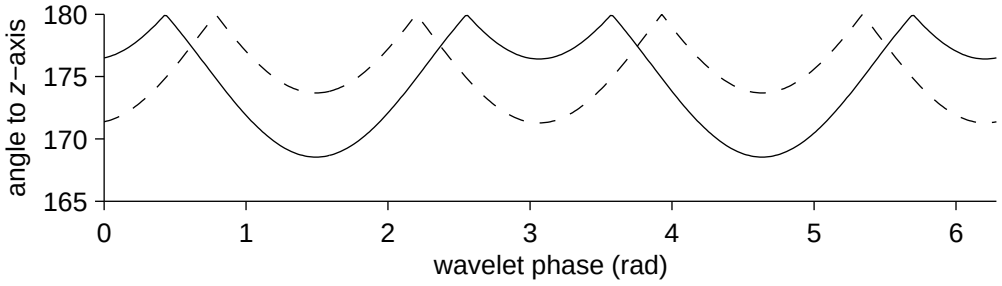

Figure 45. Variation of the nutation angle with wavelet phase after a nominal π proton pulse with a square envelope, $\phi = 0$, and a carrier frequency of 75 kHz that lasts four cycles of the carrier. The solid line is a pulse that has been optimized for $\gamma_H B_0 = 75$ kHz which requires that $\gamma_H B_1 = 19.12$ kHz and gives perfect inversion at $\phi_w = 0.4398$ rad. The dashed line is a pulse that has been optimized for $\phi_w = \pi/4$ rad which requires that $\gamma_H B_0 = 74.58$ kHz and $\gamma_H B_1 = 19.04$ kHz.

A pulse might not be capable of generating a full inversion for all wavelet phases either because the axis of rotation is outside of the xy-plane or because the required Rabi frequency changes with wavelet phase. While both of these effects are seen to some extent, the great majority of the problem comes from the first. The particular effect is actually seen in Haeberlen's (*72*) analytical treatment of continuous wave (CW) decoupling by average Hamiltonian theory.

VI. Solutions for wavelet phase dependence

Some level of wavelet phase dependence is expected for any low field experiment. The key to performing a successful pulsed experiment in the low field is to find a method that reduces these effects to an acceptable level without causing other problems that are unacceptable for the particular experiment. A number of different solutions exist with differing levels of complexity.

A. Increase pulse time

The dependence of the nutation angle on the happenstance phase of the carrier is reduced by increasing the length of the pulses. This is a reasonable solution in some cases, but may not be desirable in all cases, particularly with low γ nuclei. Increasing the pulse time by a multiple of four to give sixteen cycles of the carrier frequency produces a pulse that is capable of placing the magnetization within 3° of inversion for the on resonance case. For ^{1}H, this would increase the pulse time from 53.33 µs to 213.33 µs but for ^{15}N it increases the time from 525.88 µs to 2103.94 µs. A pulse of over 2 ms may adversely affect the pulse sequence due to the difficulty of correctly placing the long pulses and the other pulses that are meant to occur simultaneously in the sequences.

B. Only allow certain wavelet phases

Another solution would be to require that the pulses only start at certain times when the wavelet phase is near optimal. This requires slight changes in the timing of pulses and successful implementation requires somewhat better time resolution for the construction of proton pulses with the AWG than is typically utilized in the current experiments. In order to implement this, there must be enough points used such that at least one of them corresponds to a phase within an acceptable range of the phases that give a perfect inversion. For these example pulses, the desire to only use wavelet phases that invert the magnetization to within 1° would require that at least one point falls within the range of time represented by the wavelet phase change between points on the curve that are the acceptable limits. That range is only 0.16 rad requiring an AWG word rate of almost 3 MHz. Relaxing the goal to being within 2° of perfect inversion halves this requirement.

This requirement may also be reduced with a more sophisticated pulse generation technique. In the current pulse construction, the pulse starts exactly at the time represented by the first point, limiting the options of possible wavelet phase to the discrete values. A construction that allows the nominal pulse time to be slightly before the first point of the set that make up the pulse might offer better behavior. The current construction, in which the first word defining the pulse is given as the initial point in the envelope of the pulse times the carrier, assures some consistency in the

pulse construction that may also be important to generating pulses with consistent nutation.

C. Composite pulses

A third solution would be composite pulses. These require careful pulse construction so that rounding errors do not alter the relative wavelet phase between constituent pulses from what is expected. A great variety of composite pulses, all designed within the rotating frame approximation, are used to compensate for uncertainty in B_0 or B_1 or the variation of these fields over the sample. Two examples will be examined numerically to illustrate the possibility of using a similar strategy to compensate for wavelet phase effects at low field.

One of the first and most common composite pulses (*73*) is the inversion pulse $(\pi/2)_x \pi_y (\pi/2)_x$. This composite pulse is designed to compensate for incorrect settings of the Rabi frequency. Starting from longitudinal magnetization, it nominally places the magnetization on the y-axis, then rotates it about that axis before finally finishing the inversion. In this way, pulses that don't quite make it to the y-axis are moved closer to the $-z$-axis by the second pulse so that the third pulse, just like the first, can finish the inversion. Pulses that go too far during the first pulse are moved further away so that the last pulse needs to take it a little further.

The second inversion pulse considered here is a variation of the first,

$(\pi/2)_x(\pi/2)_y(\pi/2)_x$. This variation is non-obvious, based purely on the basis of the way it operates in low field.

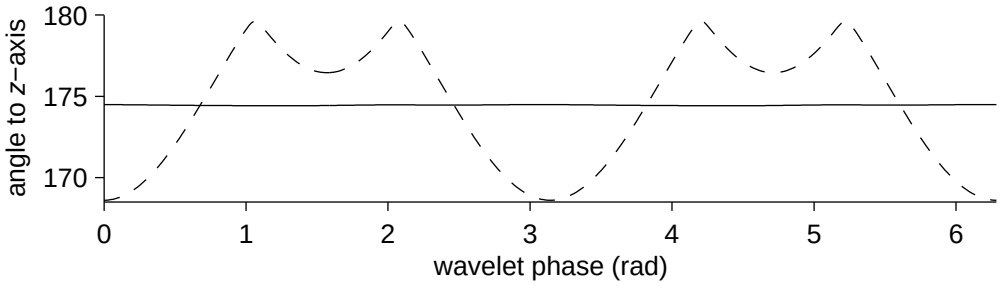

Figure 46. A well constructed composite pulse can reduce the wavelet phase dependence or simply change it. The well known $(\pi/2)_x \pi_y (\pi/2)_x$ pulse (dotted line) shows as much variation in the resultant nutation angle as is seen with single pulses. The alternative composite $(\pi/2)_x(\pi/2)_y(\pi/2)_x$ (solid line) shows very little wavelet phase dependence at the price of incomplete inversion for all. These are proton pulses with a square envelope. The carrier frequency and $\gamma_H B_0$ are set to 75 kHz and $\gamma_H B_1$ is set so that perfect inversion is possible at some wavelet phase for the first pulse and set to give the best inversion overall for the second pulse.

Composite pulses arguably do not have a single wavelet phase since each of the substituent pulses has its own wavelet phase, but it is valid to examine them based on the wavelet phase of the first pulse since the others have a definite relative phase compared to this first pulse so long there are no rounding errors. When this is done for the two composite inversion pulses, we find the dependence shown in Fig. 46. The $(\pi/2)_x \pi_y (\pi/2)_x$ pulse has the same wavelet phase dependence of the single π pulse, but shifted in phase, so is not useful. The $(\pi/2)_x(\pi/2)_y(\pi/2)_x$ pulse succeeds in having

very little wavelet phase dependence, but at the cost of never generating a particularly accurate inversion. Both come at the cost of longer pulse time.

In the current pulse construction, when a desired pulse time does not match an integer number of words, then the length is rounded, changing the time at which a pulse will occur and thus changing its relative wavelet phase slightly. When rounding is required, the pulse will be made with consistent relative wavelet phases in the composite pulse, but they may not be the desired phases. The examples of Fig. 46 use a word rate which is a multiple of the carrier frequency of the protons so that no rounding is required. It is generally not possible to choose such a frequency when pulses for two isotopes are needed, reducing the utility of this technique with the current programming.

D. Shaped pulses

Another solution is shaping the pulse envelope. Just as with composite pulses, a great variety of shaped pulses have been useful in high field NMR and new ones are easy to generate. A common motivation for shaping pulse envelopes is to narrow the range of resonance frequencies over which they are effective. This motivation is also relevant here in that the design process is greatly simplified if a given pulse acts on only one isotope. A bonus is that this strategy also mitigates the undesired dependence on wavelet phase. A few simple envelope shapes (*74*) were evaluated by numerical calculations including Hanning, Hamming, Gaussian (*75*), sinc (*76*), and half-sine. Of

these, the half-sine pulses seemed to perform the best in initial tests. Gaussian pulses also performed quite well, but would require an additional parameter, a cutoff point for the otherwise infinite pulse shape.

In another effort to improve the pulse shapes, they were filtered to remove undesirable effects. In order to do this, they were Fourier transformed to give the frequency response and undesirable frequencies were set to zero. They were then inverse Fourier transformed back into the time domain for a new pulse. This procedure returned pulses very similar to half-sine pulses in all cases, so half-sine pulses were chosen to be the pulse shape.

The half-sine pulse uses the first lobe of a sine, from the node at 0 to the node at π, inclusive of those nodes, to define the shape of the envelope. They were found to cause less nutation on distant isotopes at the expense of inducing greater nutation on nearby isotopes (Fig. 47). For most systems under consideration for hyperpolarization, this is a substantial improvement in selectivity. As with the square pulses, there is always a value of γB_0 and γB_1 that allows perfect inversion of the pulsed isotope at every wavelet phase (Fig. 48). The optimal value of γB_0 varies much less than for square pulses, but is never equivalent to the carrier frequency as the example given here that is four cycles of the carrier wave period long shows. When used at a fixed value of γB_0, they demonstrate less wavelet phase dependence for pulses of the same length (Fig. 49).

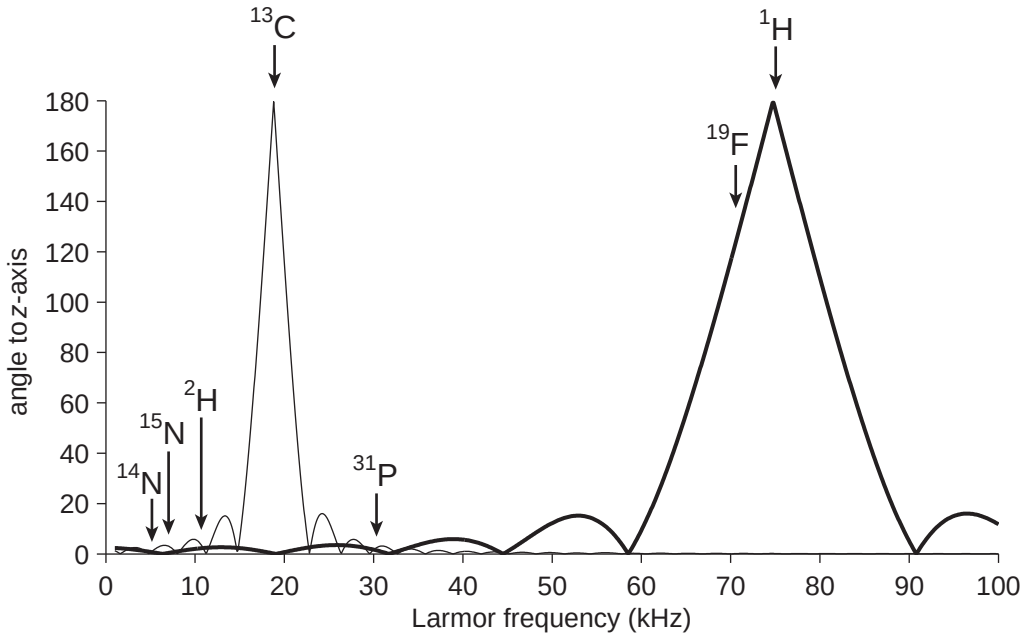

Figure 47. Pulses intended for one isotope have a significant effect on other isotopes in the sample. Here are inversion pulses for two common isotopes, ^{1}H (thick) and ^{13}C (thin). These are half-sine pulses that are six carrier wave periods of the target nucleus long. The locations of the reference frequencies for these isotopes and other common or useful isotopes are indicated by arrows.

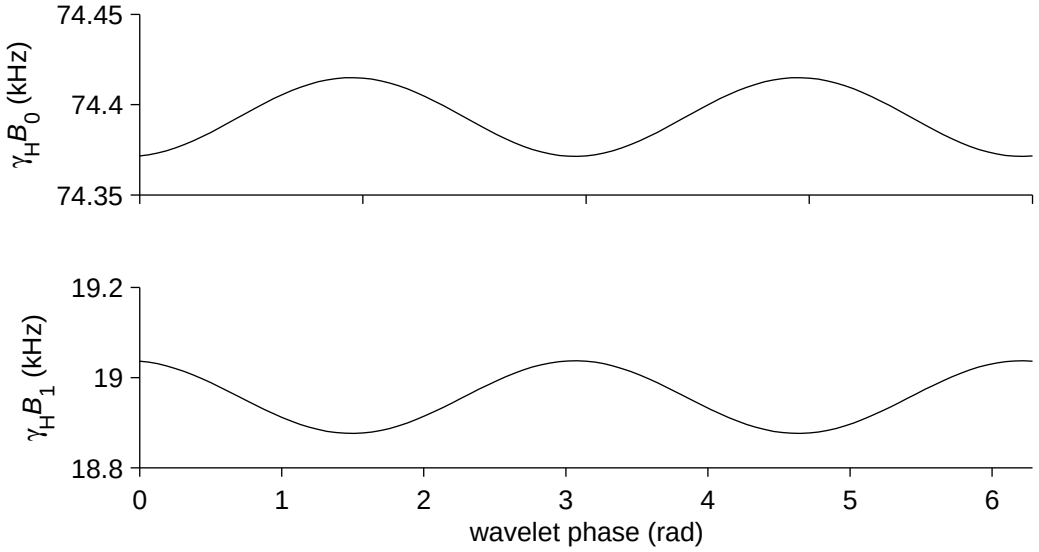

Figure 48. The optimal values for γB_0 and γB_1 for a π proton pulse with a half-sine envelope, $\phi = 0$, and a carrier frequency of 75 kHz that lasts four cycles of the carrier for the range of possible wavelet phase values. When the pulse is used with these field strengths, it gives a perfect inversion at each wavelet phase.

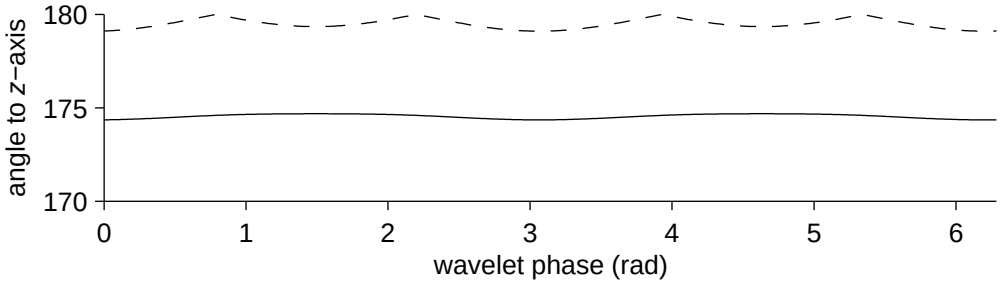

Figure 49. The nutation angle after a nominal π proton pulse with a half-sine envelope, $\phi = 0$, and a carrier frequency of 75 kHz that lasts four cycles of the carrier varies with the wavelet phase, but less than square pulses of the same length. The solid line is a pulse that has been optimized for $\gamma_H B_0 = 75$ kHz which requires that $\gamma_H B_1 = 18.91$ kHz for the greatest inversion at $\theta = \pi/4$ rad. The dashed line is a pulse that has been optimized for $\theta = \pi/4$ rad which requires that $\gamma_H B_0 = 74.40$ kHz and

$\gamma_H B_1 = 18.94$ kHz.

It might be expected that pulse shaping would change or lift the restriction that pulses be a length that is an integer or half integer multiple of the carrier frequency. This restriction is related to the specification that B_1 should not be dependent upon the wavelet phase. When pulses of this type with varying lengths are optimized for the best inversion by allowing B_0 and B_1 to vary, there is a length where B_1 does not vary and it is moved substantially from the previous length restriction (Fig. 50b). The shaping also reduces this dependence of B_1 on wavelet phase for any length pulse. Notably, near the previous length restriction, there is a position about 0.04 of the carrier period longer than the integer or half integer multiple of the carrier period where B_0 is not dependent upon the wavelet phase (Fig. 50a). This value does not vary when using different data rates to define the pulses, which makes it a good length restriction for these pulses.

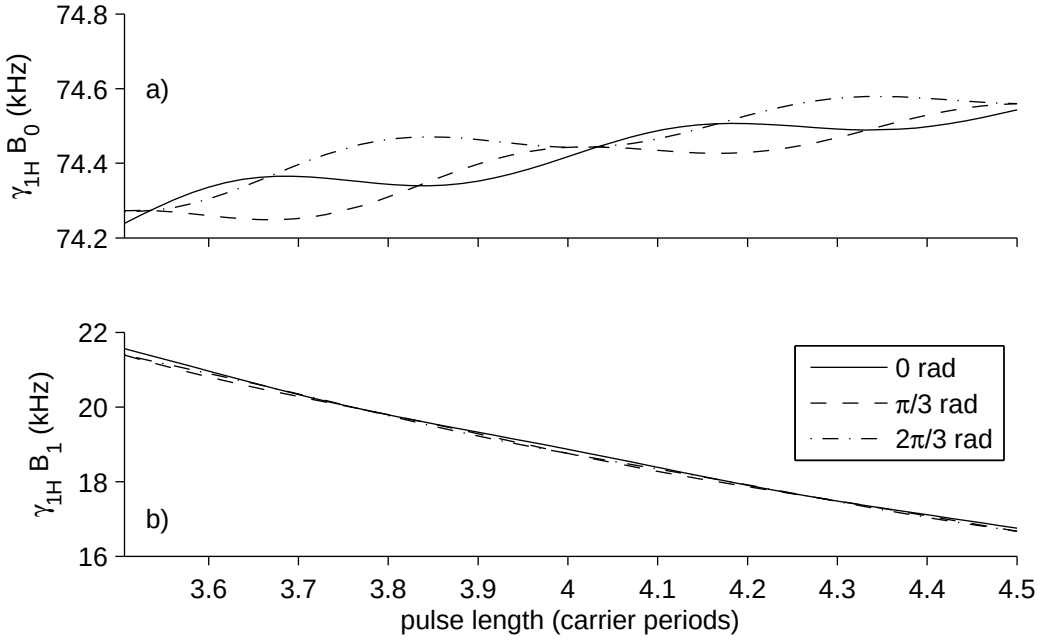

Figure 50. The optimal static field and pulse strength to give near perfect inversion with half-sine shaped pulses that are near four cycles of the carrier frequency long at a few example wavelet phases shown in the legend.

VII. Further Considerations

Hyperpolarization experiments are fundamentally different from those done with equilibrium polarization. In the case of ordinary polarization, multiple experiments can be conducted in order to gain further pieces of information about an experiment. In the case of hyperpolarization, once the polarization is lost it cannot be regained simply by waiting long enough. New methods are needed to utilize the available signal to the greatest advantage and extract information from the system as quickly as possible (*40,41*). Refocused INEPT sequences offer one route to the extraction of greater information.

Although the well known Zeeman polarization is generally the spin order of choice in an NMR experiment, other spin order types have been utilized. New experiments are currently being developed that utilize singlet spin order in varied ways so there is interest in being able to produce this spin order in many types of spin systems. Application of the spin order transfer algorithms described in the reverse sense would allow generation of singlet spin order when starting from Zeeman order.

A. Refocused INEPT

Detection on protons is desirable for better sensitivity and higher spatial resolution in MRI experiments. For inductively detected NMR and MRI, the sensitivity is proportional to the value of γ^2 at a particular polarization. One factor comes from the

magnitude of the gyromagnetic ratio. The other comes from the Faraday law which states that the voltage signal is proportional to the rate of change of the magnetic field so the higher precession of the larger gyromagnetic ratio gives a larger signal. For ^{13}C, the sensitivity gain is approximately 16 and for ^{15}N, the gain is approximately 100.

In MRI, the spatial resolution is proportional to the value of γ. This resolution is dependent upon the changes in frequency across a sample when a gradient is applied. In any application, the size of the gradient is limited by the physical limitations of the system. In the medical applications typical to MRI use, the gradient magnitude and rate of change are limited by safety considerations.

The protons added initially by molecular addition in order to reach a high polarization on the heteronucleus are ripe for use by INEPT (*19*). Refocusing is desirable to bring the antiphase peaks into phase for maximum effect in the MRI environment where field homogeneity within biological tissue is difficult to achieve. Ideally, INEPT performed by transferring polarization from a single nucleus to a single nucleus will perfectly transfer the polarization. The efficiency when performed from one heteronucleus to multiple equivalent nuclei of another isotope is readily calculated (*49*), and with optimization can lead to a similar overall gain.

Since the protons added in heteronuclear PASADENA are inequivalent and couple together, the problem is more complicated than has been treated analytically. In general these two effects will lessen the utility of the technique, but it will still demonstrate advantage over heteronuclear detection in most cases. Since every

molecule is unique, mapping the expected result with different wait times is helpful as a guide to determine the appropriate wait times. For example, succinate in basic conditions ($\mathrm{pH} = 13.3$) with the coupling constants $J_{12} = 6.68$ Hz, $J_{1S} = -6.32$ Hz, and $J_{2S} = 4.13$ Hz (*36*) would be expected to have average enhancement on the protons shown in Fig. 51 as a percentage of the starting polarization on the ^{13}C heteronucleus. In this example, an advantageous initial wait (transfer time) would be about 60 ms and the second wait (refocusing time) would be about 70 ms to give an average polarization on the protons of about 25%. This is roughly half what is expected in the ideal case of equivalent protons reducing the sensitivity advantage of detecting on protons instead of carbon from 16 to 8, still an appreciable advantage. Experimentally, such a method has been shown to increase the overall sensitivity by 6.5 (*48*).

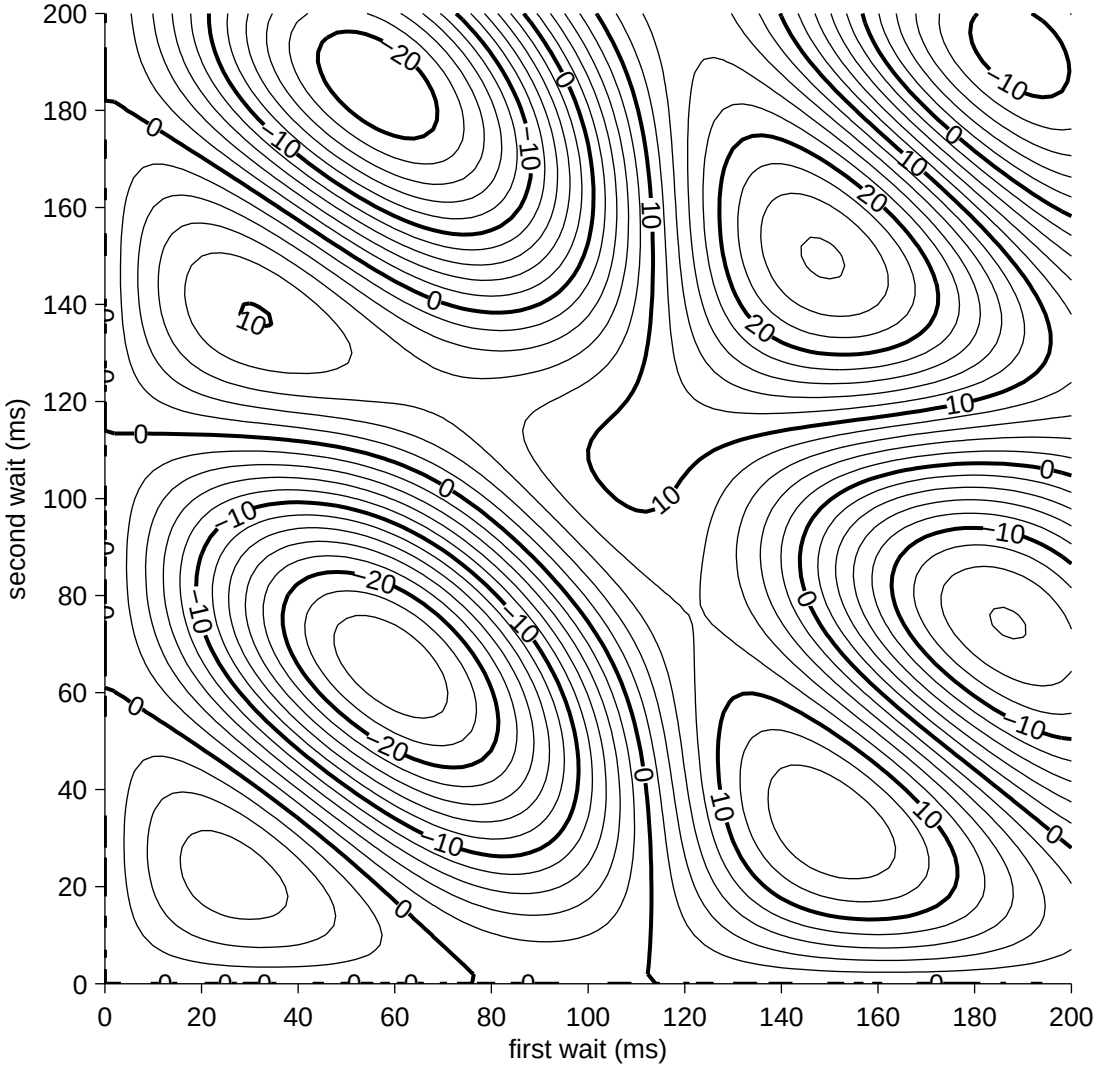

Figure 51. Expected average polarization on the two protons of succinate from molecular addition of hydrogen to a deuterated precursor in base as a percentage of the starting polarization on the heteronucleus for guiding the choice of timing constants in a refocused INEPT experiment. Major contours are spaced every 10% and minor contours are spaced every 2%. This is an ideal calculation that assumes the $4S_zI_{1z}I_{2z}$ order has relaxed to Zeeman polarization.

In cases where the chemical shift of the protons is sufficient, selective pulses can be used to restrict the transferred Zeeman spin order to one of the protons when the

molecule has been transferred to a high field for the experiment. This cannot be done for succinate, where the chemical shift difference is slight and only due to a secondary isotope effect from the single carbon label, but is useful for a number of demonstrated and proposed molecules. For TFPP, which has been demonstrated with an unselective refocused INEPT sequence (*48*), any of the three distinct protonated sites to which polarization transfer was observed could be chosen for selective transfer, since they are all separated by over 1 PPM. For choline labeled with ^{15}N, which is also an attractive molecule for biological applications, nonselective refocused INEPT has been demonstrated with molecules hyperpolarized by DNP (*77*) and it is reasonable to expect that any of the protons that couple with the ^{15}N could also be selectively polarized. Selective polarization transfer has been demonstrated to the nine equivalent methyl protons by incorporating a single selective π pulse within the refocused INEPT sequence (*49*).

B. Generation of singlet order

For applications where very long lived spin states are desirable, the lifetime of Zeeman order on a nucleus that is slow to relax can often be surpassed by the lifetime of a singlet state shared between two nuclei (*29,32,33*). Long lived spin states have been used as a method of spin labeling molecules for experiments that track their disposition through rate processes such as slow diffusion (*78*) or chemical exchange (*79*). These studies have been extended to utilizing the long lived singlet state on

protons (*80*) and heteronuclei, for example, the singlet state of $^{15}N_2O$ which has a lifetime of over 25 min (*81*).

The pulse sequence algorithms presented here performed in reverse would generate singlet order from Zeeman polarization. This would be possible from a heteronucleus to a set of protons or from a proton or isotopically distinct heteronucleus to a pair of heteronuclei, so long as the nuclei involved are all spin ½. Previous techniques for this purpose rely on chemical shift difference, which is not required here. The present sequence algorithms, using only the J-couplings, would have advantages wherever the chemical shift was small, such as in low fields or in molecules where approximate magnetic equivalence is found either by symmetry or by chance.

In performing the backwards sequence, the part of the initial condition of interest is S_z rather than $\frac{1}{2}\left(S_z - 4S_z I_{1z} I_{2z}\right)$ which is found immediately after performing the sequence in the forward direction. This initial condition for the reverse direction can be thought of as

$$\rho_r = \frac{1}{2}\left(S_z - 4I_{1z} I_{2z} S_z\right) + \frac{1}{2}\left(S_z + 4I_{1z} I_{2z} S_z\right). \tag{40}$$

The first piece will lead to singlet order. After the sequence is executed, heteronuclear decoupling on the system tuned to the isotope in the singlet state preserves the scalar spin order.

C. Conclusions

The pulse sequence algorithms presented here are capable of efficiently converting singlet spin order into Zeeman polarization. These algorithms generate polarization $P=1$ in the ideal case where 100% parahydrogen is used and relaxation during the sequence is negligible. Previously, this polarization could only be obtained for the specific case that $\theta \approx \pi/4$ and could be asymptotically approached for other values of θ with an increasing number of pulses of successively smaller angle as θ becomes bigger or smaller than $\pi/4$ (*34,35*). Relaxation ultimately will limit the efficiency with which spin order transfer can be achieved. Additionally, when transverse and longitudinal relaxation constants are not the same, the previous procedure must be compensated for this difference but it does not affect the new algorithms.

The first increase in the range of molecules to which the algorithms apply comes from introducing a more efficient use of the prior art medium θ pulse sequence algorithm. This extends the range of θ values over which $P=1$ in the ideal case to $0.3532 \lesssim \theta \leq \pi/4$. Outside of this range, the previous procedure could be used to increase polarization with modifications in the case of smaller θ values, but with compromises between achieved polarization and the duration of the pulse sequence. This fact motivates the introduction of two new pulse sequences, which make use of selective averaging of the terms in the spin Hamiltonian, effectively making θ time dependent within the sequence.

The second increase of range of molecules comes from a new pulse sequence for the small values of θ. This pulse sequence replaces the π pulse at the end of the first wait period with the onset of cyclic heteronuclear decoupling. This has the effect of removing the heteronuclear coupling terms from the Hamiltonian in operation on the system, effectively increasing the value of θ for a time so that it is large enough for the sequence to operate without losses. This small θ pulse sequence algorithm is capable of generating $P = 1$ in the ideal case for $0 < \theta \leq \pi/4$. In practical terms, J_{Δ} needs to be small enough that the calculated delay times for the sequence are not vanishingly small.

The last increase of range of molecules comes from a second new pulse sequence for large values of θ. This sequence modifies the first new sequence by applying a J-synchronized π pulse train during the first and third delays in order to change the Hamiltonian in operation during those times in the average sense. This train of pulses causes homonuclear decoupling while keeping the heteronuclear coupling terms, effectively decreasing the value of θ for a time such that the algorithm can operate without losses. The use of the J-synchronized π pulse train restricts the total time of the first and last wait to integer multiples of the synchronization period such that the ideal delay suggested by coherent averaging theory cannot be picked in many cases. Nevertheless, when this is so, numerical optimizations show that the synchronization time and heteronuclear decoupling time may be varied to yield a sequence that can be executed without losses over the range $\pi/4 \leq \theta < \pi/2$ as well as lower values where other sequences are equally effective and are faster. In practical

terms, J_Δ needs to be large enough that the delays do not become long compared to the relevant relaxation. This is the large θ pulse sequence algorithm.

In order to choose which pulse sequence algorithm is best given a particular molecule with a particular value of θ, the length of time required to generate the desired polarization is examined. This examination indicates that the small θ pulse sequence algorithm should be used in the range $0 < \theta \leq \arctan\left(1/\sqrt{2}\right)$ and the medium θ pulse sequence algorithm should be used in the range $\arctan\left(1/\sqrt{2}\right) < \theta \leq \pi/4$. Above this range, it is more difficult to determine which algorithm is best because the large θ pulse sequence algorithm generally requires longer times, so relaxation processes may remove the advantage of the algorithm. Taking a requirement that the medium θ algorithm should be able to achieve polarization of at least 90%, that algorithm requires a shorter time for $\theta \lesssim 1$ while the large θ algorithm requires a shorter time above this to give 100% polarization.

With these algorithms in hand, the challenge becomes to find the correct precursors for desirable molecules. A few example molecules that may be desirable are plotted in Fig. 52, showing a sampling of the array of molecular constants that may now be addressed with the new pulse sequence algorithms in reasonable time.

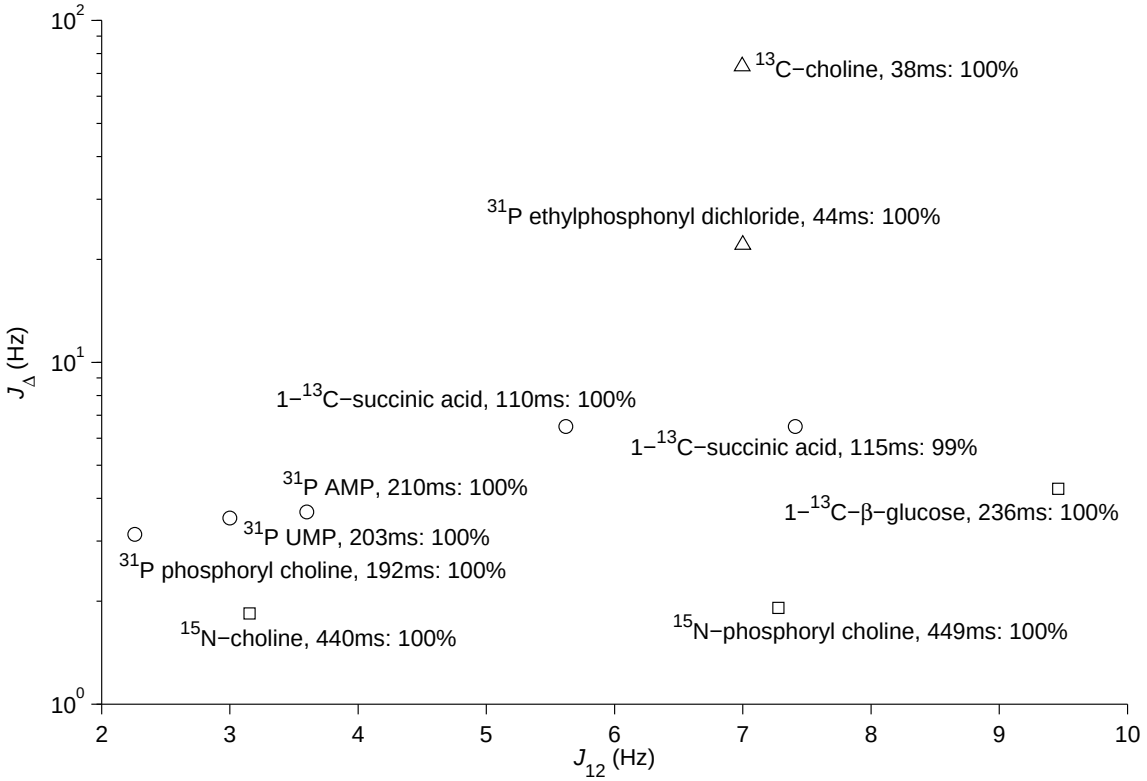

Figure 52. A selection of molecules to which the pulse sequence algorithms presented may be applied with the time required and the resulting polarization. The sequences utilized are generated by the small (△), medium (○), and large (□) θ pulse sequence algorithms.

An instrument has been built to perform the pulse sequences generated from these algorithms on real molecules for applications *in vitro* and *in vivo*. This was used to hyperpolarize a number of molecules, including succinate (*36,48,67*), the first metabolite to be hyperpolarized with heteronuclear PASADENA. This molecule has potential for imaging metabolic processes (*46*). An amphiphilic molecule, TFPP, has been developed that is sufficiently soluble for delivery and binds with lipids (*48*). When bound, the chemical shift of the hyperpolarized spin shifts so that the bound form is

discernible from that in solution, allowing a method to potentially characterize the amount of or placement of vulnerable plaques in the cardiovascular system (*43*).

In some cases, it is not attractive to detect signal on the heteronucleus. Sensitivity gains are seen in using protons for detection instead. In MRI, the resolution of the image is improved by using protons. In order to take advantage of this, refocused INEPT methods are being developed for application to complicated spin systems (*49,77*).

VIII. References

(1) Rabi, I. I.; Millman, S.; Kusch, P.; Zacharias, J. R. The Molecular Beam Resonance Method for Measuring Nuclear Magnetic Moments. The Magnetic Moments of $_3Li^6$, $_3Li^7$ and $_9F^{19}$. *Phys. Rev.* **1939**, 55, 526-535.

(2) Gorter, C. J. Negative Result of an Attempt to Detect Nuclear Magnetic Spins. *Physica* **1936**, 3, 995-998.

(3) Gorter, C. J.; Broer, L. J. F. Negative Result of an Attempt to Observe Nuclear Magnetic Resonance in Solids. *Physica* **1942**, 9, 591-596.

(4) Purcell, E. M.; Torrey, H. C.; Pound, R. V. Resonance Absorption by Nuclear Magnetic Moments in a Solid. *Phys. Rev.* **1946**, 69, 37-38.

(5) Bloch, F.; Hansen, W. W.; Packard, M. Nuclear Induction. *Phys. Rev.* **1946**, 69, 127.

(6) Purcell, E. M.; Bloembergen, N.; Pound, R. V. Resonance Absorption by Nuclear Magnetic Moments in a Single Crystal of CaF_2. *Phys. Rev.* **1946**, 70, 988.

(7) Pake, G. E. Nuclear Resonance Absorption in Hydrated Crystals: Fine Structure of the Proton Line. *J. Chem. Phys.* **1948**, 16, 327-336.

(8) Lamb, W. E. Internal Diamagnetic Fields. *Phys. Rev.* **1941**, 60, 817-819.

(9) Knight, W. D. Nuclear Magnetic Resonance Shift in Metals. *Phys. Rev.* **1949**, 76, 1259-1260.

(10) Proctor, W. G.; Yu, F. C. The Dependence of a Nuclear Magnetic Resonance Frequency upon Chemical Compound. *Phys. Rev.* **1950**, 77, 717.

(11) Dickinson, W. C. Dependence of the F^{19} Nuclear Resonance Position on Chemical Compound. *Phys. Rev.* **1950**, 77, 736-737.

(12) Proctor, W. G.; Yu, F. C. On the Nuclear Magnetic Moments of Several Stable Isotopes. *Phys. Rev.* **1951**, 81, 20-30.

(13) Gutowsky, H. S.; McCall, D. W.; Slichter, C. P. Coupling Among Nuclear Magnetic Dipoles in Molecules. *Phys. Rev.* **1951**, 84, 589-590.

(14) Williamson, M. P.; Havel, T. F.; Wuthrich, K. Solution Conformation of Proteinase Inhibitor-IIA from Bull Seminal Plasma by ^1H Nuclear Magnetic Resonance and Distance Geometry. *J. Mol. Biol.* **1985**, 182, 295-315.

(15) Gutowsky, H. S.; Holm, C. H. Rate Processes and Nuclear Magnetic Resonance Spectra .2. Hindered Internal Rotation of Amides. *J. Chem. Phys.* **1956**, 25, 1228-1234.

(16) Alger, J. R.; Shulman, R. G. NMR Studies of Enzymatic Rates *in vitro* and *in vivo* by Magnetization Transfer. *Qu. Rev. Biophys.* **1984**, 17, 83-124.

(17) Perrin, C. L.; Dwyer, T. J. Application of 2-Dimensional NMR to Kinetics of Chemical Exchange. *Chem. Rev.* **1990**, 90, 935-967.

(18) Kuhlmann, K. F.; Grant, D. M. The Nuclear Overhauser Enhancement of the Carbon-13 Magnetic Resonance Spectrum of Formic Acid. *J. Am. Chem. Soc.* **1968**, 90,

7355-7357.
(19) Morris, G. A.; Freeman, R. Enhancement of Nuclear Magnetic Resonance Signals by Polarization Transfer. *J. Am. Chem. Soc.* **1979**, 101, 760-762.
(20) Kaptein, R.; Oosterhoff, J. L. Chemically Induced Dynamic Nuclear Polarization II - (Relation with Anomalous ESR spectra). *Chem. Phys. Lett.* **1969**, 4, 195-197.
(21) Bouchiat, M. A.; Carver, T. R.; Varnum, C. M. Nuclear Polarization in He^3 Gas Induced by Optical Pumping and Dipolar Exchange. *Phys. Rev. Lett.* **1960**, 5, 373-375.
(22) Grover, B. C. Noble-Gas NMR Detection Through Noble-Gas-Rubidium Hyperfine Contact Interaction. *Phys. Rev. Lett.* **1978**, 40, 391-392.
(23) Bowers, C. R.; Weitekamp, D. P. Transformation of Symmetrization Order to Nuclear-Spin Magnetization by Chemical-Reaction and Nuclear-Magnetic-Resonance. *Phys. Rev. Lett.* **1986**, 57, 2645-2648.
(24) Bowers, C. R.; Weitekamp, D. P. Parahydrogen and Synthesis Allow Dramatically Enhanced Nuclear Alignment. *J. Am. Chem. Soc.* **1987**, 109, 5541-5542.
(25) Bowers, C. R. Parahydrogen and Synthesis Allow Dramatically Enhanced Nuclear Alignment. Ph.D. Dissertation, California Institute of Technology, Pasadena, California, 1991.
(26) Eisenschmid, T. C.; Kirss, R. U.; Deutsch, P. P.; Hommeltoft, S. I.; Eisenberg, R.; Bargon, J.; Lawler, R. G.; Balch, A. L. Para Hydrogen Induced Polarization in Hydrogenation Reactions. *J. Am. Chem. Soc.* **1987**, 109, 8089-8091.
(27) Bowers, C. R.; Jones, D. H.; Kurur, N. D.; Labinger, J. A.; Pravica, M. G.; Weitekamp, D. P. Symmetrization Postulate and Nuclear Magnetic Resonance of Reacting Systems. *Adv. Magn. Reson.* **1990**, 14, 269-291.
(28) Bowers, C. R.; Weitekamp, D. P. Nuclear Magnetic Resonance by Measuring Reaction Yield of Spin Symmetry Species. *Solid State Nucl. Magn. Reson.* **1998**, 11, 123-128.
(29) Carravetta, M.; Levitt, M. H. Long-lived Nuclear Spin States in High-field Solution NMR. *J. Am. Chem. Soc.* **2004**, 126, 6228-6229.
(30) Eisenschmid, T. C.; McDonald, J.; Eisenberg, R.; Lawler, R. G. INEPT in a Chemical Way. Polarization Transfer From Para Hydrogen to ^{31}P by Oxidative Addition and Dipolar Relaxation. *J. Am. Chem. Soc.* **1989**, 111, 7267-7269.
(31) Natterer, J.; Schedletzky, O.; Barkemeyer, J.; Bargon, J.; Glaser, S. J. Investigating Catalytic Processes with Parahydrogen: Evolution of Zero-quantum Coherence in AA ' X Spin Systems. *J. Magn. Reson.* **1998**, 133, 92-97.
(32) Carravetta, M.; Johannessen, O. G.; Levitt, M. H. Beyond the T-1 Limit: Singlet Nuclear Spin States in Low Magnetic Fields. *Phys. Rev. Lett.* **2004**, 92, 153003.
(33) Carravetta, M.; Levitt, M. H. Theory of Long-lived Nuclear Spin States in Solution Nuclear Magnetic Resonance. I. Singlet States in Low Magnetic Field. *J. Chem. Phys.* **2005**, 122, 214505.
(34) Goldman, M.; Johannesson, H. Conversion of a Proton Pair Para Order into ^{13}C Polarization by RF Irradiation, for Use in MRI. *C. R. Phys.* **2005**, 6, 575-581.

(35) Goldman, M.; Johannesson, H.; Axelsson, O.; Karlsson, M. Design and Implementation of ^{13}C Hyper Polarization from Para-hydrogen, For New MRI Contrast Agents. *C. R. Chimie* **2006**, 9, 357-363.

(36) Chekmenev, E. Y.; Hovener, J.-B.; Norton, V. A.; Harris, K.; Batchelder, L. S.; Bhattacharya, P.; Ross, B. D.; Weitekamp, D. P. PASADENA Hyperpolarization of Succinic Acid for MRI and NMR Spectroscopy. *J. Am. Chem. Soc.* **2008**, 130, 4212-4213.

(37) Albert, M. S.; Cates, G. D.; Driehuys, B.; Happer, W.; Saam, B.; Springer, C. S.; Wishnia, A. Biological Magnetic Resonance Imaging Using Laser Polarized ^{129}Xe. *Nature* **1994**, 370, 199-201.

(38) Golman, K.; Axelsson, O.; Johannesson, H.; Mansson, S.; Olofsson, C.; Petersson, J. S. Parahydrogen-induced Polarization in Imaging: Subsecond ^{13}C Angiography. *Magn. Reson. Med.* **2001**, 46, 1-5.

(39) Golman, K.; Ardenkjaer-Larsen, J. H.; Petersson, J. S.; Mansson, S.; Leunbach, I. Molecular Imaging with Endogenous Substances. *Proc. Natl. Acad. Sci. U. S. A.* **2003**, 100, 10435-10439.

(40) Bhattacharya, P.; Harris, K.; Lin, A. P.; Mansson, M.; Norton, V. A.; Perman, W. H.; Weitekamp, D. P.; Ross, B. D. Ultra-fast Three Dimensional Imaging of Hyperpolarized ^{13}C *in vivo*. *Magn. Reson. Mat. Phys. Biol. Med.* **2005**, 18, 245-256.

(41) Perman, W. H.; Bhattacharya, P.; Leupold, J.; Lin, A. P.; Harris, K. C.; Norton, V. A.; Hövener, J.-B.; Ross, B. D. Fast Volumetric Spatial-Spectral MR Imaging of Hyperpolarized ^{13}C-Labeled Compounds Using Multiple Echo 3D bSSFP. *Magn. Reson. Imag.* **2010**, 28, 459-465.

(42) Chekmenev, E. Y.; Chow, S. K.; Tofan, D.; Weitekamp, D. P.; Ross, B. D.; Bhattacharya, P. Fluorine-19 NMR Chemical Shift Probes Molecular Binding to Lipid Membranes. *J. Phys. Chem. B* **2008**, 112, 6285-6287.

(43) Chekmenev, E. Y.; Reynolds, W. F.; Chow, S.-K.; Hövener, J. B.; Norton, V. A.; Tran, T. T.; Chan, H. C.; Wagner, S. R.; Perman, W. H.; Weitekamp, D. P.; Ross, B. D.; Bhattacharya, P. In *Experimental NMR Conference* Asilomar, California, 2009.

(44) Gallagher, F. A.; Kettunen, M. I.; Day, S. E.; Hu, D. E.; Ardenkjaer-Larsen, J. H.; in't Zandt, R.; Jensen, P. R.; Karlsson, M.; Golman, K.; Lerche, M. H.; Brindle, K. M. Magnetic Resonance Imaging of pH *in vivo* Using Hyperpolarized ^{13}C-labelled Bicarbonate. *Nature* **2008**, 453, 940-943.

(45) Golman, K.; in't Zandt, R.; Lerche, M.; Pehrson, R.; Ardenkjaer-Larsen, J. H. Metabolic Imaging by Hyperpolarized ^{13}C Magnetic Resonance Imaging for *in vivo* Tumor Diagnosis. *Can. Res.* **2006**, 66, 10855-10860.

(46) Ross, B. D.; Bhattacharya, P.; Wagner, S.; Tran, T.; Sailasuta, N. Hyperpolarized MR Imaging: Neurologic Applications of Hyperpolarized Metabolism. *Am. J. Neuroradiol.* **2010**, 31, 24-33.

(47) Larson, P. E. Z.; Kerr, A. B.; Chen, A. P.; Lustig, M. S.; Zierhut, M. L.; Hu, S.; Cunningham, C. H.; Pauly, J. M.; Kurhanewicz, J.; Vigneron, D. B. Multiband Excitation Pulses for Hyperpolarized ^{13}C Dynamic Chemical-shift Imaging. *J. Magn. Reson.* **2008**,

194, 121-127.
(48) Chekmenev, E. Y.; Norton, V. A.; Weitekamp, D. P.; Bhattacharya, P. Hyperpolarized ^{1}H NMR Employing Low Gamma Nucleus for Spin Polarization Storage. *J. Am. Chem. Soc.* **2009**, 131, 3164-3165.
(49) Pfeilsticker, J. A.; Ollerenshaw, J. E.; Norton, V. A.; Weitekamp, D. P. A Selective ^{15}N-to-^{1}H Polarization Transfer Sequence for More Sensitive Detection of ^{15}N-Choline. *J. Magn. Reson.* **2010**, *In Press*.
(50) Smith, S. A.; Levante, T. O.; Meier, B. H.; Ernst, R. R. Computer-Simulations in Magnetic-Resonance - an Object-Oriented Programming Approach. *J. Magn. Reson. Ser. A* **1994**, 106, 75-105.
(51) Osborn, J. A.; Jardine, F. H.; Young, J. F.; Wilkinson, G. The Preparation and Properties of Tris(triphenylphosphine)halogenorhodium(I) and Some Reactions Thereof Including Catalytic Homogeneous Hydrogenation of Olefins and Acetylenes and Their Derivatives. *J. Chem. Soc. A* **1966**, 1711-1732.
(52) Eisenberg, R.; Eisenschmid, T. C.; Chinn, M. S.; Kirss, R. U. Parahydrogen Induced Polarization and Polarization Transfer in Hydrogenation and Oxidative Addition Reactions - A Mechanistic Probe. *Adv. Chem. Ser.* **1992**, 47-74.
(53) Duckett, S. B.; Sleigh, C. J. Applications of the Parahydrogen Phenomenon: A Chemical Perspective. *Prog. Nuc. Magn. Reson. Spec.* **1999**, 34, 71-92.
(54) Lit, E. S.; Mallon, F. K.; Tsai, H. Y.; Roberts, J. D. Conformational Changes of Butanedioic Acid as a Function of pH as Determined From Changes in Vicinal Proton-proton NMR Couplings. *J. Am. Chem. Soc.* **1993**, 115, 9563-9567.
(55) Siddall, T. H.; Prohaska, C. A. Conformation of Organophosphorus Compounds. I. Proton Magnetic Resonance Studies of Some Phosphinates, Phosphinic Acids, Phosphinyl Chlorides and Phosphonyl Dichlorides. *J. Am. Chem. Soc.* **1962**, 84, 2502-2506.
(56) Dessy, R. E.; Flautt, T. J.; Jaffe, H. H.; Reynolds, G. F. Nuclear Magnetic Resonance Spectra of Some Dialkylmercury Compounds. *J. Chem. Phys.* **1959**, 30, 1422-1425.
(57) Govindaraju, V.; Young, K.; Maudsley, A. A. Proton NMR Chemical Shifts and Coupling Constants for Brain Metabolites. *NMR Biomed.* **2000**, 13, 129-153.
(58) Hovener, J. B.; Chekmenev, E. Y.; Harris, K. C.; Perman, W. H.; Robertson, L. W.; Ross, B. D.; Bhattacharya, P. PASADENA Hyperpolarization of ^{13}C Biomolecules: Equipment Design and Installation. *Magn. Reson. Mat. Phys. Biol. Med.* **2009**, 22, 111-121.
(59) Hovener, J. B.; Chekmenev, E. Y.; Harris, K. C.; Perman, W. H.; Tran, T. T.; Ross, B. D.; Bhattacharya, P. Quality Assurance of PASADENA Hyperpolarization for ^{13}C Biomolecules. *Magn. Reson. Mat. Phys. Biol. Med.* **2009**, 22, 123-134.
(60) *LabVIEW™,* version 8.5; National Instruments: Austin, Texas, 2007.
(61) *MATLAB®,* version R2008a; The Mathworks, Inc.: Natick, Massachusetts, 1984-2008.
(62) Levitt, M. H.; Freeman, R.; Frenkiel, T. Broad-band Heteronuclear Decoupling. *J.*

Magn. Reson. **1982**, 47, 328-330.
(63) Bloch, F.; Siegert, A. Magnetic Resonance for Nonrotating Fields. *Phys. Rev.* **1940**, 57, 522-527.
(64) Gridnev, I. D.; Higashi, N.; Asakura, K.; Imamoto, T. Mechanism of Asymmetric Hydrogenation Catalyzed by a Rhodium Complex of (S,S)-1,2-bis(tert-butylmethylphosphino)ethane. Dihydride Mechanism of Asymmetric Hydrogenation. *J. Am. Chem. Soc.* **2000**, 122, 7183-7194.
(65) Gridnev, I. D.; Imamoto, T. On the Mechanism of Stereoselection in Rh-catalyzed Asymmetric Hydrogenation: A General Approach for Predicting the Sense of Enantioselectivity. *Accounts Chem. Res.* **2004**, 37, 633-644.
(66) Golman, K.; Axelsson, O.; Johannesson, H.; Mansson, S.; Olofsson, C.; Petersson, J. S. Parahydrogen-induced polarization in imaging: Subsecond C-13 angiography. *Magn. Reson. Med.* **2001**, 46, 1-5.
(67) Bhattacharya, P.; Chekmenev, E. Y.; Perman, W. H.; Harris, K. C.; Lin, A. P.; Norton, V. A.; Tan, C. T.; Ross, B. D.; Weitekamp, D. P. Towards Hyperpolarized ^{13}C-Succinate Imaging of Brain Cancer. **2007**, 186, 150-155.
(68) Vold, R. L.; Waugh, J. S.; Klein, M. P.; Phelps, D. E. Measurement of Spin Relaxation in Complex Systems. *J. Chem. Phys.* **1968**, 48, 3831-3832.
(69) Torchia, D. A. Measurement of Proton-enhanced ^{13}C T_1 Values by a Method Which Supresses Artifacts. *J. Magn. Reson.* **1978**, 30, 613-616.
(70) Levitt, M. H. *Spin Dynamics: Basics of Nuclear Magnetic Resonance*; John Wiley & Sons Ltd.: Chichester, 2001.
(71) Goldman, M. *Quantum Description of High-Resolution NMR in Liquids*; Oxford University Press, Inc.: Oxford, 1988.
(72) Haeberlen, U. *High Resolution NMR in Solids: Selective Averaging*; Academic Press: New York, 1976.
(73) Levitt, M. H.; Freeman, R. NMR Population-Inversion Using a Composite Pulse. *J. Magn. Reson.* **1979**, 33, 473-476.
(74) Borgnat, P.; Lesage, A.; Caldarelli, S.; Emsley, L. Narrowband Linear Selective Pulses for NMR. *J. Magn. Reson. A* **1996**, 119, 289-294.
(75) Bauer, C.; Freeman, R.; Frenkiel, T.; Keeler, J.; Shaka, A. J. Gaussian Pulses. *J. Magn. Reson.* **1984**, 58, 442-457.
(76) Temps, A. J.; Brewer, C. F. Synthesis of Arbitrary Frequency Domain Transmitting Pulses Applicable to Pulsed NMR Instruments. *J. Magn. Reson.* **1984**, 56, 355-372.
(77) Sarkar, R.; Comment, A.; Vasos, P. R.; Jannin, S.; Gruetter, R.; Bodenhausen, G.; Hall, H. l. n.; Kirik, D.; Denisov, V. P. Proton NMR of ^{15}N-Choline Metabolites Enhanced by Dynamic Nuclear Polarization. *J. Am. Chem. Soc.* **2009**, 131, 16014-16015.
(78) Ferrage, F.; Zoonens, M.; Warschawski, D. E.; Popot, J.-L.; Bodenhausen, G. Slow Diffusion of Macromolecular Assemblies by a New Pulsed Field Gradient NMR Method. *J. Am. Chem. Soc.* **2003**, 125, 2541-2545.
(79) Wenter, P.; Bodenhausen, G.; Dittmer, J.; Pitsch, S. Kinetics of RNA Refolding in

Dynamic Equilibrium by ^{1}H-Detected ^{15}N Exchange NMR Spectroscopy. *J. Am. Chem. Soc.* **2006**, 128, 7579-7587.

(80) Cavadini, S.; Dittmer, J.; Antonijevic, S.; Bodenhausen, G. Slow Diffusion By Singlet State NMR Spectroscopy. *J. Am. Chem. Soc.* **2005**, 127, 15744-15748.

(81) Pileio, G.; Carravetta, M.; Hughes, E.; Levitt, M. H. The Long-Lived Nuclear Singlet State of ^{15}N-Nitrous Oxide in Solution. *J. Am. Chem. Soc.* **2008**, 130, 12582-12583.